

Next-to-Leading Order Unitarity Fits in the Extended Georgi-Machacek Model

Debtosh Chowdhury *, Poulami Mondal † and Subrata Samanta ‡

Department of Physics, Indian Institute of Technology Kanpur, Kanpur 208016, India

(Dated: June 10, 2025)

Abstract

The Georgi-Machacek (GM) model is a triplet scalar extension of the Standard Model (SM) that preserves custodial symmetry (CS) due to an explicit global $SU(2)_L \otimes SU(2)_R$ symmetry in the scalar potential at tree-level. However, it is also possible to construct a triplet extended scalar sector of the SM without imposing a global $SU(2)_L \otimes SU(2)_R$ symmetry in the potential while still maintaining custodial symmetry at tree-level. This is referred to as the extended GM (eGM) model. We compute one-loop corrections to all $2 \rightarrow 2$ bosonic scattering amplitudes in the GM and eGM models and place next-to-leading order (NLO) unitarity bounds on the scalar quartic couplings. Further, we derive the bounded-from-below (BFB) conditions on the scalar quartic couplings demanding the stability of the scalar potential in the field subspaces. We show that the BFB conditions with all combinations of three non-zero scalar fields provide a very good approximation of the all field BFB conditions for both models while being computationally more efficient. With these theoretical constraints, we perform a global fit of the GM and eGM models to the latest Higgs signal strength results from the 13 TeV Large Hadron Collider. We observe that the global fit disfavors the regions where $\kappa_V > 1.05$, $\kappa_V < 0.95$, and $\kappa_f > 1.05$, $\kappa_f < 0.92$ at a 95.4% confidence level for both models. The global fit results demonstrate that NLO unitarity and stability bounds play a significant role in constraining the allowed parameter space of both models. We obtain an upper limit on the absolute values of the scalar quartic couplings to be 1.91 (2.51) in the GM (eGM) model. We find that in both models, the absolute mass differences between the heavy Higgs bosons are less than 410 GeV if their masses are below 1.1 TeV. Unlike the GM model, the masses of scalar particles within each CS multiplet are no longer degenerate in the eGM model. We find that the maximal mass splitting among the members of each CS multiplet in the eGM model is restricted to be smaller than 210 GeV.

Keywords: Beyond Standard Model, Higgs Physics, Multi-Higgs Models, Renormalization Group

* E-mail: debtoshc@iitk.ac.in

† E-mail: poulamim@iitk.ac.in

‡ E-mail: samantaphy20@iitk.ac.in

CONTENTS

| | |
|---|----|
| I. Introduction | 2 |
| II. Model | 4 |
| III. Boundedness of the scalar potential | 8 |
| IV. Unitarity constraints at one-loop | 9 |
| A. Partial-wave analysis | 9 |
| B. $2 \rightarrow 2$ scattering amplitudes | 10 |
| V. HEPfit | 13 |
| VI. Global fit constraints | 14 |
| A. Theoretical constraints | 14 |
| B. h signal strengths | 15 |
| VII. Results | 17 |
| VIII. Conclusions | 26 |
| Acknowledgments | 27 |
| A. Quartic couplings from physical masses | 28 |
| B. Bounded-from-below constraints in the field subspace | 29 |
| C. Necessary and sufficient bounded-from-below conditions | 33 |
| D. Results for one-loop scattering amplitudes | 34 |
| E. Two-loop renormalization group equations | 46 |
| F. Supplementary figures | 52 |
| References | 56 |

I. INTRODUCTION

Discovery of the Higgs boson [1, 2] has already played a significant role in understanding the electroweak symmetry breaking (EWSB) mechanism and its connection to the generation of the masses of elementary particles in the Standard Model (SM). However, the origin of EWSB has not yet been settled. Results from the latest ATLAS and CMS Run 2 data allow for a deviation within $\sim 10\%$ in the Higgs signal strength values [3–21]. Thus the

data does not preclude the existence of additional multiplets (doublet or higher) in the scalar sector of the SM. Such higher multiplets leave an imprint on the EWSB mechanism that can be detected via the SM-like Higgs couplings to the vector bosons. Among these higher multiplets, the scalar $SU(2)_L$ triplet extensions of the SM have various interesting phenomenological aspects at the LHC [22–42] and future colliders [43–50]. In addition to the existence of singly-charged scalars, scalar triplets also predict doubly-charged scalars unlike the models with Higgs doublets. These doubly-charged scalars couple to massive vector boson pairs at tree-level and open up the possibility that the SM-like Higgs boson's couplings to WW and ZZ could be larger than that in the SM [34, 41]. The vacuum expectation values (VEVs) of these triplets gets constrained from the SM-like Higgs signal strength data and, therefore, affects the mass spectra of heavier Higgs bosons in the model. Additionally, the presence of doubly-charged Higgs in triplet models leads to phenomenologically interesting signatures in the colliders. For example, this doubly-charged Higgs boson can decay into a pair of same-sign W bosons and hence provides further constraints on triplet VEV [51–54]. Furthermore, B -physics and electroweak precision observables (EWPO) put indirect constraints [30, 55–57] on the extended scalar sector of the beyond SM (BSM). Among the EWPO, the ρ parameter, defined as,

$$\rho = \frac{M_W^2}{M_Z^2 \cos^2 \theta_W},$$

where θ_W is the weak-mixing angle, plays a significant role in constraining the structure and parameters in BSM models. Global fit analyses [58] suggest that,

$$\rho = 1.00038 \pm 0.00020.$$

Minimal triplet scalar extension of the SM needs one complex triplet scalar and one real triplet scalar under $SU(2)_L$ with hypercharge, $Y = 1$ and $Y = 0$, respectively, such that the ρ parameter at the tree-level remains unity, owing to the consequence of an approximate global $SU(2)$ symmetry called custodial symmetry (CS). One such extension is the Georgi-Machacek (GM) model [22, 23], which preserves the CS as in the SM due to the explicit global $SU(2)_L \otimes SU(2)_R$ symmetry on the scalar potential at the tree-level. However, it is possible to construct a triplet extended scalar sector of the SM without requiring the global $SU(2)_L \otimes SU(2)_R$ symmetry in the potential while the custodial symmetry remains intact at the tree-level. This is dubbed as the extended GM (eGM) model, as mentioned in [59]. Unlike the GM model, the masses of scalar particles within each CS multiplet are no longer degenerate in the eGM model, and therefore, the eGM model has a much richer collider prospect.

Prior to the SM Higgs discovery, perturbative unitarity bounds were used to place an upper limit on the SM Higgs boson mass [60–73]. Dicus and Mathur [60], and Lee, Quigg, and Thacker [61, 62] established an upper limit of SM quartic coupling, $\lambda \leq 8\pi/3$, demanding the unitarity of $2 \rightarrow 2$ partial-wave scattering amplitudes. A number of authors extended this work to one-loop level and derived an upper bound on the running coupling, $\lambda \lesssim 2–2.5$, in a weakly interacting SM Higgs scenario [63, 65, 67–71]. A similar methodology was used to test the reliability of the perturbative calculations at the two-loop level and showed that an increase of one order in perturbation theory does not revise the above-stated limit on the running coupling λ [72, 73]. Therefore, perturbative unitarity delineates the region in which

perturbative calculations can be trusted, as performed in most phenomenological studies. Perturbative unitarity constraints have been used to bound large quartic couplings as well as exotic Higgs masses in the two-Higgs doublet model (2HDM) with a softly broken Z_2 symmetry [74, 75]. Clearly, it is imperative to study the constraints arising from perturbative unitarity of $2 \rightarrow 2$ partial-wave scattering amplitudes in a weakly interacting Higgs sector of GM and eGM models. Few authors have studied the tree-level perturbative unitarity bounds on the quartic couplings in the GM model [28, 38, 76]. In this work, we compute, for the first time, one-loop corrections to all the $2 \rightarrow 2$ Higgs boson and longitudinal vector boson scattering amplitudes in the GM and the eGM models. Specifically, we consider ϕ^4 -like interactions which are enhanced, $\mathcal{O}(\lambda_i \lambda_j / 16\pi^2)$, in the limit $s \gg |\lambda_i|v^2 \gg M_W^2$, $s \gg |\mu_i|v$. We further derive the 3-field bounded-from-below (BFB) conditions on the scalar quartic couplings of the GM and the eGM models. We show that the allowed parameter space coming from BFB conditions due to all possible combinations of 3-field directions and BFB conditions for all 13-field directions [28, 77] share large overlapping regions for both the GM and eGM models. Hence, the 3-field BFB conditions are a very good approximation of the full 13-field BFB conditions [28, 77] in both the GM and eGM models.

Our aim in this paper is to highlight the importance of theoretical constraints on the global fit. The question we ask is: which regions of the parameter space are allowed from the global fit to the latest Run 2 LHC data on the Higgs signal strengths with the improved theoretical constraints, such as next-to-leading order (NLO) unitarity, 3-field BFB constraints. The global fit results establish that the allowed parameter space of the eGM model gets significantly constrained once we impose perturbative NLO unitarity and BFB conditions. Furthermore, we revisit the GM model [22] and assess its status given these improved theoretical and updated experimental constraints. Similar global fits were previously performed on the GM model with tree-level unitarity bounds in [32, 36]. Our analysis shows that a large part of the parameter space in the GM model is disfavored by NLO unitarity bounds, which were otherwise viable from the tree-level unitarity bounds. These enhanced theoretical bounds will guide theorists and experimentalists in the search for new physics at present and upcoming collider experiments. Also, the inclusion of the latest Run 2 LHC data notably refines the upper limit of the triplet VEV.

The structure of this paper is as follows: The model is defined in Section II. Bounded-from-below conditions and NLO unitarity constraints are discussed in Section III and Section IV, respectively. We explain our global fit set-up in Section V and list all relevant constraints in Section VI. The results from the global fits are presented in Section VII. We conclude in Section VIII. Explicit expressions of quartic couplings in terms of the physical Higgs masses are given in Appendix A. Our results for the BFB conditions are provided in Appendices B and C, respectively, while Appendix D contains the results for the one-loop scattering amplitudes. Finally, Appendix E includes the one-loop and two-loop renormalization group equations (RGEs), and the supplementary figures are placed in Appendix F.

II. MODEL

We have extended the scalar sector of the SM, augmented by a real triplet ξ with hypercharge $Y = 0$, and a complex triplet χ with $Y = 1$. The most general $SU(2)_L \otimes U(1)_Y$ invariant

scalar potential reads [59],

$$\begin{aligned}
V = & -m_\phi^2(\phi^\dagger\phi) - m_\xi^2(\xi^\dagger\xi) - m_\chi^2(\chi^\dagger\chi) + \mu_1(\chi^\dagger t_a \chi) \xi_a + \mu_2(\phi^\dagger \tau_a \phi) \xi_a \\
& + \mu_3 \left[(\phi^T \epsilon \tau_a \phi) \tilde{\chi}_a + \text{h.c.} \right] + \lambda_\phi (\phi^\dagger \phi)^2 + \lambda_\xi (\xi^\dagger \xi)^2 + \lambda_\chi (\chi^\dagger \chi)^2 \\
& + \tilde{\lambda}_\chi |\tilde{\chi}^\dagger \chi|^2 + \lambda_{\phi\xi} (\phi^\dagger \phi) (\xi^\dagger \xi) + \lambda_{\phi\chi} (\phi^\dagger \phi) (\chi^\dagger \chi) + \lambda_{\chi\xi} (\chi^\dagger \chi) (\xi^\dagger \xi) \\
& + \kappa_1 |\xi^\dagger \chi|^2 + \kappa_2 (\phi^\dagger \tau_a \phi) (\chi^\dagger t_a \chi) + \kappa_3 \left[(\phi^T \epsilon \tau_a \phi) (\chi^\dagger t_a \xi) + \text{h.c.} \right], \quad (1)
\end{aligned}$$

where $\phi = (\phi^+ \ \phi^0)^T$ is the SM Higgs doublet with $Y = 1/2$, $\xi = (\xi^+ \ \xi^0 \ - \xi^{++})^T$, and $\chi = (\chi^{++} \ \chi^+ \ \chi^0)^T$. The charge conjugate of the complex triplet is defined as $\tilde{\chi} = (\chi^{0*} \ - \chi^{+*} \ \chi^{++*})^T$. Note that τ_a and t_a are the 2-dimensional and 3-dimensional representations of the $SU(2)$ generators, respectively, written in the spherical basis and, in general, are not hermitian. All the model parameters are taken to be real to avoid explicit CP violation. We refer Eq. (1) as the scalar potential of the ‘generalized two-triplet model’ in our paper.

After the EWSB, we redefine the neutral components of the fields as,

$$\phi^0 = \frac{v_\phi}{\sqrt{2}} + \frac{1}{\sqrt{2}} (\phi' + i\phi'') , \quad \chi^0 = v_\chi + \frac{1}{\sqrt{2}} (\chi' + i\chi'') , \quad \xi^0 = v_\xi + \xi' , \quad (2)$$

where v_ϕ and v_ξ (v_χ) are the VEVs of the SM Higgs doublet and real (complex) triplet, respectively. All the VEVs are taken to be real in order to avoid spontaneous CP violation.

Given the VEV structure in Eq. (2), one can derive the following expression for the ρ parameter at the tree-level,

$$\rho = \frac{v_\phi^2 + 4(v_\xi^2 + v_\chi^2)}{v_\phi^2 + 8v_\chi^2} , \quad \text{with} \quad v_\phi^2 + 4(v_\chi^2 + v_\xi^2) = v^2 \approx (246 \text{ GeV})^2 .$$

At the tree-level, $\rho = 1$ requires, $v_\chi = v_\xi$. We ensure $\rho = 1$ remains intact at the tree-level by putting $v_\chi = v_\xi$ and imposing the following condition [59],

$$\left. \frac{\partial V}{\partial \chi} \right|_{\substack{\phi^0 = v_\phi, \chi^0 = v_\chi, \\ \xi^0 = v_\xi, v_\chi = v_\xi}} = \left. \frac{\partial V}{\partial \xi} \right|_{\substack{\phi^0 = v_\phi, \chi^0 = v_\chi, \\ \xi^0 = v_\xi, v_\chi = v_\xi}} . \quad (3)$$

As a consequence, four constraints are being imposed on the model parameters [59],

$$m_\chi^2 = 2m_\xi^2 , \quad \mu_2 = \sqrt{2}\mu_3 , \quad \lambda_{\chi\xi} = 2\lambda_\chi - 4\lambda_\xi , \quad \kappa_2 = 4\lambda_{\phi\xi} - 2\lambda_{\phi\chi} + \sqrt{2}\kappa_3 . \quad (4)$$

This choice gives rise to a triplet scalar extension of the SM, preserving custodial symmetry at the tree-level. Following [59], we refer to this choice as the extended Georgi-Machacek (eGM) model.¹ One should keep in mind that this is not an extension of the well-known Georgi-Machacek model [22]. In the eGM model, the Goldstone bosons (G^+, G^0) show up in the longitudinal mode of massive W^+ and Z^0 gauge bosons, and the following mass

¹ The Yukawa interactions between the lepton doublets and the Higgs triplets are not being considered, since we have assumed v_χ to be $\mathcal{O}(1)$ in our analysis [26].

eigenstates emerge: three CP-even eigenstates (F^0, H, h), one CP-odd eigenstate (A), two singly-charged scalars (F^+, H^+), and one doubly-charged scalar (F^{++}). The mixings among the states in the eGM model are given below,

$$F^{++} = \chi^{++}, \quad \begin{bmatrix} G^0 \\ A \end{bmatrix} = \begin{bmatrix} c_\beta & s_\beta \\ -s_\beta & c_\beta \end{bmatrix} \begin{bmatrix} \phi'' \\ \chi'' \end{bmatrix}, \quad \begin{bmatrix} h \\ H \\ F^0 \end{bmatrix} = R_\alpha^{-1} R_0 \begin{bmatrix} \phi' \\ \xi' \\ \chi' \end{bmatrix}, \quad \begin{bmatrix} G^+ \\ H^+ \\ F^+ \end{bmatrix} = R_\delta^{-1} R_\beta R_+ \begin{bmatrix} \phi^+ \\ \xi^+ \\ \chi^+ \end{bmatrix}.$$

The form of the rotation matrices R_i ($i = \alpha, \beta, \delta, 0, +$) are as follows,

$$R_{\alpha(\beta)} = \begin{bmatrix} c_{\alpha(\beta)} & s_{\alpha(\beta)} & 0 \\ -s_{\alpha(\beta)} & c_{\alpha(\beta)} & 0 \\ 0 & 0 & 1 \end{bmatrix}, \quad R_\delta = \begin{bmatrix} 1 & 0 & 0 \\ 0 & c_\delta & s_\delta \\ 0 & -s_\delta & c_\delta \end{bmatrix}, \quad R_0 = \begin{bmatrix} 1 & 0 & 0 \\ 0 & \frac{1}{\sqrt{3}} & \sqrt{\frac{2}{3}} \\ 0 & -\sqrt{\frac{2}{3}} & \frac{1}{\sqrt{3}} \end{bmatrix}, \quad R_+ = \begin{bmatrix} 1 & 0 & 0 \\ 0 & \frac{1}{\sqrt{2}} & \frac{1}{\sqrt{2}} \\ 0 & -\frac{1}{\sqrt{2}} & \frac{1}{\sqrt{2}} \end{bmatrix},$$

with $\tan \beta = 2\sqrt{2}v_\chi/v_\phi$, where c_θ and s_θ stand for $\cos \theta$ and $\sin \theta$, respectively. The mass-squared eigenvalues of the CP-even sector can be written as,

$$\begin{aligned} m_h^2 &= (\mathcal{M}_n^2)_{11} c_\alpha^2 + (\mathcal{M}_n^2)_{22} s_\alpha^2 - 2 (\mathcal{M}_n^2)_{12} s_\alpha c_\alpha, \\ m_H^2 &= (\mathcal{M}_n^2)_{11} s_\alpha^2 + (\mathcal{M}_n^2)_{22} c_\alpha^2 + 2 (\mathcal{M}_n^2)_{12} s_\alpha c_\alpha, \\ m_{F^0}^2 &= \frac{1}{2} v^2 s_\beta^2 (4\lambda_\xi - \lambda_\chi) - \frac{3}{2\sqrt{2}} v^2 c_\beta^2 \kappa_3 + \frac{1}{\sqrt{2}} c_\beta^2 s_\beta^{-1} \mu_2 v + \frac{1}{\sqrt{2}} s_\beta \mu_1 v, \end{aligned} \quad (5)$$

where

$$\tan 2\alpha = \frac{2 (\mathcal{M}_n^2)_{12}}{(\mathcal{M}_n^2)_{22} - (\mathcal{M}_n^2)_{11}}, \quad \text{with } \alpha \in \left[-\frac{\pi}{2}, \frac{\pi}{2} \right]. \quad (6)$$

\mathcal{M}_n^2 is the mass-squared matrix in the basis $\{\phi', \frac{\xi' + \sqrt{2}\chi'}{\sqrt{3}}\}$, whose elements are given below,

$$\begin{aligned} (\mathcal{M}_n^2)_{11} &= 2v^2 c_\beta^2 \lambda_\phi, \\ (\mathcal{M}_n^2)_{12} &= \frac{\sqrt{3}}{2} v^2 s_\beta c_\beta \kappa_3 + \sqrt{\frac{3}{2}} v^2 s_\beta c_\beta \lambda_{\phi\xi} - \frac{\sqrt{3}}{2} c_\beta \mu_2 v, \\ (\mathcal{M}_n^2)_{22} &= v^2 s_\beta^2 (\lambda_\chi - \lambda_\xi) - \frac{1}{2\sqrt{2}} s_\beta \mu_1 v + \frac{1}{\sqrt{2}} c_\beta^2 s_\beta^{-1} \mu_2 v. \end{aligned}$$

The CP-odd neutral scalar (A) and the doubly-charged scalar (F^{++}) mass-squared eigenvalues are as follows,

$$\begin{aligned} m_A^2 &= \frac{1}{\sqrt{2}} s_\beta^{-1} \mu_2 v - \frac{1}{2\sqrt{2}} v^2 \kappa_3, \\ m_{F^{++}}^2 &= -\frac{1}{2\sqrt{2}} v^2 c_\beta^2 (\sqrt{2}\kappa_2 + \kappa_3) + \frac{1}{2} v^2 s_\beta^2 \tilde{\lambda}_\chi + \frac{1}{\sqrt{2}} c_\beta^2 s_\beta^{-1} \mu_2 v + \frac{1}{\sqrt{2}} s_\beta \mu_1 v. \end{aligned} \quad (7)$$

The singly-charged mass-squared eigenvalues are given by,

$$\begin{aligned} m_{H^+}^2 &= (\mathcal{M}_c^2)_{11} c_\delta^2 + (\mathcal{M}_c^2)_{22} s_\delta^2 - 2 (\mathcal{M}_c^2)_{12} s_\delta c_\delta, \\ m_{F^+}^2 &= (\mathcal{M}_c^2)_{11} s_\delta^2 + (\mathcal{M}_c^2)_{22} c_\delta^2 + 2 (\mathcal{M}_c^2)_{12} s_\delta c_\delta, \end{aligned} \quad (8)$$

where

$$\tan 2\delta = \frac{2 (\mathcal{M}_c^2)_{12}}{(\mathcal{M}_c^2)_{22} - (\mathcal{M}_c^2)_{11}}, \quad \text{with} \quad \delta \in \left[-\frac{\pi}{2}, \frac{\pi}{2} \right]. \quad (9)$$

\mathcal{M}_c^2 is the mass-squared matrix in the basis $\{-s_\beta\phi^+ + c_\beta\frac{\xi^+ + \chi^+}{\sqrt{2}}, \frac{-\xi^+ + \chi^+}{\sqrt{2}}\}$, with the matrix elements,

$$\begin{aligned} (\mathcal{M}_c^2)_{11} &= -\frac{1}{8}v^2 \left(\kappa_2 + \sqrt{2}\kappa_3 \right) + \frac{1}{\sqrt{2}}s_\beta^{-1}\mu_2 v, \\ (\mathcal{M}_c^2)_{12} &= -\frac{1}{8}v^2 c_\beta \left(\kappa_2 - \sqrt{2}\kappa_3 \right), \\ (\mathcal{M}_c^2)_{22} &= -\frac{1}{8}v^2 c_\beta^2 \left(\kappa_2 + 5\sqrt{2}\kappa_3 \right) + \frac{1}{4}v^2 s_\beta^2 \kappa_1 + \frac{1}{\sqrt{2}}c_\beta^2 s_\beta^{-1}\mu_2 v + \frac{1}{\sqrt{2}}s_\beta \mu_1 v. \end{aligned}$$

In our analysis, we trade the mixing angle (δ) between the singly charged Higgs bosons with the heavy Higgs boson mass, m_A , and as a result, we get the following relation,

$$m_A^2 = m_{H^+}^2 c_\delta^2 + m_{F^+}^2 s_\delta^2 - (m_{F^+}^2 - m_{H^+}^2) c_\beta^{-1} s_\delta c_\delta. \quad (10)$$

From Eq. (10), it can be easily seen that m_A and m_{H^+} are mass degenerate in the limit $\delta = 0$. In the eGM model, the absolute mass difference between $m_{F^{++}}$ and m_{F^0} , obtained from Eq. (7) and Eq. (5), is independent of the trilinear couplings, μ_1 and μ_2 . All other mass differences of physical scalars depend on both the quartic and trilinear parameters of the potential.

Georgi and Machacek constructed a global $SU(2)_L \otimes SU(2)_R$ symmetric potential [22] by adding a bi-doublet Φ and a bi-triplet Δ scalars to the SM potential, where

$$\Phi = \begin{pmatrix} \phi^{0*} & \phi^+ \\ -\phi^- & \phi^0 \end{pmatrix}, \quad \Delta = \begin{pmatrix} \chi^{0*} & \xi^+ & \chi^{++} \\ -\chi^- & \xi^0 & \chi^+ \\ \chi^{--} & -\xi^- & \chi^0 \end{pmatrix}. \quad (11)$$

The GM potential conserves $\rho = 1$ by construction and is written, in the conventions of Ref. [31], as

$$\begin{aligned} V(\Phi, \Delta) &= \frac{1}{2}m_1^2 \text{Tr}[\Phi^\dagger \Phi] + \frac{1}{2}m_2^2 \text{Tr}[\Delta^\dagger \Delta] + \lambda_1 (\text{Tr}[\Phi^\dagger \Phi])^2 + \lambda_2 (\text{Tr}[\Delta^\dagger \Delta])^2 \\ &\quad + \lambda_3 \text{Tr}[(\Delta^\dagger \Delta)^2] + \lambda_4 \text{Tr}[\Phi^\dagger \Phi] \text{Tr}[\Delta^\dagger \Delta] + \lambda_5 \text{Tr}[\Phi^\dagger \tau^a \Phi \tau^b] \text{Tr}[\Delta^\dagger t^a \Delta t^b] \\ &\quad + \mu_1 \text{Tr}[\Phi^\dagger \tau^a \Phi \tau^b] (P^\dagger \Delta P)_{ab} + \mu_2 \text{Tr}[\Delta^\dagger t^a \Delta t^b] (P^\dagger \Delta P)_{ab}. \end{aligned} \quad (12)$$

Here τ^a 's and t^a 's are the $SU(2)$ generators for the doublet and triplet representations, respectively, and the matrix P diagonalizes the adjoint representation of the $SU(2)$ generator [31]. Similar to the eGM model, the GM model also has one doubly charged, two singly charged, and four neutral scalars, one of them being the SM-like Higgs boson. They form one fiveplet, one triplet, and two singlets by their transformation properties under the custodial $SU(2)$ symmetry. In the GM model, the physical scalars in each custodial multiplet are mass degenerate. The field structures and the masses of the physical scalars of the GM model are given in Ref. [31].

III. BOUNDEDNESS OF THE SCALAR POTENTIAL

For a given theory, one of the constraints is to ensure that the scalar potential must be bounded from below in any direction of the field space. Various methodologies are extensively used in the literature to study the vacuum stability of the extended scalar potentials such as copositivity [78–80], geometric approaches [81–86], and other mathematical techniques [87–89]. However, it is mathematically challenging to compute the necessary and sufficient bounded-from-below (BFB) conditions for the general quartic potential with multiple scalar fields. The BFB conditions, taking into account all combinations of two non-zero scalar fields, were derived in [26] for the GM model and in [90] and [91] for the generalized two-triplet model. Ref. [92] provides necessary and sufficient conditions on the couplings of the Type II Seesaw model that are valid for all field directions. The BFB conditions considering all field directions has been studied in [28] and [77] for the GM model, while [77] also computed the all field BFB conditions for the generalized two-triplet model. The necessary and sufficient bounded-from-below conditions for a generic quartic scalar potential of a large number of fields cannot always be recast into a fully analytical compact form as pointed out in [77]. In this section, we compute the strict copositivity criteria at the tree-level, taking into account all combinations of three non-zero scalar fields for the GM, the eGM, and the generalized two-triplet model. Following the strategy of reparameterizing the field space as given in [77, 85, 92], we also derive all field BFB conditions for the eGM model at the tree-level.

At large values of the fields, there should not exist any field direction that renders the potential to be unbounded from below. Strict positivity condition on the quartic part of the potential, given in Eq. (1), has to be imposed to avoid such unboundedness, i.e.,

$$V^{(4)} \equiv \lambda_\phi(\phi^\dagger\phi)^2 + \lambda_\xi(\xi^\dagger\xi)^2 + \lambda_\chi(\chi^\dagger\chi)^2 + \tilde{\lambda}_\chi|\tilde{\chi}^\dagger\chi|^2 + \lambda_{\phi\xi}(\phi^\dagger\phi)(\xi^\dagger\xi) + \lambda_{\phi\chi}(\phi^\dagger\phi)(\chi^\dagger\chi) + \lambda_{\chi\xi}(\chi^\dagger\chi)(\xi^\dagger\xi) + \kappa_1|\xi^\dagger\chi|^2 + \kappa_2(\phi^\dagger\tau_a\phi)(\chi^\dagger t_a\chi) + \kappa_3[(\phi^T\epsilon\tau_a\phi)(\chi^\dagger t_a\xi) + \text{h.c.}] > 0. \quad (13)$$

To compute the BFB conditions on the quartic parameters, we impose strict copositivity criteria for the potential of a specific direction in the field space. Taking into account all such directions with only two non-vanishing fields at once, we obtain the following BFB conditions for the eGM model,

$$\begin{aligned} \lambda_\phi > 0, \quad \lambda_\chi > 0, \quad 4\lambda_\chi - 8\lambda_\xi + \kappa_1 + 4\sqrt{\lambda_\xi\lambda_\chi} > 0, \\ \lambda_{\phi\xi} + 2\sqrt{\lambda_\phi\lambda_\xi} > 0, \quad \lambda_\xi > 0, \quad 2\lambda_\chi - 4\lambda_\xi + 2\sqrt{\lambda_\xi(\lambda_\chi + \tilde{\lambda}_\chi)} > 0, \\ \lambda_{\phi\chi} + 2\sqrt{\lambda_\phi(\lambda_\chi + \tilde{\lambda}_\chi)} > 0, \quad \lambda_\chi - \lambda_\xi > 0, \quad 4\lambda_{\phi\chi} - 4\lambda_{\phi\xi} - \sqrt{2}\kappa_3 + 4\sqrt{\lambda_\phi\lambda_\chi} > 0, \\ 4\lambda_{\phi\xi} + \sqrt{2}\kappa_3 + 4\sqrt{\lambda_\phi\lambda_\chi} > 0, \quad \lambda_\chi + \tilde{\lambda}_\chi > 0, \quad 2\lambda_\chi - 4\lambda_\xi + \kappa_1 + 2\sqrt{\lambda_\xi(\lambda_\chi + \tilde{\lambda}_\chi)} > 0. \end{aligned} \quad (14)$$

The quartic parameters get further constrained once we consider three or more simultaneously non-vanishing field directions in the field space. For instance, if we consider the field directions where only the neutral components of the fields ϕ^0, ξ^0 , and, χ^0 are non-zero, we

get the following BFB conditions for the eGM model,

$$6\lambda_{\phi\xi} + 3\sqrt{2}\kappa_3 + 4\sqrt{3\lambda_\phi(\lambda_\chi - \lambda_\xi)} > 0, \quad 6\lambda_{\phi\xi} - \sqrt{2}\kappa_3 + 4\sqrt{3\lambda_\phi(\lambda_\chi - \lambda_\xi)} > 0. \quad (15)$$

The methodology for obtaining the above conditions is discussed in depth in Appendix B, where we have also computed the BFB conditions taking into account all such combinations with three simultaneously non-vanishing fields for the eGM model and for the generalized two-triplet model. The BFB conditions with all non-zero field directions are given in Appendix C for the eGM model.

We obtain the minimal set of BFB conditions considering all possible two non-vanishing field directions for the GM model,

$$\begin{aligned} \lambda_1 > 0, \quad & \lambda_2 + \lambda_3 > 0, \quad & \lambda_4 + 2\sqrt{\lambda_1(\lambda_2 + \lambda_3)} > 0, \\ 3\lambda_2 + \lambda_3 > 0, \quad & 4\lambda_4 - |\lambda_5| + 4\sqrt{2\lambda_1(2\lambda_2 + \lambda_3)} > 0. \end{aligned} \quad (16)$$

The above results agree except for the fourth condition involving λ_4 in Eq. (3.3) of Ref. [26]. Along with that, we get a more stringent BFB constraint, $3\lambda_2 + \lambda_3 > 0$, from the two field directions where ξ^0 and χ^{++} (χ^0) are considered to be non-zero. If we consider the combination where only neutral components of the fields ϕ^0 , ξ^0 , and, χ^0 are non-zero, we get these additional BFB conditions on top of the conditions given in Eq. (16),

$$\lambda_4 + \frac{1}{2}\lambda_5 + 2\sqrt{\lambda_1\left(\lambda_2 + \frac{1}{3}\lambda_3\right)} > 0, \quad \lambda_4 - \frac{1}{6}\lambda_5 + 2\sqrt{\lambda_1\left(\lambda_2 + \frac{1}{3}\lambda_3\right)} > 0. \quad (17)$$

In Appendix B, we have listed down the BFB conditions by taking into account all such combinations with three simultaneously non-vanishing fields for the GM model. In our numerical analysis in Section VII, we will compare the BFB constraints for two, three, and all thirteen non-vanishing field directions for both models.

IV. UNITARITY CONSTRAINTS AT ONE-LOOP

A. Partial-wave analysis

In this section, we aim to study the unitarity bounds on the quartic parameters of Eq. (1). Perturbative unitarity constraints come from demanding the unitarity of the S -matrix, which reads as,

$$\left|a_\ell^{2 \rightarrow 2} - \frac{1}{2}i\right|^2 + \sum_{k>2} \left|a_\ell^{2 \rightarrow k}\right|^2 = \frac{1}{4}. \quad (18)$$

Here, $a_\ell^{2 \rightarrow k}$'s are the eigenvalues of the S -matrix consisting of ℓ -th partial-wave amplitudes of $2 \rightarrow k$ scattering.² In the limit, $s \gg |\lambda_i|v^2$, $s \gg |\mu_i|v$, $2 \rightarrow 3$ partial-wave amplitudes can be neglected since $|a_\ell^{2 \rightarrow 3}|^2 \sim \lambda_i^4 v^2/s$, where μ_i (λ_i)'s represent some linear combinations of

² Note that, for $k > 2$, the scattering matrix is diagonalized in the eigenbasis of the $2 \rightarrow 2$ scattering matrix.

scalar cubic (quartic) couplings of the theory. The next leading order contribution comes from $2 \rightarrow 4$ scattering amplitudes, which scale as $|a_\ell^{2 \rightarrow 4}|^2 \sim \lambda_i^4$. In the SM, the $2 \rightarrow 4$ amplitudes are significantly smaller compared to the $2 \rightarrow 2$ partial-wave amplitudes because of the smallness of the quartic coupling [93]. Therefore, in our analysis, only the $2 \rightarrow 2$ amplitudes will be taken into account. In the rest of the paper, we remove the superscript $2 \rightarrow 2$ from partial-wave amplitudes. Under this consideration, Eq. (18) gives an upper limit on the eigenvalues of the S -matrix,

$$\left| a_\ell - \frac{1}{2}i \right|^2 \leq \frac{1}{4}. \quad (19)$$

At the tree-level, each of the eigenvalues, $a_\ell \in \mathbb{R}$, leads to a strong bound, $|\text{Re}(a_\ell)| \leq 1/2$. At one-loop and beyond, $a_\ell \notin \mathbb{R}$, thus the above-stated limit gets weaker when we calculate the one-loop and the higher order corrections to the S -matrix. Note that the unitarity bounds over the real line are employed in the tree-level analysis, and the complete unitarity circle in the complex plane is utilized once the loop corrections are incorporated into the unitarity calculations. In the limit, $s \gg |\lambda_i|v^2 \gg M_W^2$, $s \gg |\mu_i|v$ the most dominant contribution comes from the $\ell = 0$ partial-wave at the tree-level. Therefore, we will only consider $\ell = 0$ in our analysis. To calculate the partial-wave amplitude (a_0) at one-loop level, we adopt the approach of Ref. [74]. For a given process $i \rightarrow f$, the corresponding matrix element is

$$(a_0)_{i,f}(s) = \frac{1}{16\pi s} \int_{-s}^0 dt \mathcal{M}_{i \rightarrow f}(s, t),$$

where $\mathcal{M}_{i \rightarrow f}$ represents the sum of all possible scattering amplitudes with an initial state i and final state f . As the $SU(2)_L \otimes U(1)_Y$ symmetry is intact at high energies, the S -matrix can be sub-divided into smaller block diagonal forms consisting of two-particle states with their respective total charge (Q) and hypercharge (Y). Following this prescription, the basis states are written in Table I. We have included $1/\sqrt{2}$ symmetry factor in the identical initial or final states. However, this block diagonal structure does not hold beyond the tree-level due to hypercharge interactions. At the one-loop level, in general, the off-block diagonal elements are non-zero due to the wave function renormalization terms. For a given scattering process with total charge Q , if the tree-level blocks have unique eigenvalues, then off-block diagonal elements do not contribute to the tree-level eigenvalues at the one-loop, while the contributions can appear at the two-loop and beyond.

B. $2 \rightarrow 2$ scattering amplitudes

Goldstone-boson equivalence theorem is a useful theoretical tool to study scattering amplitudes in high energy regime [62, 94, 95]. This theorem states that, at energies, $\sqrt{s} \gg M_W$, an amplitude involving k longitudinally polarized vector bosons (W_L^\pm, Z_L, h, \dots) at the external states can be related to an amplitude with k external Goldstone bosons (w^\pm, z, h, \dots) as,

$$\mathcal{M}(W_L^\pm, Z_L, h, \dots) = (iC)^k \mathcal{M}(w^\pm, z, h, \dots).$$

| $Y \backslash Q$ | 0 | 1/2 | 1 | 3/2 | 2 |
|------------------|---|---|--|---|---|
| 0 | $\phi^{0*}\phi^0$ $\phi^+\phi^-$ $\chi^{++}\chi^{--}$ | $\frac{\xi^0\xi^0}{\sqrt{2}}$ $\xi^+\xi^-$ | $\chi^{0*}\chi^0$ $\chi^+\chi^-$ | $\phi^0\xi^0$ $\phi^+\xi^-$ | $\phi^{0*}\chi^0$ $\chi^+\phi^-$ |
| | | | | $\frac{\phi^0\phi^0}{\sqrt{2}}$ | $\chi^0\xi^0$ $\chi^+\xi^-$ |
| | | | | | $\phi^0\chi^0$ $\frac{\chi^0\chi^0}{\sqrt{2}}$ |
| 1 | $\phi^{0*}\phi^+$ $\chi^-\chi^{++}$ | $\xi^0\xi^+$ $\phi^+\xi^0$ | $\chi^{0*}\chi^+$ $\chi^{++}\phi^-$ | $\phi^0\xi^+$ $\phi^+\xi^0$ | $\phi^{0*}\chi^+$ $\chi^{++}\xi^-$ |
| | | | | $\phi^0\phi^+$ $\chi^0\xi^+$ | $\xi^0\chi^+$ $\phi^+\chi^0$ |
| 2 | $\frac{\xi^+\xi^+}{\sqrt{2}}$ | $\chi^{0*}\chi^{++}$ | $\phi^+\xi^+$ $\phi^{0*}\chi^{++}$ | $\frac{\phi^+\phi^+}{\sqrt{2}}$ $\xi^0\chi^{++}$ | $\xi^+\chi^+$ $\phi^+\chi^{++}$ |
| 3 | \times | \times | | $\xi^+\chi^{++}$ | $\phi^+\chi^{++}$ |
| 4 | \times | \times | \times | \times | $\frac{\chi^{++}\chi^{++}}{\sqrt{2}}$ |

TABLE I. Two-particle basis states broken down by their total charge Q and total hypercharge Y . We have omitted the charge conjugated states as they give the same eigenvalues. The blocks with total weak isospin $|T_3| = 0, 1/2, 1, 3/2, 2$ are shown in green, lime green, olive, yellow, and brown, respectively.

In the limit, $s \gg |\lambda_i|v^2 \gg M_W^2$, $s \gg |\mu_i|v$, only one-particle irreducible (1PI) diagrams with two internal lines survive at the one-loop.³ We choose $\overline{\text{MS}}$ scheme to renormalize the quartic couplings in the one-loop computation to satisfy the Goldstone theorem with $C = 1$ [95].

The renormalized parameter (λ) can be defined in terms of the bare parameter (λ^0) as,

$$\lambda_i^0 = \lambda_i + \delta\lambda_i, \quad \kappa_i^0 = \kappa_i + \delta\kappa_i.$$

Following the convention given in [74], the counterterms for a given parameter λ can be written as,

$$\delta\lambda = \frac{1}{16\pi^2\epsilon}\beta_\lambda, \quad \text{with} \quad \beta_\lambda = 16\pi^2\mu^2 \frac{d\lambda}{d\mu^2}, \quad (20)$$

where μ is the renormalization scale. We have verified from our calculations that the counter-terms required in order to cancel the infinities in the one-loop S -matrix are nothing but the

³ We have chosen this energy regime to simplify our computations. These conditions are examined uniformly throughout the energy regime of interest [65, 96].

beta functions given in the literature [97, 98],⁴

$$\begin{aligned}
\beta_{\lambda_\phi} &= 12\lambda_\phi^2 + 3\lambda_{\phi\xi}^2 + \frac{1}{4}\kappa_2^2 + \kappa_3^2 + \frac{3}{2}\lambda_{\phi\chi}^2, \\
\beta_{\lambda_\xi} &= 44\lambda_\xi^2 + \kappa_1\lambda_{\chi\xi} + \frac{1}{2}\kappa_1^2 + \frac{3}{2}\lambda_{\chi\xi}^2 + \lambda_{\phi\xi}^2, \\
\beta_{\lambda_\chi} &= 8\tilde{\lambda}_\chi \left(\tilde{\lambda}_\chi + \lambda_\chi \right) + 2\kappa_1\lambda_{\chi\xi} + \frac{1}{2}\kappa_1^2 + \frac{1}{4}\kappa_2^2 + 14\lambda_\chi^2 + 3\lambda_{\chi\xi}^2 + \lambda_{\phi\chi}^2, \\
\beta_{\tilde{\lambda}_\chi} &= 6\tilde{\lambda}_\chi \left(\tilde{\lambda}_\chi + 2\lambda_\chi \right) + \frac{1}{2}\kappa_1^2 - \frac{1}{4}\kappa_2^2, \\
\beta_{\kappa_1} &= \kappa_1 \left(4\tilde{\lambda}_\chi + 5\kappa_1 + 8\lambda_\xi + 2\lambda_\chi + 8\lambda_{\chi\xi} \right) - \kappa_3^2, \\
\beta_{\kappa_2} &= 2\kappa_2 \left(\lambda_\chi - 2\tilde{\lambda}_\chi + \lambda_\phi + 2\lambda_{\phi\chi} \right) + 2\kappa_3^2, \\
\beta_{\kappa_3} &= \kappa_3 \left(\kappa_2 - \kappa_1 \right) + 2\kappa_3 \left(\lambda_{\chi\xi} + \lambda_\phi + 2\lambda_{\phi\xi} + \lambda_{\phi\chi} \right), \\
\beta_{\lambda_{\phi\xi}} &= 2\lambda_{\phi\xi} \left(2\lambda_{\phi\xi} + 10\lambda_\xi + 3\lambda_\phi \right) + \lambda_{\phi\chi} \left(\kappa_1 + 3\lambda_{\chi\xi} \right) + 2\kappa_3^2, \\
\beta_{\lambda_{\phi\chi}} &= 2\lambda_{\phi\chi} \left(\lambda_{\phi\chi} + 2\tilde{\lambda}_\chi + 4\lambda_\chi + 3\lambda_\phi \right) + 2\lambda_{\phi\xi} \left(\kappa_1 + 3\lambda_{\chi\xi} \right) + 2\kappa_3^2 + \kappa_2^2, \\
\beta_{\lambda_{\chi\xi}} &= 4\lambda_{\chi\xi} \left(\tilde{\lambda}_\chi + 5\lambda_\xi + 2\lambda_\chi + \lambda_{\chi\xi} \right) + 2\kappa_1 \left(2\lambda_\xi + \lambda_\chi \right) + \kappa_1^2 + \kappa_3^2 + 2\lambda_{\phi\xi}\lambda_{\phi\chi}. \tag{21}
\end{aligned}$$

The complete set of one-loop and two-loop beta functions for the Yukawa, gauge, and quartic couplings in the theory are given in Appendix E. Up to symmetry factors, one-loop amplitude for a generic 1PI diagram involving four-point vertices is given by,

$$\mathcal{M}_{1\text{PI}}^{2\rightarrow 2} = \frac{\lambda_i\lambda_j}{16\pi^2} \left[\frac{1}{\epsilon} + 2 - \ln \left(\frac{-p^2 - i0_+}{\mu^2} \right) \right],$$

where the quartic couplings, λ_i and λ_j are evaluated at the energy scale, $\mu^2 = s$. For a given electric charge (Q) and hypercharge (Y), the S -matrix at the one-loop can be expressed as [74, 99],

$$256\pi^3 \mathbf{a}_0 = -16\pi^2 \mathbf{b}_0 + (i\pi - 1) \mathbf{b}_0 \cdot \mathbf{b}_0 + 3\beta_{\mathbf{b}_0}, \tag{22}$$

where \mathbf{b}_0 is the tree-level S -matrix and $\beta_{\mathbf{b}_0}$ represents the matrix carrying some linear combinations of the beta functions defined in Eq. (20). For example, if $b_0 = a\lambda_i + b\lambda_j$, then $\beta_{b_0} = a\beta_{\lambda_i} + b\beta_{\lambda_j}$, $\forall a, b \in \mathbb{R}$. Our results of the S -matrix elements at the one-loop are given in Appendix D. These results solely come from the 1PI one-loop corrections to the tree-level processes, and wave function corrections are ignored in the energy regime of interest [74, 99]. For the potential given in Eq. (1), we have found 16, 15, 11, 3, and 1 unique tree-level eigenvalues for the blocks with $Q = 0, 1, 2, 3, 4$, respectively. Out of these, a total of 19 eigenvalues appeared to be independent, which is in agreement with the results given

⁴ Note that, $\beta_{\text{Eq. (20)}} = \frac{1}{2}\beta_{\text{Ref. [97]}}$.

in the literature [38, 91],

$$\begin{aligned}
-16\pi a_{0;1} &= 2\lambda_{\chi\xi} + \kappa_1, \\
-16\pi a_{0;2}^\pm &= \lambda_\chi - 2\tilde{\lambda}_\chi + \lambda_\phi \pm \sqrt{\kappa_2^2 + \left(-\lambda_\chi + 2\tilde{\lambda}_\chi + \lambda_\phi\right)^2}, & -16\pi a_{0;3} &= \lambda_{\phi\chi} + \frac{\kappa_2}{2}, \\
-16\pi a_{0;4}^\pm &= 4\lambda_\xi + \lambda_\chi + 2\tilde{\lambda}_\chi \pm \sqrt{2\kappa_1^2 + \left(-4\lambda_\xi + \lambda_\chi + 2\tilde{\lambda}_\chi\right)^2}, & -16\pi a_{0;5} &= 2\lambda_{\chi\xi} + 4\kappa_1, \\
-16\pi a_{0;6}^\pm &= \lambda_{\phi\xi} + \frac{\lambda_{\phi\chi}}{2} - \frac{\kappa_2}{4} \pm \sqrt{\kappa_3^2 + \left(\frac{\kappa_2}{4} + \lambda_{\phi\xi} - \frac{\lambda_{\phi\chi}}{2}\right)^2}, & -16\pi a_{0;7} &= 2\lambda_\chi, \\
-16\pi a_{0;8}^\pm &= \lambda_{\phi\xi} + \frac{\lambda_{\phi\chi}}{2} + \frac{\kappa_2}{2} \pm \sqrt{4\kappa_3^2 + \left(\frac{\kappa_2}{2} - \lambda_{\phi\xi} + \frac{\lambda_{\phi\chi}}{2}\right)^2}, & -16\pi a_{0;9} &= \lambda_{\phi\chi} - \kappa_2, \\
-16\pi a_{0;10}^\pm &= \lambda_{\chi\xi} + \lambda_\phi - \frac{\kappa_1}{2} \pm \sqrt{2\kappa_3^2 + \left(\frac{\kappa_1}{2} - \lambda_{\chi\xi} + \lambda_\phi\right)^2}, & -16\pi a_{0;11} &= 2\lambda_\chi + 6\tilde{\lambda}_\chi,
\end{aligned}$$

and $-16\pi a_{0;i}$ ($i = 12, 13, 14$) being the eigenvalues of the following matrix,

$$\begin{bmatrix} 20\lambda_\xi & 2\sqrt{3}\lambda_{\phi\xi} & \sqrt{2}(\kappa_1 + 3\lambda_{\chi\xi}) \\ 2\sqrt{3}\lambda_{\phi\xi} & 6\lambda_\phi & \sqrt{6}\lambda_{\phi\chi} \\ \sqrt{2}(\kappa_1 + 3\lambda_{\chi\xi}) & \sqrt{6}\lambda_{\phi\chi} & 8\lambda_\chi + 4\tilde{\lambda}_\chi \end{bmatrix}. \quad (23)$$

The eigenvalues of the S -matrix at the tree-level can be found in Refs. [28, 76] for the scalar quartic couplings in the GM model.

V. HEPFIT

To constrain the parameters in the GM and the eGM models, we employ a Bayesian fit with Markov Chain Monte Carlo (MCMC) simulations. We use the open-source code **HEPfit** [100] to calculate various theoretical and experimental observables that depend on the model parameters and feed them into the parallelized **BAT** library [101] with Message Passing Interface (MPI). It offers to sample the parameter space and find out allowed regions with all sorts of constraints in a given new physics (NP) model. Approximately, each fit runs over 16 parallel chains, generating a total of 6.4×10^8 iterations.

In our global fits, we consider the lightest CP-even scalar to be the SM-like Higgs with fixed mass $m_h = 125.09$ GeV [102], and $v = 246.22$ GeV, in both the GM and eGM models. All the other SM parameters are fixed to their best-fit values [56]. To perform a Bayesian fit for any NP model, we need to choose a set of input parameters and their corresponding priors to sample the parameter space. Here, we use a different set of input parameters compared to [32] for the GM model to achieve good sampling and implement the eGM model into **HEPfit** for the first time. We list the input parameters of the GM and the eGM models and their priors in Table II and III, respectively. In the case of the eGM model, we make observables for heavy scalar masses within the range: $m_A, m_{F^0}, m_{F^{++}} \in [130, 1100]$ GeV. The triplet VEV outside of the chosen prior range is expected to be excluded from flavor observables (see [30] for the GM model). In this work, we assume that all the exotic Higgs

masses are heavier than 125 GeV and focus on the parameter space that is within the reach of the LHC. For the GM model, we adopt the notation used in Ref. [31], where v_Δ represents the triplet VEV, and m_1, m_3 , and m_5 denote the masses of the custodial singlet, triplet, and fiveplet, respectively. The relations between the quartic couplings and physical masses of the GM model can be found in [26]. For the eGM model, we provide the expressions of quartic couplings in terms of the physical masses in Appendix A.

| Parameter | v_Δ | α | λ_3, λ_5 | m_1, m_3, m_5 |
|-----------|---------------|-------------------|------------------------|-------------------|
| Range | $[0, 60]$ GeV | $[-\pi/2, \pi/2]$ | $[-4\pi, 4\pi]$ | $[130, 1100]$ GeV |

TABLE II. Priors on the input parameters of GM model.

The Bayesian statistics, in principle, do not provide a unique rule for choosing prior and posterior distributions. However, it is recommended to choose flat priors for the parameters on which the model observables depend linearly [103]. In order to keep our fit results to be as much prior independent as possible, we choose flat priors for all the input parameters. Following [32, 103], we use both mass and mass-squared priors in separate global fits and combine the 95.4% allowed regions for both priors while showing the combined fit results in our paper.

| Parameter | v_χ | α, δ | λ_χ | $\tilde{\lambda}_\chi, \kappa_1, \kappa_3$ | m_H, m_{H^+}, m_{F^+} |
|-----------|---------------|-------------------|----------------|--|-------------------------|
| Range | $[0, 60]$ GeV | $[-\pi/2, \pi/2]$ | $[0, 4\pi]$ | $[-4\pi, 4\pi]$ | $[130, 1100]$ GeV |

TABLE III. Priors on the input parameters of eGM model.

VI. GLOBAL FIT CONSTRAINTS

A. Theoretical constraints

From the theory perspective, we include the following constraints in our fits:

- Higgs potential must satisfy the stability bounds due to all possible three simultaneously non-vanishing field directions in the field space up to the scale 1 TeV.⁵
- Yukawa and quartic couplings of the theory are assumed to be in the perturbative regime (i.e., their magnitudes are smaller than $\sqrt{4\pi}$ and 4π , respectively) up to the scale 1 TeV.⁶ For the renormalization group running, we use two-loop renormalization group equations.
- Eigenvalues of the S -matrix of $2 \rightarrow 2$ scattering up to NLO given in Eq. (22) should satisfy the unitarity bounds at the scale 1 TeV.⁷ We further demand that the NLO

⁵ In our analysis, the stability bounds refer to the bounded-from-below conditions on the scalar potential. The metastability of the potential is not considered here and will be addressed in a future study.

⁶ The choice of this scale depends on the energy upto which the theory is assumed to be weakly interacting.

⁷ This scale is well above the electroweak scale and we can safely use the NLO unitarity conditions given in Eq. (22).

corrections to the LO eigenvalues should be smaller in magnitude. To quantify this, we define [74],

$$R'_1 = \frac{|a_0^{\text{NLO}}|}{|a_0^{\text{LO}}|}, \quad (24)$$

where a_0^{NLO} stands for NLO corrections calculated in the eigenbasis of the matrix, \mathbf{a}_0^{LO} .

Therefore, the perturbative expansion is not valid at NLO when $R'_1 \geq 1$. Similar criteria were used in case of the SM [93] and later in the 2HDM [74, 75] to analyze perturbative unitarity. However, there are certain directions in the parameter space that lead to accidental cancellations in the LO amplitudes. For example, $a_0^{\text{LO}} = \kappa_2 - \lambda_{\phi\chi}$ is small when $\kappa_2 \approx \lambda_{\phi\chi}$, while the NLO correction can be large since it depends on other quartic couplings of the theory (see Eq. (23)). Therefore, while doing R'_1 test, we impose a cut on the tree-level eigenvalues, $|a_0^{\text{LO}}| > 0.02$, such that the fit does not encounter any such accidental cancellations for reasonable values of the quartic couplings. Furthermore, it is worth noting that the bounds on the eigenvalues of the S -matrix are obtained at the TeV energy regime. However, the running of the VEVs destabilizes the custodial symmetric vacua [97].⁸ Therefore, the constraints on the model parameters given in Eq. (4) no longer hold in the high energy limit for the eGM model. The global $SU(2)_L \otimes SU(2)_R$ symmetry for the GM model also breaks down in the high energy limit. In order to make it consistent with the S -matrix computations, we consider the most general potential (Eq. (1)) containing ten quartic couplings, and we use the one-loop unitarity conditions on these couplings. The S -matrix elements at one-loop are given in Appendix D, where the quartic couplings are running couplings. The two-loop renormalization group equations (RGEs) are computed using PyR@TE [104]. Explicit expressions of two-loop RGEs are given in Appendix E. Among the Yukawa's, we only consider the contributions coming from the third-generation fermions.

B. h signal strengths

For a given process of producing the SM-like Higgs h via the channel i and decay to final state f , the signal strength for the production (μ_i) and for the decay (μ_f) are given by,

$$\mu_i = \frac{\sigma_i}{(\sigma_i)_{\text{SM}}}, \quad \text{and} \quad \mu_f = \frac{\mathcal{B}(h \rightarrow f)}{\mathcal{B}_{\text{SM}}(h \rightarrow f)},$$

where σ_i 's are the production cross sections via i^{th} channel where $i \in \{ggF, bbh, \text{VBF}, Wh, Zh, t\bar{t}h, th\}$, and $\mathcal{B}(h \rightarrow f)$'s are the decay branching fractions for the final state f where $f \in \{ZZ, WW, \gamma\gamma, Z\gamma, \mu\mu, bb, \tau\tau\}$. Signal strength for the combined process with production channel (i) and the decay mode (f) of h can be defined as,

$$\mu_i^f \equiv \mu_i \cdot \mu_f = r_i \cdot \frac{r_f}{\sum_{\substack{f' \in \{ZZ, WW, Z\gamma, \\ \gamma\gamma, \mu\mu, bb, \tau\tau\}}} r_{f'} \cdot \mathcal{B}_{\text{SM}}(h \rightarrow f')} ,$$

⁸ Note that, the self-energy corrections also break the symmetry if the loop effects of $U(1)_Y$ gauge coupling, top Yukawa coupling, and new Higgs bosons are taken into account. As a result, the predictions of the Peskin-Takeuchi parameters (S , T , and U) deviate from their SM values [27].

| | Signal strength | Value | Correlation matrix | | | | | | \mathcal{L} [fb $^{-1}$] | Source |
|--|---------------------------------------|------------------|--------------------|-------|-------|-------|-------|-------|-----------------------------|--------|
| | $\mu_{\text{ggF,bbh}}^{\gamma\gamma}$ | 1.04 ± 0.10 | 1 | -0.13 | 0 | 0 | 0 | 0 | 139 | [20] |
| | $\mu_{\text{VBF}}^{\gamma\gamma}$ | 1.20 ± 0.26 | -0.13 | 1 | 0 | 0 | 0 | 0 | | |
| | $\mu_{\text{Vh}}^{\gamma\gamma}$ | 1.5 ± 0.55 | 0 | 0 | 1 | -0.37 | 0 | -0.11 | | |
| | $\mu_{\text{Zh}}^{\gamma\gamma}$ | -0.2 ± 0.55 | 0 | 0 | -0.37 | 1 | 0 | 0 | | |
| | $\mu_{\text{tth}}^{\gamma\gamma}$ | 0.89 ± 0.31 | 0 | 0 | 0 | 0 | 1 | -0.44 | | |
| | $\mu_{\text{th}}^{\gamma\gamma}$ | 3 ± 3.5 | 0 | 0 | -0.11 | 0 | -0.44 | 1 | | |
| | μ_{ggF}^{ZZ} | 0.95 ± 0.1 | 1 | -0.22 | -0.27 | 0 | 139 | [4] | | |
| | μ_{VBF}^{ZZ} | 1.19 ± 0.45 | -0.22 | 1 | 0 | 0 | | | | |
| | μ_{Vh}^{ZZ} | 1.43 ± 1.0 | -0.27 | 0 | 1 | -0.18 | | | | |
| | μ_{tth}^{ZZ} | 1.69 ± 1.45 | 0 | 0 | -0.18 | 1 | | | | |
| | $\mu_{\text{incl.}}^{ZZ}$ | 1.0 ± 0.1 | | | | | | | | |
| | $\mu_{\text{ggF,bbh}}^{WW}$ | 1.15 ± 0.135 | | | | | 139 | [19] | | |
| | μ_{VBF}^{WW} | 0.93 ± 0.21 | | | | | | | | |
| | $\mu_{\text{ggF,bbh,VBF}}^{WW}$ | 1.09 ± 0.11 | | | | | | | | |
| | $\mu_{\text{VBF}}^{\tau\tau}$ | 0.90 ± 0.18 | 1 | -0.24 | 0 | 0 | 139 | [13] | | |
| | $\mu_{\text{ggF,bbh}}^{\tau\tau}$ | 0.96 ± 0.31 | -0.24 | 1 | -0.29 | 0 | | | | |
| | $\mu_{\text{Vh}}^{\tau\tau}$ | 0.98 ± 0.60 | 0 | -0.29 | 1 | 0 | | | | |
| | $\mu_{\text{tth,th}}^{\tau\tau}$ | 1.06 ± 1.18 | 0 | 0 | 0 | 1 | | | | |
| | μ_{VBF}^{bb} | 0.95 ± 0.37 | | | | | 126 | [9] | | |
| | μ_{Vh}^{bb} | 0.95 ± 0.26 | | | | | | | | |
| | μ_{Zh}^{bb} | 1.08 ± 0.24 | | | | | | | | |
| | μ_{Vh}^{bb} | 1.02 ± 0.17 | | | | | | | | |
| | $\mu_{\text{tth,th}}^{bb}$ | 0.35 ± 0.35 | | | | | | | | |
| | $\mu_{\text{pp}}^{\mu\mu}$ | 1.2 ± 0.6 | | | | | 139 | [7] | | |
| | $\mu_{\text{pp}}^{Z\gamma}$ | 2.0 ± 0.95 | | | | | | | | |

TABLE IV. Latest Run 2 data on h signal strengths measured by ATLAS at $\sqrt{s} = 13$ TeV. Correlations below 0.1 are treated to be zero. The colors in the first column represent the corresponding decay channels in Figure 6.

where r_i and r_f are the ratios of the σ_i 's and the partial decay width Γ^f 's with respect to their corresponding SM values. Therefore, the signal strength for a particular decay mode implicitly depends on all the other h -decay modes. In the κ -framework [3], the modifiers for SM h coupling to vector bosons and fermions at the tree-level in both the GM and eGM models are given by,⁹

$$\kappa_V = c_\alpha c_\beta - \sqrt{\frac{8}{3}} s_\alpha s_\beta, \quad \text{and} \quad \kappa_f = \frac{c_\alpha}{c_\beta}. \quad (25)$$

⁹ Note that, the definitions of s_β and c_β are opposite to that given in Ref. [31] because our definition of $\tan \beta$ is inversely related to their definitions.

| | Signal strength | Value | Correlation matrix | \mathcal{L} [fb $^{-1}$] | Source |
|--|---------------------------------------|-----------------|----------------------|-----------------------------|--------|
| | $\mu_{\text{ggh,bbh}}^{\gamma\gamma}$ | 1.07 ± 0.11 | | | |
| | $\mu_{\text{VBF}}^{\gamma\gamma}$ | 1.04 ± 0.32 | | | |
| | $\mu_{\text{Vh}}^{\gamma\gamma}$ | 1.34 ± 0.34 | | 137 | [11] |
| | $\mu_{\text{tth,th}}^{\gamma\gamma}$ | 1.35 ± 0.31 | | | |
| | $\mu_{\text{ggh,bbh,tth,th}}^{ZZ}$ | 0.95 ± 0.13 | 1 -0.11 | | |
| | $\mu_{\text{VBF,Vh}}^{ZZ}$ | 0.82 ± 0.34 | -0.11 1 | 137 | [10] |
| | μ_{ggh}^{WW} | 0.92 ± 0.11 | 1 -0.13 0 0 | | |
| | μ_{VBF}^{WW} | 0.71 ± 0.26 | -0.13 1 0 0 | | |
| | μ_{Zh}^{WW} | 2.0 ± 0.7 | 0 0 1 0 | 138 | [16] |
| | μ_{Wh}^{WW} | 2.2 ± 0.6 | 0 0 0 1 | | |
| | $\mu_{\text{incl.}}^{\tau\tau}$ | 0.93 ± 0.12 | | | |
| | $\mu_{\text{ggh}}^{\tau\tau}$ | 0.97 ± 0.19 | | | |
| | $\mu_{\text{qqh}}^{\tau\tau}$ | 0.68 ± 0.23 | | 138 | [15] |
| | $\mu_{\text{Vh}}^{\tau\tau}$ | 1.80 ± 0.44 | | | |
| | μ_{qqh}^{bb} | 1.59 ± 0.60 | 1 -0.75 | | |
| | μ_{ggh}^{bb} | -2.7 ± 3.89 | -0.75 1 | 90.8 | [21] |
| | $\mu_{\text{ggh,tth}}^{\mu\mu}$ | 0.66 ± 0.67 | 1 -0.24 | | |
| | $\mu_{\text{VBF,Vh}}^{\mu\mu}$ | 1.85 ± 0.86 | -0.24 1 | 137 | [8] |
| | $\mu_{\text{pp}}^{Z\gamma}$ | 2.4 ± 0.9 | | 138 | [14] |

TABLE V. Latest Run 2 data on h signal strengths measured by CMS at $\sqrt{s} = 13$ TeV. Correlations below 0.1 are treated to be zero. The colors in the first column represent the corresponding decay channels in Figure 6.

At the leading order (LO), the h decays into $\gamma\gamma$ and $Z\gamma$ channels are mediated via exotic charged Higgs bosons (F^{++}, F^+, H^+) at the one-loop. Due to the non-degenerate masses in the eGM model, both F^{++} and F^+ contribute separately to the above loop-mediated decay modes. The general expressions of $r_{\gamma\gamma}$ and $r_{Z\gamma}$ involving the SM constituents and the exotic charged particles are given in [105]. The experimental input values of h signal strengths from the latest ATLAS and CMS Run 2 data at a center-of-mass energy of 13 TeV are displayed in Table IV and V, respectively. ATLAS and CMS combination for Run 1 data on h signal strengths measurements are given in Table 2 of [103].

VII. RESULTS

In this section, we present the allowed parameter space considering the above-mentioned theoretical constraints and the 95.4% probability regions from the combined fits to the

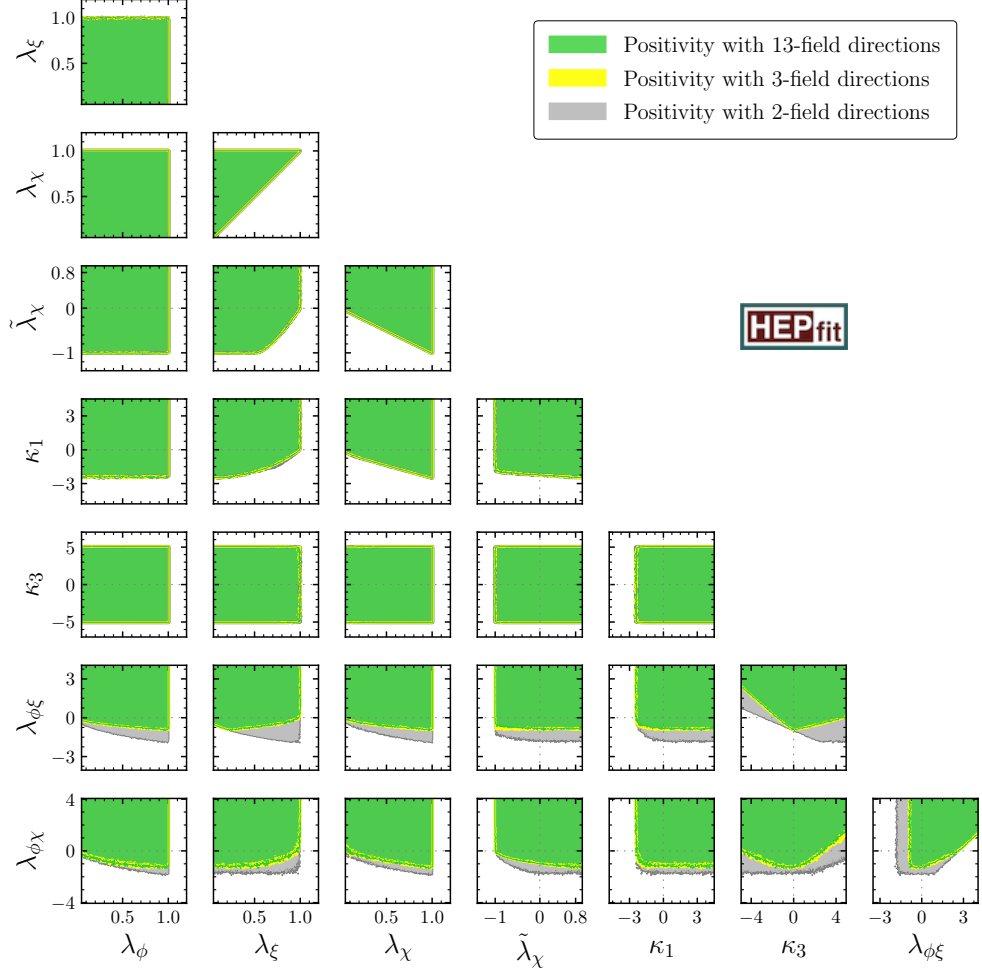


FIG. 1. Allowed regions on the quartic coupling planes of the eGM model with different BFB constraints. The grey (yellow) regions show the boundedness of the potential in the 2-field (3-field) directions, while the green areas are allowed if we use BFB conditions considering all thirteen non-zero scalar field directions.

latest Run-2 LHC results on the SM-like Higgs signal strengths for both the GM and eGM models. For the theoretical constraints, we assume flat likelihoods, and the allowed regions represent 100% probability contours. In Figure 1, we compare three different bounded-from-below (BFB) constraints on the quartic coupling planes of the eGM model. The grey (yellow) regions manifest allowed parameter space that satisfies the BFB conditions with all possible combinations of any two (three) non-vanishing field directions. The green areas show the allowed parameter space if we impose the BFB conditions, considering all thirteen fields have non-zero values. From the Figure 1, we see that the 3-field BFB constraints largely overlap with the 13-field BFB constraints in the quartic coupling planes of the eGM model. For example, in Figure 2, we show the allowed regions in the λ_5 vs. λ_4 (left panel) and κ_3 vs. $\lambda_{\phi\xi}$ (right panel) planes with three different BFB constraints for the GM and the eGM models, respectively. The grey, yellow, and green colors in Figure 2 have the same meaning as in Figure 1. The magenta dashed boundary lines in the right panel of Figure 2 depict the 2-field BFB conditions for the eGM model, $4\lambda_{\phi\xi} + \sqrt{2}\kappa_3 > -4\sqrt{\lambda_\phi \lambda_\chi}$ and

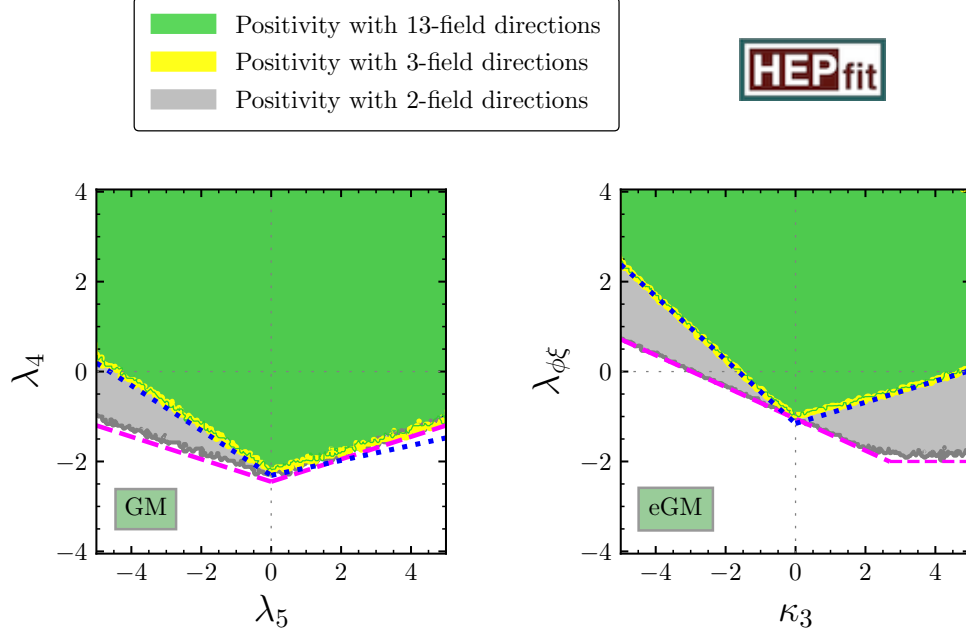


FIG. 2. Comparison of different BFB conditions in the λ_5 vs. λ_4 plane (left) of the the GM model and κ_3 vs. $\lambda_{\phi\xi}$ plane (right) of the eGM model. The grey, yellow, and green areas are allowed if we use the BFB conditions with all possible 2-field, 3-field, and 13-field directions at once, respectively. The magenta dashed boundary lines originated from the BFB conditions with all possible two non-vanishing field directions at once, while the blue dotted boundary lines originated from the BFB conditions with at least three scalar fields to be non-zero.

$\lambda_{\phi\xi} > -2\sqrt{\lambda_\phi\lambda_\xi}$. In the left panel of Figure 2, the magenta dashed boundary lines represent the 2-field BFB conditions for the GM model, $4\lambda_4 - |\lambda_5| > -4\sqrt{2\lambda_1(2\lambda_2 + \lambda_3)}$ [26]. Blue dotted lines represent the boundary lines coming from one of the necessary conditions with three non-vanishing field directions given in Eq. (15) for the eGM model and in Eq. (17) for the GM model. The comparison of these three different BFB constraints in all other planes of the GM model is given in Figure 11 of Appendix F. Note that these BFB conditions are imposed on the tree-level potential, and all the quartic couplings are interpreted at the scale of M_Z .¹⁰

Thus, the BFB conditions with all possible 3-field directions provide a very good approximation of the full 13-field BFB conditions [28, 77] for both models. Since the later conditions depend on more than one field-dependent parameter (see Eq. (C2) for the eGM model), the computational cost is significantly high for this case compared to the 3-field BFB case. Therefore, in the rest of our analysis, we shall consider the BFB conditions with all possible 3-field directions to reduce computational cost.

Next, we compare different unitarity constraints on the parameter spaces for both the GM and eGM models. In Figure 3 (Figure 4), we show the allowed regions, at the M_Z scale, in the quartic coupling planes of the GM (eGM) model with LO, NLO unitarity, and NLO

¹⁰ To compare the three different BFB conditions in Figures 1, 2, and 11, we sample the parameter space of the quartic couplings in the following ranges: (i) $\lambda_\phi, \lambda_\xi, \lambda_\chi, \tilde{\lambda}_\chi \in [-1, 1]$ and $\lambda_{\phi\xi}, \lambda_{\phi\chi}, \kappa_1, \kappa_3 \in [-5, 5]$ for the eGM model, (ii) $\lambda_1, \lambda_2, \lambda_3 \in [-1, 1]$ and $\lambda_4, \lambda_5 \in [-5, 5]$ for the GM model.

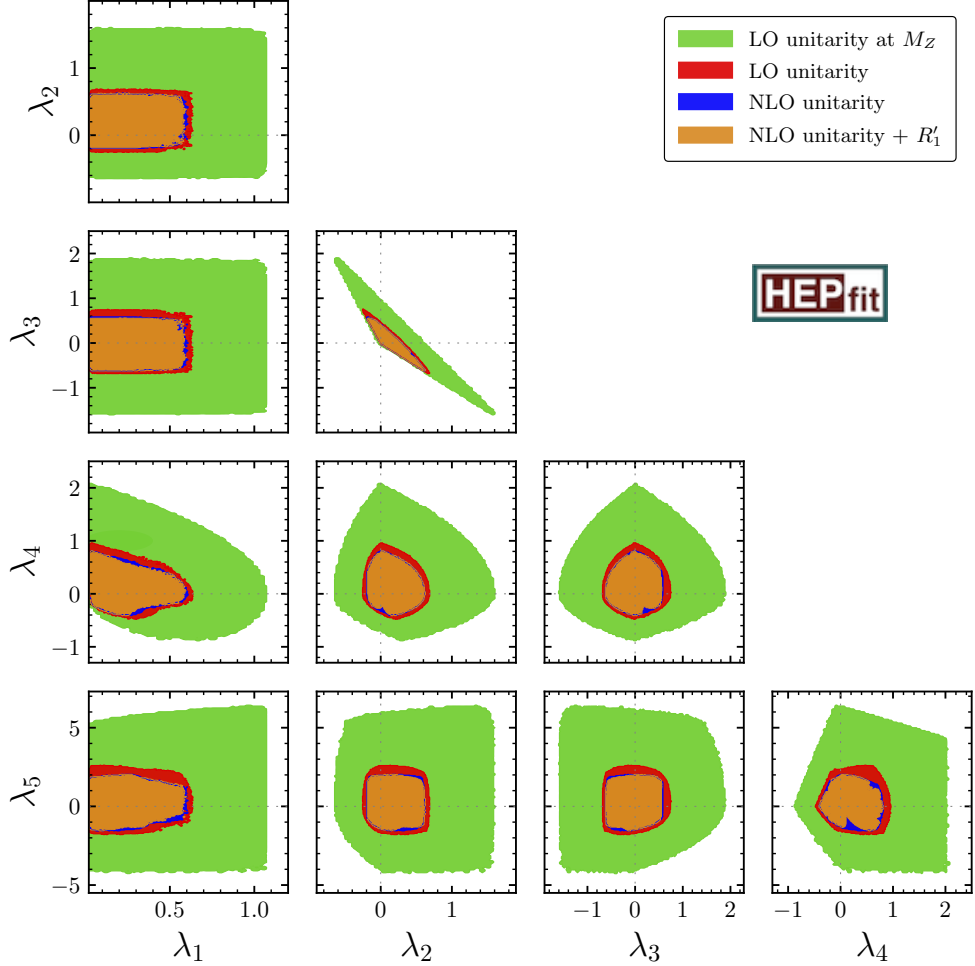


FIG. 3. Allowed regions in the λ_i vs. λ_j planes of the GM model. The red (blue) colored areas show the allowed parameter space if we use LO (NLO) unitarity bounds. The brown regions are obtained with the additional condition that the NLO value should be smaller than LO value in magnitude (if the LO value is not accidentally small), and the green areas are allowed if we impose the unitarity conditions at the scale M_Z . All the λ_i values are given at M_Z scale. Note that all these allowed regions satisfy the 3-field BFB conditions on the potential.

unitarity with R'_1 (see Eq. (24)), in the colors red, blue, and brown, respectively. All these regions satisfy the 3-field BFB conditions on the potential. Unless stated, the aforementioned unitarity bounds are imposed on the two-loop renormalization group improved quartic scalar couplings at the scale 1 TeV. It is distinctly evident from Figures 3 and 4 that the NLO unitarity constraint sets substantially stringent bounds on the parameter space compared to the LO unitarity. The allowed regions get further shrunk when we include the perturbativity NLO unitarity condition ($R'_1 < 1$). In some of the panels in Figures 3 and 4, we observe sharp cuts around the origin once the perturbative unitarity is considered. An explanation of such features in the quartic coupling planes is given in Appendix F. If we use LO unitarity conditions at the M_Z scale instead, the parameter space gets much more relaxed. These regions are shown in green color in the same planes of Figures 3 and 4. Numerically, the quartic couplings for the GM (eGM) model can have a maximum absolute value as large as

2.7, 2.2, 2.2 (4.1, 3.1, 3.1) if we apply LO unitarity, NLO unitarity, R'_1 -perturbative NLO unitarity, respectively. These values are obtained from the Figures 3 and 4.

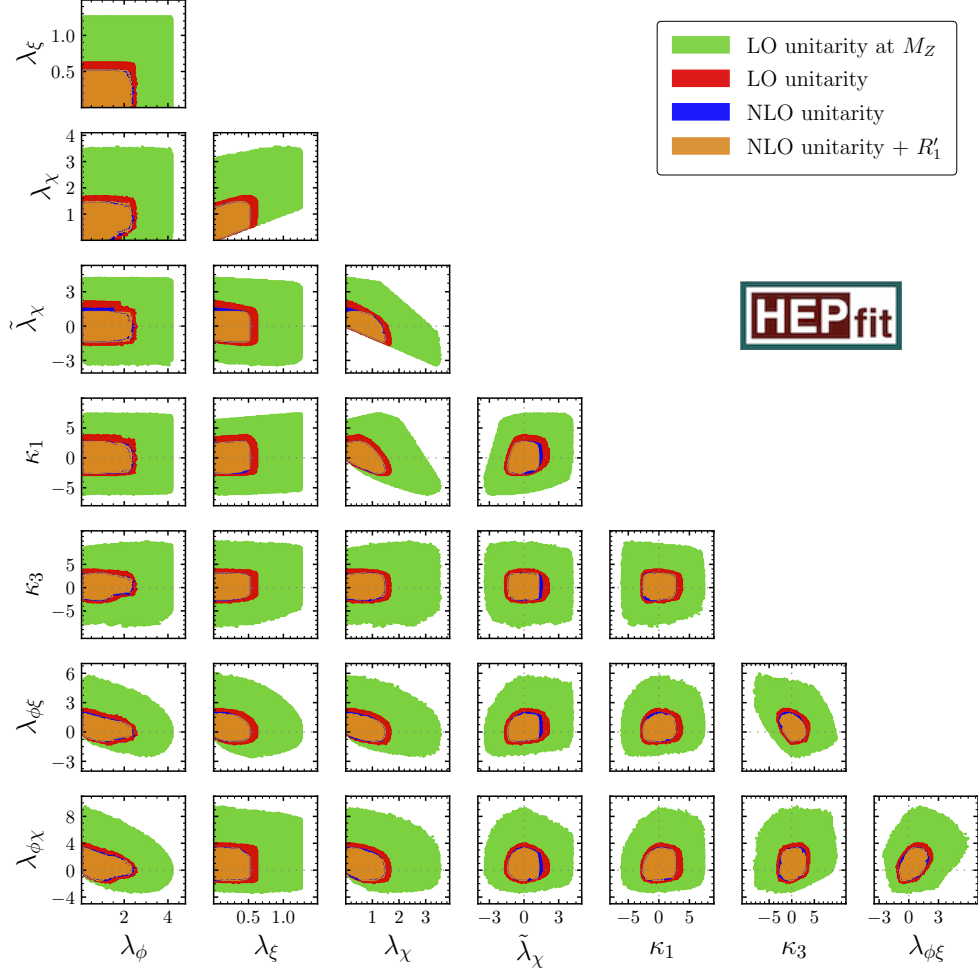


FIG. 4. Allowed regions in the quartic coupling planes of the eGM model. The colors of the shaded regions have the same meaning here as in Figure 3. All the allowed regions satisfy the 3-field BFB conditions on the potential.

A comparison among different unitarity conditions for the GM model is displayed on the λ_4 vs. λ_5 plane in the right panel of Figure 5. The green, red, blue, and brown solid lines correspond to the contours of the same color as in Figure 3. The red dashed contour is the result of imposing LO unitarity with LO RGEs and it is almost always more stringent than the choice of LO unitarity with NLO RGEs. This is due to the fact that LO RGEs run the quartic couplings into non-perturbative values at a much lower energy scale in comparison with NLO RGE running. Therefore, larger values of quartic couplings are allowed at the M_Z scale if one uses NLO RGE. The cyan contour represents the allowed regions when we demand R'_1 perturbative condition with imposing constraint on the LO unitarity eigenvalues only and the contour shows some distinct pinch-cuts towards the origin. A weaker bound comes from Eq. (19) if we consider only the real part of the NLO unitarity eigenvalues, i.e., $|\text{Re}(a_\ell)| \leq 1/2$. This contour is represented by a blue dotted line, and as expected it is always less stringent than the blue solid contour. The violet contour corresponds to

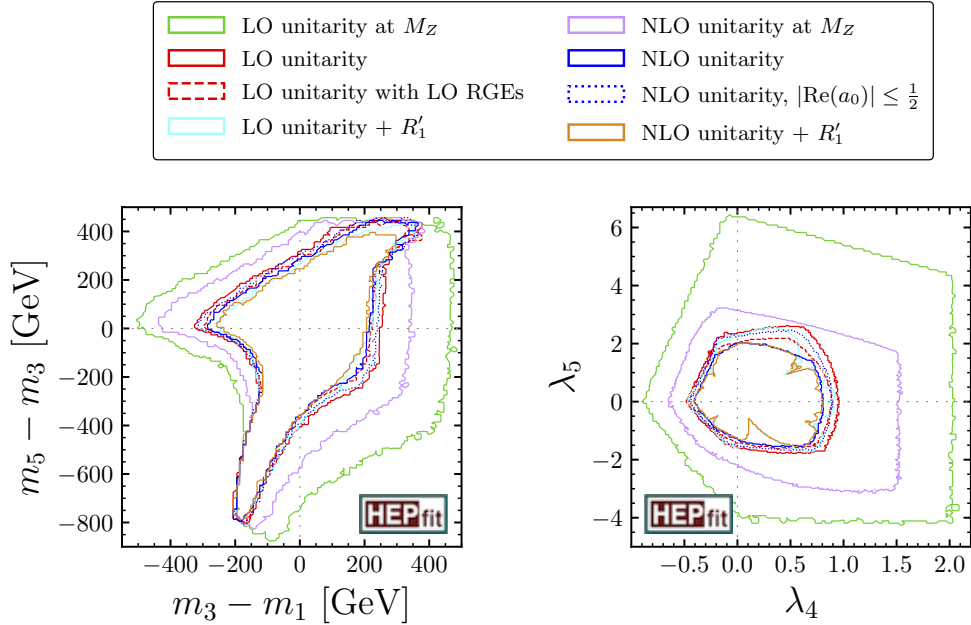


FIG. 5. Comparison among different unitarity constraints in the $m_3 - m_1$ vs. $m_5 - m_3$ plane (left) and λ_4 vs. λ_5 plane (right) of GM model. The green, red, blue, and brown contours have the same meaning as in Figure 3. The red dashed contour shows the effects of LO RGEs to the LO unitarity conditions, and the cyan contour demonstrates the impact of R'_1 -perturbative condition without imposing NLO unitarity bounds. The dotted blue contour shows the allowed regions if we consider only real parts of the S -matrix eigenvalues while imposing unitarity bounds at one-loop, and the violet contour represents the allowed area if we impose NLO unitarity conditions at the scale M_Z . All the allowed regions satisfy the 3-field BFB conditions on the potential.

the allowed regions satisfying NLO unitarity conditions at the scale M_Z . This yields only a stronger constraint than the LO unitarity evaluated at M_Z . The left panel in Figure 5 shows how these constraints on the quartic couplings translate into the mass difference planes of the heavy Higgs bosons in the GM model. The different unitarity constraints follow the same ordering as in the right panel.

In the top left (top right) panel of Figure 6, we display the impacts of the individual signal strengths with different final states on the v_Δ vs. α plane (v_χ vs. α plane) for the GM (eGM) model. For small v_χ and the region where α is not close to zero, the ZZ , WW , and $\gamma\gamma$ signal strengths are most restrictive. Whereas, for large v_χ values, the most significant constraint around $\alpha = 0$ region comes from $h \rightarrow b\bar{b}$ data. Amongst the loop-mediated decays, the $h \rightarrow \gamma\gamma$ channel stringently constrains v_χ vs. α plane compared to the $h \rightarrow Z\gamma$ channel. The combined fit with all signal strengths favors the negative values of α with $|\alpha| < 0.45$, and the triplet VEV v_χ cannot exceed ≈ 30 GeV at a 95.4% confidence level (CL) for both models. This result shows a significant improvement over the previous global fit reported in Ref. [32], where the upper limit of triplet VEV was ≈ 45 GeV in the GM model.¹¹ In the decoupling limit, $\alpha, v_\chi \rightarrow 0$ [28], all additional Higgs bosons become heavy, and the couplings of the SM-like Higgs approach towards its SM values, which translate into

¹¹ Figure 6 shows that the allowed region from the $\gamma\gamma$ signal strength in the eGM model (red region) is smaller than that in the GM model. The $\gamma\gamma$ signal strength receives contributions from charged scalar

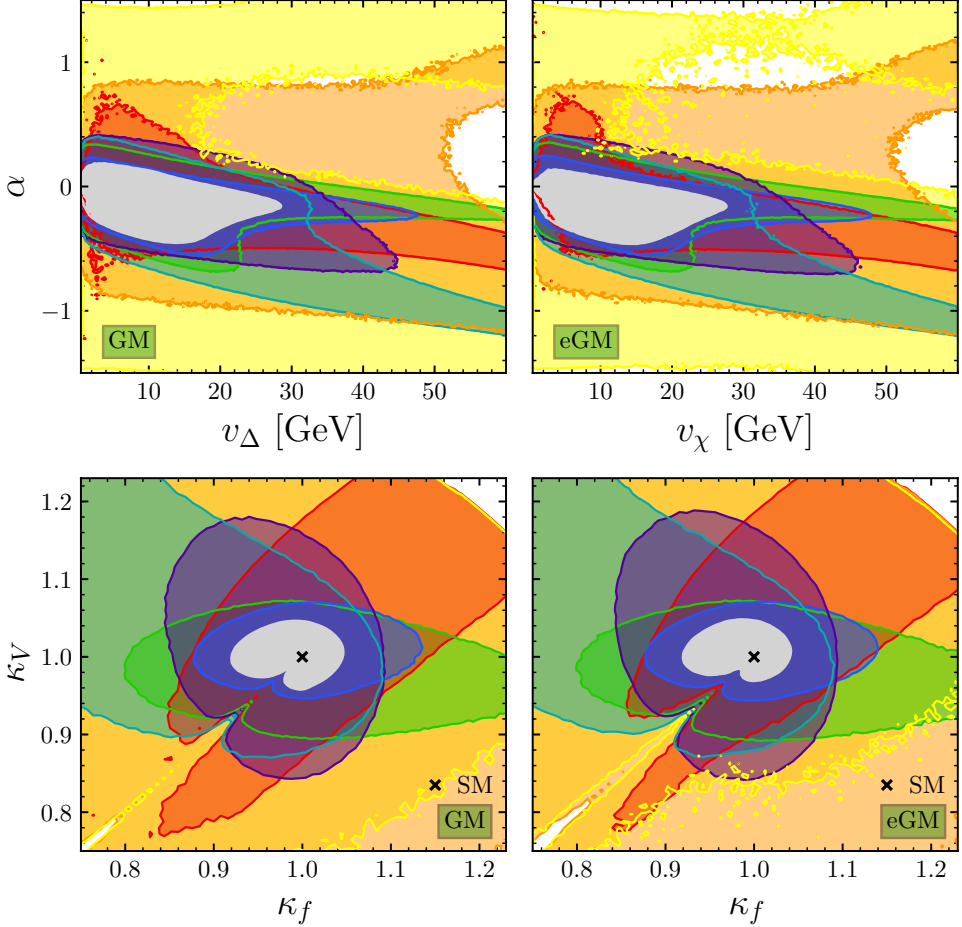
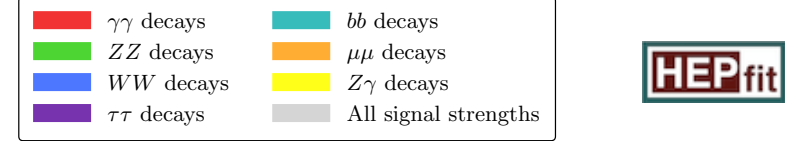


FIG. 6. 95.4% probability regions show the impact of the Higgs signal strengths for different final states in the v_χ vs. α planes (top) and the κ_f vs. κ_V planes (bottom). The individual fits to full Run 1 and Run 2 data from h decays to $\gamma\gamma$, ZZ , WW , $\tau\tau$, bb , $\mu\mu$, and $Z\gamma$ in red, green, blue, purple, cyan, orange, and yellow, respectively. The results from the combined fits are shown in the grey color shaded regions, where the cross indicates the expected value for the SM Higgs boson.

$\kappa_V = \kappa_f = 1$ (see Eq. (25)). Away from the decoupling limit, κ_V and κ_f are no longer unity at the tree-level. In the bottom left (right) panel of Figure 6, we show the allowed ranges in κ_f vs. κ_V plane for all different final states for the GM (eGM) model. The SM predictions of

loops which depend on the scalar couplings in the potential. The relationships between the GM and eGM couplings are provided in Table 3 of Ref. [59]. Since no theoretical constraints have been imposed here, certain allowed coupling values in the GM model are not accessible in the eGM model given the chosen prior ranges listed in Tables II and III. Consequently, the parameter space of the eGM model is more constrained than the GM model. This also reflects on the allowed parameter space once all the signal strength channels are combined (grey region). Once the theoretical constraints are considered the allowed couplings in both models remain well below the chosen prior ranges, eliminating this apparent discrepancy.

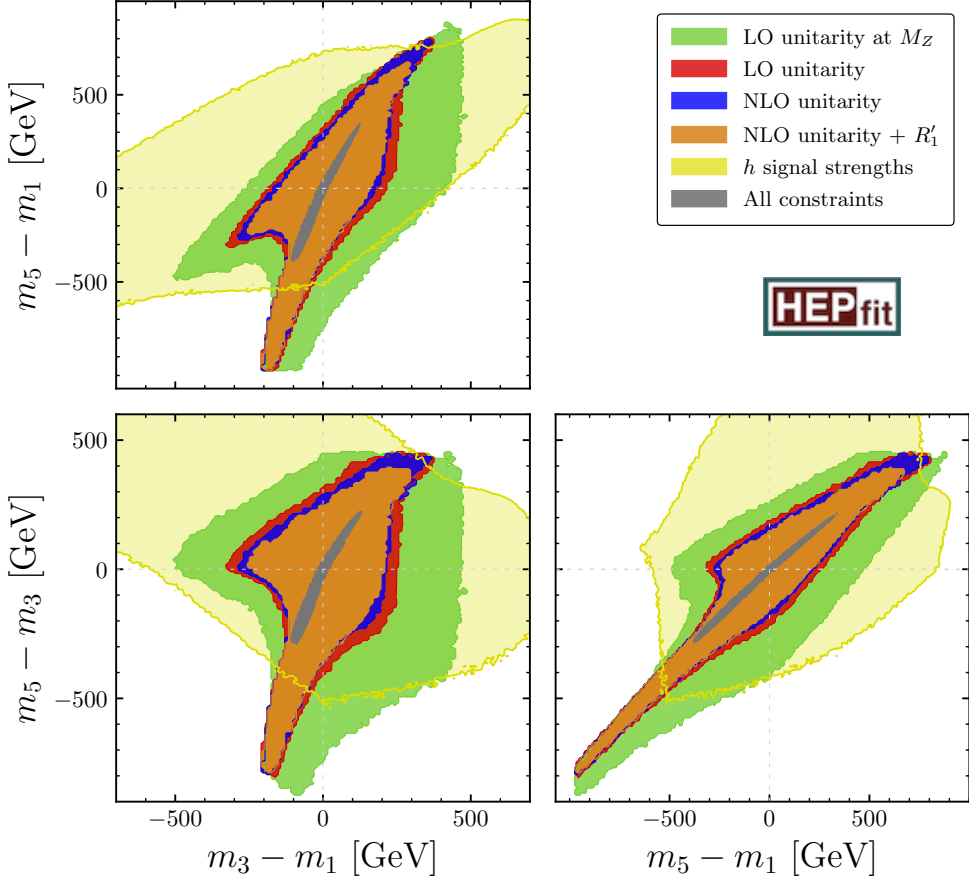


FIG. 7. Allowed regions in the mass difference planes of the GM model. The green, red, blue, and brown areas have the same meaning as the regions of the same color in Figure 3. The yellow regions are allowed from the Higgs signal strengths measurements with a 95.4% CL. Finally, the grey areas are allowed with a 95.4% CL from the combined fits to the theory and Higgs signal strengths constraints.

$\kappa_f = 1$ and $\kappa_V = 1$ lie within the allowed regions (grey shaded area) of all signal strengths. In the combined fit, we find that the Higgs signal strength data disfavor the region where $\kappa_V > 1.05$, $\kappa_V < 0.95$, and $\kappa_f > 1.05$, $\kappa_f < 0.92$ at a 95.4% CL for both models. At leading order, the SM-like Higgs boson h couplings to $\gamma\gamma$ and $Z\gamma$ are modified by κ_f , κ_V , and contributions from charged scalars loops [105]. To quantify new physics effects on these couplings, we define [105], $r_{VV} \equiv \Gamma(h \rightarrow VV)/\Gamma_{\text{SM}}(h \rightarrow VV)$ with $VV = \{\gamma\gamma, Z\gamma, gg\}$, where $\Gamma(h \rightarrow VV)$ denotes the partial decay width of the $h \rightarrow VV$ channel. The 95.4% CL contours in the $r_{V\gamma}$ vs. r_{gg} ($V = \gamma, Z$) planes are shown in Figure 13 of Appendix F. The maximal deviations of $r_{\gamma\gamma}$ and $r_{Z\gamma}$ from their SM values are approximately 25% and 10%, respectively, in both models.

In Figure 7, we present the effects of different theoretical constraints and the latest Higgs signal strength data on the mass differences of the heavy Higgs bosons in the GM model. The green, red, blue, and brown areas correspond to the same regions as in Figure 3. The yellow shaded areas show the allowed region from the Higgs signal strength data at a 95.4% CL. The combined fit (grey shaded area) allows for a maximal mass splitting among three

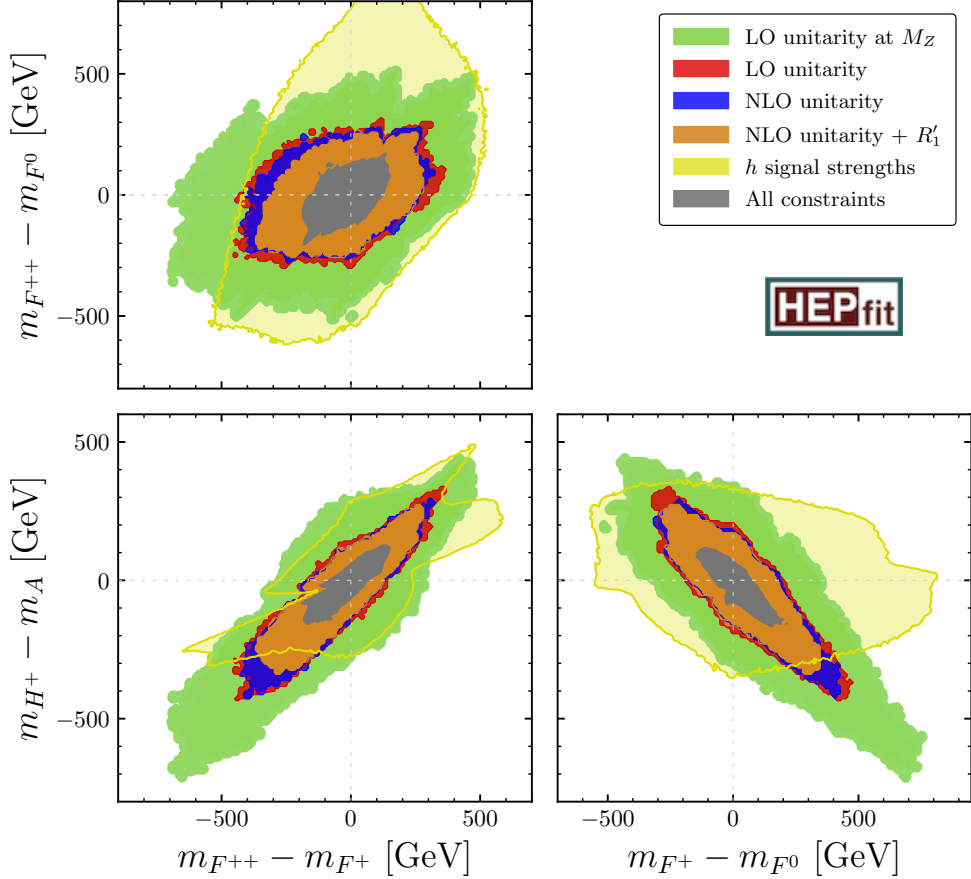


FIG. 8. Effects of different constraints in the planes of heavy Higgs boson mass difference within the members of each CS multiplet in eGM model. The shaded regions are allowed from various constraints and the colors have the same meaning as in Figure 7.

multiplets (m_1 , m_3 , and m_5) to be around 400 GeV in the GM model. Note that the largest possible absolute value of these mass differences is reduced by about 100 GeV compared to what was allowed in the previous global fit for the GM model [32]. Compared to other mass differences, the mass difference, $m_3 - m_1$ is stringently constrained from the theoretical constraints and is restricted to be smaller than 130 GeV in magnitude. On the other hand, Figure 8 shows the effect of all these constraints on the mass splittings within the members of each CS multiplet in the eGM model. At a 95.4% CL, these mass differences can maximally reach 210 GeV in the eGM model. We have observed that the mass splitting within the CS five-plet, $m_{F^{++}} - m_{F^0}$ receives the strongest constraint from the theory bounds among other mass differences.

In summary, Figure 9 shows the 95.4% probability limits of the quartic couplings and heavy Higgs mass differences once all constraints are taken into account. The mass differences of the heavy Higgs bosons are restricted to be smaller than 410 GeV for both models.¹² The

¹² In principle, the allowed values of the mass difference of the heavy Higgs bosons in the GM model remain valid in the eGM model provided both models are subject to the same parameter constraints. However, the global fit results indicate that, under all constraints, the allowed mass differences among certain heavy Higgs bosons tend to be smaller in the eGM model than in the GM model. This occurs because the credibility intervals in the mass difference planes of the eGM model are prone to be conservative estimates

maximum magnitude of κ_3 (λ_5) can reach 2.51 (1.91) without violating the aforementioned theoretical bounds in the eGM (GM) model.

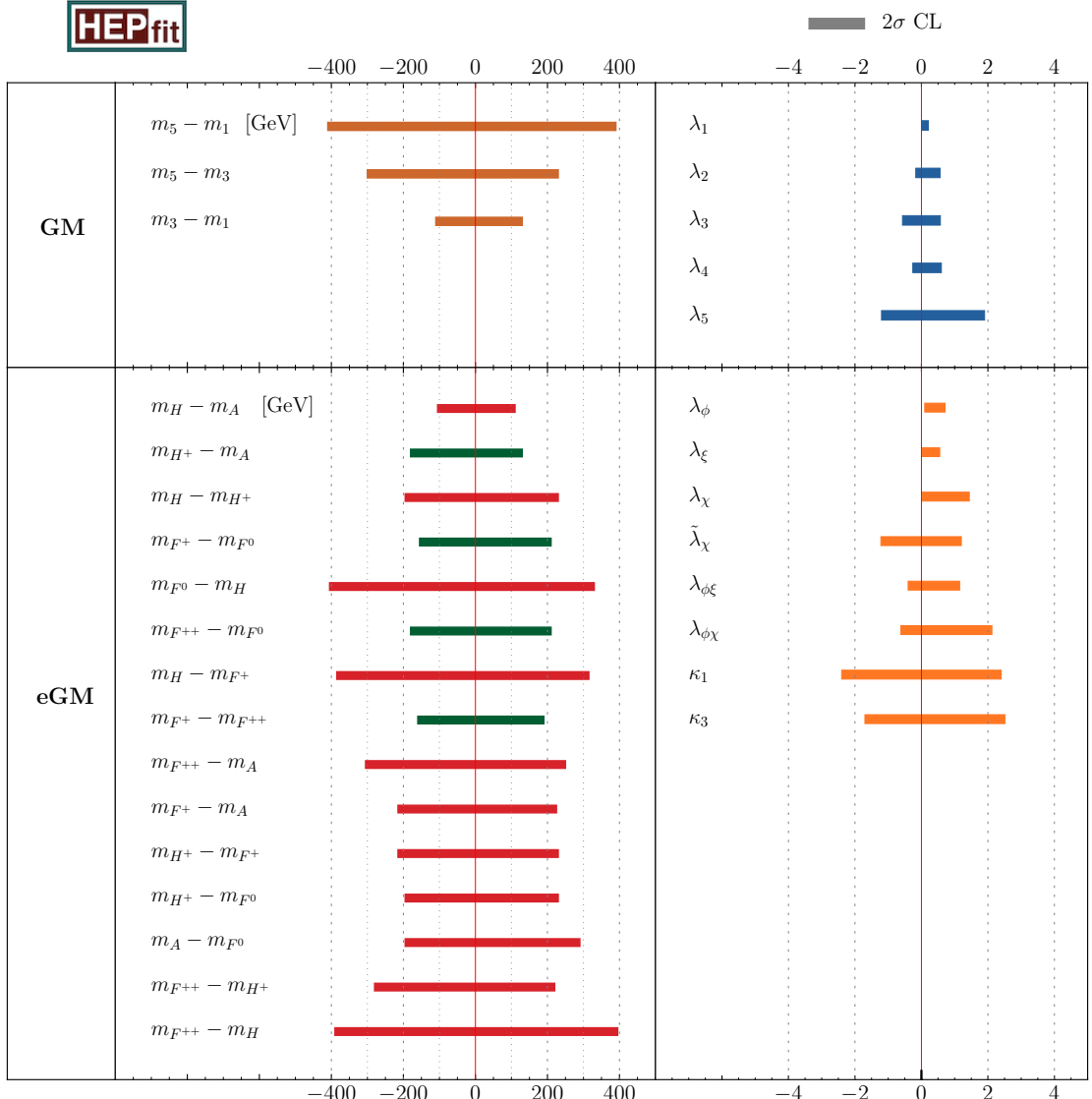


FIG. 9. Limits on the mass differences of the heavy Higgs bosons and quartic couplings from the global fit in both the GM and eGM models. The horizontal bands denote the 95.4% confidence interval. The mass differences between the members of each CS multiplet in the eGM model are shown in green. The limits on these mass parameters are obtained from the Figures 7, 8, 14 and 15.

VIII. CONCLUSIONS

Triplet scalar extension of the SM, which preserves the custodial symmetry (CS) due to the global $SU(2)_L \times SU(2)_R$ symmetry on the scalar potential at tree-level, results in the well-

when the NLO unitarity bounds are imposed on the model parameters (see Figure 15). Hence, the 95.4% probability limits on the mass differences of heavy Higgs bosons in the eGM model, as shown in Figure 9, may be relaxed by increasing the number of iterations or by modifying the sampling procedure.

known GM model. On the contrary, keeping the custodial symmetry intact at the tree-level in a triplet extended scalar sector of the SM only via the conditions given in Eq. (4) [59], gives rise to the extended GM (eGM) model. We have derived the BFB conditions taking into account all combinations of three non-zero scalar fields for the GM, the eGM, and the generalized two-triplet model at the tree-level. We have observed that the BFB conditions with all possible 3-field directions are a very good approximation of all 13-field BFB conditions in both the GM and eGM models and significantly reduce computational cost. We have computed, for the first time, one-loop corrections to the tree-level eigenvalues of S -matrix for all $2 \rightarrow 2$ bosonic scatterings, and placed unitarity bounds on the two-loop renormalization group improved quartic couplings in the GM and the eGM models. We have found that the allowed parameter space of both the GM and eGM models gets more constrained once we impose NLO unitarity conditions in comparison to the LO unitarity constraint. Imposing perturbativity conditions with NLO unitarity further reduces the allowed parameter space. Considering the NLO unitarity and 3-field BFB conditions, we have observed that the allowed values of the quartic couplings cannot exceed 2.2 (3.1) in magnitude in the GM (eGM) model. We have performed global fits to the latest SM-like Higgs signal strength data from the LHC with NLO unitarity and 3-field BFB conditions in both models.

We compare the impact on the parameter space due to the individual Higgs signal strengths on leading order h couplings using the Run 1 and latest Run 2 data from the CMS and ATLAS detectors. Taking into account all the available Higgs signal strength data, we find that the triplet VEV, v_χ , and mixing angle, $|\alpha|$, cannot exceed 30 GeV and 0.45, respectively. In other words, Higgs signal strength data disfavors the regions where $\kappa_V > 1.05$, $\kappa_V < 0.95$, and $\kappa_f > 1.05$, $\kappa_f < 0.92$ at a 95.4% CL in both the GM and eGM models. At one-loop, the maximal deviation of $r_{\gamma\gamma}$ and $r_{Z\gamma}$ from their SM values are roughly 25% and 10% in both models, respectively.

Combining all theoretical constraints and the latest h signal strength data, we find the following ranges of the model parameters, with a 95.4% CL, while marginalizing over all other parameters: The values of the quartic couplings cannot exceed 1.91 (2.51) in magnitude in the GM (eGM) model. The mass differences between the heavy Higgs bosons are restricted to be smaller than 410 GeV in both models. The largest possible absolute value of these mass differences is reduced by about 100 GeV than that was allowed from the fits previously done in the literature [32] for the GM model. One significant feature of the eGM model is the non-zero mass splitting within the members of each CS multiplet at the tree-level. From the global fit, we have shown that the maximal mass splitting between the members of each CS multiplet cannot exceed 210 GeV in the eGM model. One such mass difference between the doubly-charged Higgs (F^{++}) and CP-even Higgs (F^0) does not depend on the trilinear parameters, μ_1 and μ_2 , and therefore strongly constrained from the theory bounds. While a detailed collider analysis is beyond the scope of this paper, our analysis would impact the search strategies of heavy Higgs bosons at the LHC and the other future colliders. It will be worthwhile to examine the bounds of the eGM model using electroweak precision observables or flavor observables, which will be addressed in future studies [106].

ACKNOWLEDGMENTS

We thank Joydeep Chakrabortty, Sanmay Ganguly, Anirban Kundu, Swagata Mukherjee, Christopher W. Murphy, and Sudhir K. Vempati for useful discussions. We are indebted

to Gilbert Moultaka and Palash B. Pal for their valuable comments on the manuscript. We are grateful to Ayan Paul and Luca Silvestrini for numerous discussions regarding the `HEPfit` code. This work is supported by the SERB (Govt. of India) under grant SERB/CRG/2021/007579. SS acknowledges funding from the MHRD (Govt. of India) under the Prime Minister's Research Fellows (PMRF) Scheme, 2023. PM and DC acknowledge funding from the SERB (Govt. of India) under grant SERB/CRG/2021/007579. DC also acknowledges funding from an initiation grant IITK/PHY/2019413 at IIT Kanpur.

Appendix A: Quartic couplings from physical masses

In this appendix, we provide the expressions of the quartic couplings (λ_i, κ_i) in terms of the physical masses for the eGM model.

$$\begin{aligned}
\lambda_\phi &= \frac{1}{2v^2 c_\beta^2} \left(m_h^2 c_\alpha^2 + m_H^2 s_\alpha^2 \right), \\
\lambda_\xi &= \frac{1}{3v^2 s_\beta^2} \left(m_h^2 s_\alpha^2 + m_H^2 c_\alpha^2 + 2m_{F^0}^2 + 3 \left(M_2^2 - 2m_A^2 \right) c_\beta^2 - \frac{3}{2} M_1^2 \right), \\
\lambda_\chi &= \frac{2}{3v^2 s_\beta^2} \left(2m_h^2 s_\alpha^2 + 2m_H^2 c_\alpha^2 + m_{F^0}^2 - 3m_A^2 c_\beta^2 \right), \\
\tilde{\lambda}_\chi &= \frac{2}{v^2 s_\beta^2} \left[m_{F^{++}}^2 - M_1^2 + c_\beta^2 \left(2M_2^2 - 3m_A^2 \right) \right] \\
&\quad + \frac{2c_\beta^2}{v^2 s_\beta^2 (c_{2\delta} - c_\beta s_{2\delta})} \left[2m_{F^+}^2 - 2m_{H^+}^2 + c_{2\delta} \left(4m_A^2 - 2m_{F^+}^2 - 2m_{H^+}^2 \right) \right], \\
\lambda_{\phi\xi} &= \frac{1}{v^2 s_\beta c_\beta} \left(s_\beta c_\beta \left(2m_A^2 - M_2^2 \right) + \sqrt{\frac{2}{3}} \left(M_H^2 - m_h^2 \right) c_\alpha s_\alpha \right), \\
\lambda_{\phi\chi} &= \frac{2}{v^2} \left[m_A^2 + \sqrt{\frac{2}{3}} \frac{s_{2\alpha}}{s_{2\beta}} \left(m_H^2 - m_h^2 \right) \right] - \frac{2}{v^2 (c_{2\delta} - c_\beta s_{2\delta})} \left[2s_\delta^2 m_{F^+}^2 - 2c_\delta^2 m_{H^+}^2 \right. \\
&\quad \left. + \left(M_2^2 + m_A^2 \right) c_{2\delta} - \left(M_2^2 - m_A^2 \right) c_\beta s_{2\delta} \right], \\
\kappa_1 &= \frac{4}{v^2 s_\beta^2 (c_{2\delta} - c_\beta s_{2\delta})} \left[-M_1^2 c_{2\delta} + \left(c_\delta^2 m_{F^+}^2 - s_\delta^2 m_{H^+}^2 \right) s_\beta^2 + 2 \left(M_2^2 - m_A^2 \right) c_\beta^2 c_{2\delta} \right. \\
&\quad \left. + \left(m_{F^+}^2 - m_{H^+}^2 \right) c_\beta^2 + c_\beta s_{2\delta} \left(M_1^2 + m_A^2 - m_{F^+}^2 - m_{H^+}^2 - \left(2M_2^2 - 3m_A^2 \right) c_\beta^2 \right) \right], \\
\kappa_3 &= \frac{2\sqrt{2}}{v^2} \left(M_2^2 - m_A^2 \right), \tag{A1}
\end{aligned}$$

where we have defined,

$$M_1^2 = \frac{\mu_1 s_\beta v}{\sqrt{2}}, \quad M_2^2 = \frac{\mu_2 v}{\sqrt{2} s_\beta}. \tag{A2}$$

These eight quartic couplings can be reduced to five λ_i ($i = 1, 2, 3, 4, 5$), in the limit $\delta = 0$, $m_A = m_{H^+}$, and $m_{F^0} = m_{F^+} = m_{F^{++}}$, which are consistent with the relations given in [26].

Appendix B: Bounded-from-below constraints in the field subspace

Here, we consider the subspaces of the potential where only two or three fields are non-vanishing at once. At large field values, only quartic terms in the potential dominate as shown in Eq. (13). In the field space, first we consider a field direction where only electrically neutral components, χ^0 and ξ^0 are non-vanishing. The corresponding potential reads,

$$V^{(4)} = \lambda_\chi |\chi^0|^4 + \lambda_{\chi\xi} |\chi^0|^2 (\xi^0)^2 + \lambda_\xi (\xi^0)^4. \quad (\text{B1})$$

Due to the bi-quadratic form of the potential in Eq. (B1), the necessary and sufficient BFB conditions in this direction are nothing but the criteria for strict copositivity of the potential [107], given by,

$$\lambda_\chi > 0 \wedge \lambda_\xi > 0 \wedge \lambda_{\chi\xi} + 2\sqrt{\lambda_\chi \lambda_\xi} > 0. \quad (\text{B2})$$

Similarly, if we consider the field direction where only ϕ^0 , ξ^0 , and, χ^+ are non-vanishing,

$$\begin{aligned} V^{(4)} = & \lambda_\phi |\phi^0|^4 + \lambda_\xi (\xi^0)^4 + (\lambda_\chi + \tilde{\lambda}_\chi) |\chi^+|^4 + \lambda_{\phi\xi} |\phi^0|^2 (\xi^0)^2 \\ & + \lambda_{\phi\chi} |\phi^0|^2 |\chi^+|^2 + (\lambda_{\chi\xi} + \kappa_1) |\chi^+|^2 (\xi^0)^2. \end{aligned} \quad (\text{B3})$$

The above equation can be written in a matrix form $x^T \Lambda x$, in the basis $x^T = \{|\phi^0|^2, (\xi^0)^2, |\chi^+|^2\}$, where Λ is given by,

$$\Lambda = \begin{bmatrix} \lambda_\phi & \frac{\lambda_{\phi\xi}}{2} & \frac{\lambda_{\phi\chi}}{2} \\ \frac{\lambda_{\phi\xi}}{2} & \lambda_\xi & \frac{\kappa_1 + \lambda_{\chi\xi}}{2} \\ \frac{\lambda_{\phi\chi}}{2} & \frac{\kappa_1 + \lambda_{\chi\xi}}{2} & \lambda_\chi + \tilde{\lambda}_\chi \end{bmatrix}. \quad (\text{B4})$$

The symmetric matrix Λ is strictly copositive (i.e., $x^T \Lambda x > 0$) if and only if [107, 108],

$$\begin{aligned} \lambda_\phi > 0, & \quad \lambda_\chi + \tilde{\lambda}_\chi > 0, & \quad a_1 = \lambda_{\phi\xi} + 2\sqrt{\lambda_\phi \lambda_\xi} > 0, \\ \lambda_\xi > 0, \quad b_1 = \lambda_{\phi\chi} + 2\sqrt{\lambda_\phi (\lambda_\chi + \tilde{\lambda}_\chi)} > 0, & \quad c_1 = \lambda_{\chi\xi} + \kappa_1 + 2\sqrt{\lambda_\xi (\lambda_\chi + \tilde{\lambda}_\chi)} > 0, \\ \lambda_{\phi\xi} \sqrt{\lambda_\chi + \tilde{\lambda}_\chi} + \lambda_{\phi\chi} \sqrt{\lambda_\xi} + (\lambda_{\chi\xi} + \kappa_1) \sqrt{\lambda_\phi} + 2\sqrt{\lambda_\phi \lambda_\xi (\lambda_\chi + \tilde{\lambda}_\chi)} + \sqrt{a_1 b_1 c_1} > 0. \end{aligned} \quad (\text{B5})$$

Among these 3-field directions, we write down the part of the potential where only neutral components of the fields ϕ^0 , ξ^0 , and χ^0 are non-vanishing,

$$\begin{aligned} V^{(4)} = & \lambda_\phi |\phi^0|^4 + \lambda_\xi (\xi^0)^4 + \lambda_\chi |\chi^0|^4 + \lambda_{\phi\xi} |\phi^0|^2 (\xi^0)^2 + \lambda_{\chi\xi} |\chi^0|^2 (\xi^0)^2 \\ & + \left(\lambda_{\phi\chi} + \frac{\kappa_2}{2} \right) |\phi^0|^2 |\chi^0|^2 + \frac{\kappa_3}{\sqrt{2}} [(\phi^0)^2 \xi^0 \chi^{0*} + \text{h.c.}]. \end{aligned} \quad (\text{B6})$$

Following the methodology given in [85, 92], we define,

$$x = \sqrt{\frac{|\chi^0|^2}{(\xi^0)^2}} \in \mathbb{R}_+, \quad X = \frac{(\xi^0)^2}{|\phi^0|^2} \in \mathbb{R}_+, \quad \zeta = \frac{1}{2} \frac{[(\phi^0)^2 \xi^0 \chi^{0*} + \text{h.c.}]}{|\phi^0|^2 \sqrt{|\chi^0|^2 (\xi^0)^2}}, \quad (\text{B7})$$

where x , X , and ζ are three independent variables.¹³ The quartic potential in Eq. (B6) can be written as,

$$\frac{V^{(4)}}{|\phi^0|^4} = \lambda_\phi + \left(\lambda_{\phi\xi} + \sqrt{2}\kappa_3\zeta x + \left(\lambda_{\phi\chi} + \frac{\kappa_2}{2} \right) x^2 \right) X + \left(\lambda_\xi + \lambda_{\chi\xi}x^2 + \lambda_\chi x^4 \right) X^2, \quad (\text{B8})$$

where ζ takes the values $\zeta = 0, \pm 1$.¹⁴ The potential in Eq. (B6) is strictly copositive if and only if,

$$\begin{aligned} \lambda_\phi &> 0, & \lambda_\chi &> 0, & a_2 = \lambda_{\phi\xi} + 2\sqrt{\lambda_\phi\lambda_\xi} &> 0, \\ \lambda_\xi &> 0, & b_2 = \lambda_{\chi\xi} + 2\sqrt{\lambda_\chi\lambda_\xi} &> 0, & c_2 = 2\lambda_{\phi\chi} + \kappa_2 + 4\sqrt{\lambda_\phi\lambda_\chi} &> 0, \\ 2\lambda_{\phi\xi} + (2\lambda_{\phi\chi} + \kappa_2)x^2 - 2\sqrt{2}|\kappa_3|x + 4\sqrt{\lambda_\phi(\lambda_\xi + \lambda_{\chi\xi}x^2 + \lambda_\chi x^4)} &> 0, \\ 2\lambda_{\phi\xi}\sqrt{\lambda_\chi} + 2\lambda_{\chi\xi}\sqrt{\lambda_\phi} + (2\lambda_{\phi\chi} + \kappa_2)\sqrt{\lambda_\xi} + 4\sqrt{\lambda_\phi\lambda_\xi\lambda_\chi} + \sqrt{2a_2b_2c_2} &> 0. \end{aligned} \quad (\text{B9})$$

The condition given in the third line of Eq. (B9) contains a field dependent parameter, x . We check this condition numerically by scanning over the range of $x \in \mathbb{R}_+$. Considering all such directions with three simultaneously non-vanishing fields, we get a minimal set of necessary and sufficient 3-field BFB conditions:

$$\begin{aligned} \lambda_\phi &> 0, & \Lambda_1 = \lambda_{\phi\xi} + 2\sqrt{\lambda_\phi\lambda_\xi} &> 0, & \Lambda_2 = 2\lambda_{\chi\xi} + \kappa_1 + 4\sqrt{\lambda_\xi\lambda_\chi} &> 0, \\ \lambda_\xi &> 0, & \Lambda_3 = \lambda_{\chi\xi} + 2\sqrt{\lambda_\chi\lambda_\xi} &> 0, & \Lambda_4 = 2\lambda_{\phi\chi} + \kappa_2 + 4\sqrt{\lambda_\phi\lambda_\chi} &> 0, \\ \lambda_\chi &> 0, & \Lambda_5 = \lambda_\chi + 2\sqrt{\lambda_\chi(\lambda_\chi + \tilde{\lambda}_\chi)} &> 0, & \Lambda_6 = 2\lambda_{\phi\chi} - \kappa_2 + 4\sqrt{\lambda_\phi\lambda_\chi} &> 0, \\ \lambda_\chi + \tilde{\lambda}_\chi &> 0, & \Lambda_7 = \lambda_{\chi\xi} + 2\sqrt{\lambda_\xi(\lambda_\chi + \tilde{\lambda}_\chi)} &> 0, & \Lambda_8 = \lambda_{\phi\chi} + 2\sqrt{\lambda_\phi(\lambda_\chi + \tilde{\lambda}_\chi)} &> 0, \\ \Lambda_9 = \lambda_{\chi\xi} + \kappa_1 + 2\sqrt{\lambda_\xi(\lambda_\chi + \tilde{\lambda}_\chi)} &> 0, \\ 2\lambda_{\phi\chi}\sqrt{\lambda_\phi} + 4\lambda_\phi\sqrt{\lambda_\chi} + \sqrt{\lambda_\phi\Lambda_4\Lambda_6} &> 0, \\ 8\lambda_\xi\sqrt{\lambda_\chi} + (4\lambda_{\chi\xi} + \kappa_1)\sqrt{\lambda_\xi} + 2\sqrt{2\lambda_\xi\Lambda_2\Lambda_3} &> 0, \\ 4(\lambda_\chi + \tilde{\lambda}_\chi)\sqrt{\lambda_\xi} + (2\lambda_{\chi\xi} + \kappa_1)\sqrt{\lambda_\chi} + \Lambda_2\sqrt{\lambda_\chi + \tilde{\lambda}_\chi} &> 0, \\ \lambda_{\chi\xi}\sqrt{\lambda_\chi} + 2(\lambda_\chi + \tilde{\lambda}_\chi)\sqrt{\lambda_\xi} + \Lambda_3\sqrt{\lambda_\chi + \tilde{\lambda}_\chi} &> 0, \\ 4\lambda_\xi\sqrt{\lambda_\chi + \tilde{\lambda}_\chi} + (2\lambda_{\chi\xi} + \kappa_1)\sqrt{\lambda_\xi} + 2\sqrt{\lambda_\xi\Lambda_7\Lambda_9} &> 0, \\ \lambda_{\phi\xi}\sqrt{\lambda_\chi + \tilde{\lambda}_\chi} + \lambda_{\phi\chi}\sqrt{\lambda_\xi} + \Lambda_9\sqrt{\lambda_\phi} + \sqrt{\Lambda_1\Lambda_8\Lambda_9} &> 0, \end{aligned}$$

¹³ Here, the parameter, ζ can be seen as a cosine of angles in the field space.

¹⁴ It is worth to note that the parameter, ζ varies in the bounded domain, $\zeta \in [-1, 1]$, if we consider four fields at once.

$$\begin{aligned}
& \lambda_{\phi\xi}\sqrt{\lambda_\chi + \tilde{\lambda}_\chi} + \lambda_{\phi\chi}\sqrt{\lambda_\xi} + \Lambda_7\sqrt{\lambda_\phi} + \sqrt{\Lambda_1\Lambda_7\Lambda_8} > 0, \\
& \lambda_{\chi\xi}\sqrt{\lambda_\chi + \tilde{\lambda}_\chi} + 2\lambda_\chi\sqrt{\lambda_\xi} + \Lambda_9\sqrt{\lambda_\chi} + \sqrt{2\Lambda_3\Lambda_5\Lambda_9} > 0, \\
& 2\lambda_{\phi\chi}\sqrt{\lambda_\chi} + 4(\lambda_\chi + \tilde{\lambda}_\chi)\sqrt{\lambda_\phi} + \sqrt{\Lambda_4\Lambda_6(\lambda_\chi + \tilde{\lambda}_\chi)} > 0, \\
& 2\lambda_{\chi\xi}\sqrt{\lambda_\chi} + 4\lambda_\chi\sqrt{\lambda_\xi} + \Lambda_2\sqrt{\lambda_\chi + \tilde{\lambda}_\chi} + 2\sqrt{\Lambda_2\Lambda_5\Lambda_7} > 0, \\
& 2\lambda_{\phi\chi}\sqrt{\lambda_\chi} + 4\lambda_\chi\sqrt{\lambda_\phi} + \Lambda_4\sqrt{\lambda_\chi + \tilde{\lambda}_\chi} + 2\sqrt{\Lambda_4\Lambda_5\Lambda_8} > 0, \\
& 2\lambda_{\phi\xi}\sqrt{\lambda_\chi} + 4\lambda_\chi\sqrt{\lambda_\phi} + \Lambda_6\sqrt{\lambda_\chi + \tilde{\lambda}_\chi} + 2\sqrt{\Lambda_5\Lambda_6\Lambda_8} > 0, \\
& 2\lambda_{\phi\xi}\sqrt{\lambda_\chi} + (2\lambda_{\phi\chi} - \kappa_2)\sqrt{\lambda_\xi} + \Lambda_2\sqrt{\lambda_\phi} + \sqrt{\Lambda_1\Lambda_2\Lambda_6} > 0, \\
& 2\lambda_{\phi\xi}\sqrt{\lambda_\chi} + (2\lambda_{\phi\chi} + \kappa_2)\sqrt{\lambda_\xi} + \Lambda_2\sqrt{\lambda_\phi} + \sqrt{\Lambda_1\Lambda_2\Lambda_4} > 0, \\
& 2\lambda_{\phi\xi}\sqrt{\lambda_\chi} + (2\lambda_{\phi\chi} - \kappa_2)\sqrt{\lambda_\xi} + 2\Lambda_3\sqrt{\lambda_\phi} + \sqrt{2\Lambda_1\Lambda_3\Lambda_6} > 0, \\
& 2\lambda_{\phi\xi}\sqrt{\lambda_\chi} + (2\lambda_{\phi\chi} + \kappa_2)\sqrt{\lambda_\xi} + 2\Lambda_3\sqrt{\lambda_\phi} + \sqrt{2\Lambda_1\Lambda_3\Lambda_4} > 0, \\
& \lambda_{\phi\xi} + \lambda_{\phi\chi}x^2 - |\kappa_3|x + 2\sqrt{\lambda_\phi(\lambda_\xi + \lambda_{\chi\xi}x^2 + (\lambda_\chi + \tilde{\lambda}_\chi)x^4)} > 0, \\
& 2\lambda_{\phi\xi} + (2\lambda_{\phi\chi} + \kappa_2)x^2 - 2\sqrt{2}|\kappa_3|x + 4\sqrt{\lambda_\phi(\lambda_\xi + \lambda_{\chi\xi}x^2 + \lambda_\chi x^4)} > 0, \\
& 2\lambda_{\chi\xi} + \kappa_1 + (2\lambda_{\chi\xi} + \kappa_1)x^2 - 2|\kappa_1|x + 4\sqrt{\lambda_\xi(\lambda_\chi + (2\lambda_\chi + 4\tilde{\lambda}_\chi)x^2 + \lambda_\chi x^4)} > 0, \quad (\text{B10})
\end{aligned}$$

For the eGM model, the minimal set of necessary and sufficient 3-field BFB conditions read as,

$$\begin{aligned}
\lambda_\phi > 0, \quad \Sigma_1 = \lambda_{\phi\xi} + 2\sqrt{\lambda_\phi\lambda_\xi} > 0, \quad \Sigma_2 = 4\lambda_\chi - 8\lambda_\xi + \kappa_1 + 4\sqrt{\lambda_\xi\lambda_\chi} > 0, \\
\lambda_\xi > 0, \quad \lambda_\chi + \tilde{\lambda}_\chi > 0, \quad \Sigma_3 = 2\lambda_\chi - 4\lambda_\xi + 2\sqrt{\lambda_\chi\lambda_\xi} > 0, \\
\lambda_\chi > 0, \quad \Sigma_5 = \lambda_\chi + 2\sqrt{\lambda_\chi(\lambda_\chi + \tilde{\lambda}_\chi)} > 0, \quad \Sigma_4 = \sqrt{2}\kappa_3 + 4\left(\sqrt{\lambda_\chi\lambda_\phi} + \lambda_{\phi\xi}\right) > 0, \\
& \Sigma_6 = 4\left(\sqrt{\lambda_\chi\lambda_\phi} - \lambda_{\phi\xi} + \lambda_{\phi\chi}\right) - \sqrt{2}\kappa_3 > 0, \\
& \Sigma_7 = 2\lambda_\chi - 4\lambda_\xi + 2\sqrt{\lambda_\xi(\lambda_\chi + \tilde{\lambda}_\chi)} > 0, \\
& \Sigma_8 = \lambda_{\phi\chi} + 2\sqrt{\lambda_\phi(\lambda_\chi + \tilde{\lambda}_\chi)} > 0, \\
& \Sigma_9 = 2\lambda_\chi - 4\lambda_\xi + \kappa_1 + 2\sqrt{\lambda_\xi(\lambda_\chi + \tilde{\lambda}_\chi)} > 0, \\
& 2\lambda_{\phi\chi}\sqrt{\lambda_\phi} + 4\lambda_\phi\sqrt{\lambda_\chi} + \sqrt{\lambda_\phi\Sigma_4\Sigma_6} > 0, \\
& 8\lambda_\xi\sqrt{\lambda_\chi} + (8\lambda_\chi - 16\lambda_\xi) + \kappa_1)\sqrt{\lambda_\xi} + 2\sqrt{2\lambda_\xi\Sigma_2\Sigma_3} > 0, \\
& 4(\lambda_\chi + \tilde{\lambda}_\chi)\sqrt{\lambda_\xi} + (4\lambda_\chi - 8\lambda_\xi + \kappa_1)\sqrt{\lambda_\chi} + \Sigma_2\sqrt{\lambda_\chi + \tilde{\lambda}_\chi} > 0,
\end{aligned}$$

$$\begin{aligned}
& (2\lambda_\chi - 4\lambda_\xi)\sqrt{\lambda_\chi} + 2(\lambda_\chi + \tilde{\lambda}_\chi)\sqrt{\lambda_\xi} + \Sigma_3\sqrt{\lambda_\chi + \tilde{\lambda}_\chi} > 0, \\
& 4\lambda_\xi\sqrt{\lambda_\chi + \tilde{\lambda}_\chi} + (4\lambda_\chi - 8\lambda_\xi + \kappa_1)\sqrt{\lambda_\xi} + 2\sqrt{\lambda_\xi\Sigma_7\Sigma_9} > 0, \\
& \lambda_{\phi\xi}\sqrt{\lambda_\chi + \tilde{\lambda}_\chi} + \lambda_{\phi\chi}\sqrt{\lambda_\xi} + \Sigma_9\sqrt{\lambda_\phi} + \sqrt{\Sigma_1\Sigma_8\Sigma_9} > 0, \\
& \lambda_{\phi\xi}\sqrt{\lambda_\chi + \tilde{\lambda}_\chi} + \lambda_{\phi\chi}\sqrt{\lambda_\xi} + \Sigma_7\sqrt{\lambda_\phi} + \sqrt{\Sigma_1\Sigma_7\Sigma_8} > 0, \\
& (2\lambda_\chi - 4\lambda_\xi)\sqrt{\lambda_\chi + \tilde{\lambda}_\chi} + 2\lambda_\chi\sqrt{\lambda_\xi} + \Sigma_9\sqrt{\lambda_\chi} + \sqrt{2\Sigma_3\Sigma_5\Sigma_9} > 0, \\
& 2\lambda_{\phi\chi}\sqrt{\lambda_\chi} + 4(\lambda_\chi + \tilde{\lambda}_\chi)\sqrt{\lambda_\phi} + \sqrt{\Sigma_4\Sigma_6(\lambda_\chi + \tilde{\lambda}_\chi)} > 0, \\
& (4\lambda_\chi - 8\lambda_\xi)\sqrt{\lambda_\chi} + 4\lambda_\chi\sqrt{\lambda_\xi} + \Sigma_2\sqrt{\lambda_\chi + \tilde{\lambda}_\chi} + 2\sqrt{\Sigma_2\Sigma_5\Sigma_7} > 0, \\
& 2\lambda_{\phi\chi}\sqrt{\lambda_\chi} + 4\lambda_\chi\sqrt{\lambda_\phi} + \Sigma_4\sqrt{\lambda_\chi + \tilde{\lambda}_\chi} + 2\sqrt{\Sigma_4\Sigma_5\Sigma_8} > 0, \\
& 2\lambda_{\phi\chi}\sqrt{\lambda_\chi} + 4\lambda_\chi\sqrt{\lambda_\phi} + \Sigma_6\sqrt{\lambda_\chi + \tilde{\lambda}_\chi} + 2\sqrt{\Sigma_5\Sigma_6\Sigma_8} > 0, \\
& 2\lambda_{\phi\xi}\sqrt{\lambda_\chi} + (4\lambda_{\phi\chi} - \sqrt{2}\kappa_3 - 4\lambda_{\phi\xi})\sqrt{\lambda_\xi} + \Sigma_2\sqrt{\lambda_\phi} + \sqrt{\Sigma_1\Sigma_2\Sigma_6} > 0, \\
& 2\lambda_{\phi\xi}\sqrt{\lambda_\chi} + (\sqrt{2}\kappa_3 + 4\lambda_{\phi\xi})\sqrt{\lambda_\xi} + \Sigma_2\sqrt{\lambda_\phi} + \sqrt{\Sigma_1\Sigma_2\Sigma_4} > 0, \\
& 2\lambda_{\phi\xi}\sqrt{\lambda_\chi} + (4\lambda_{\phi\chi} - \sqrt{2}\kappa_3 - 4\lambda_{\phi\xi})\sqrt{\lambda_\xi} + 2\Sigma_3\sqrt{\lambda_\phi} + \sqrt{2\Sigma_1\Sigma_3\Sigma_6} > 0, \\
& 2\lambda_{\phi\xi}\sqrt{\lambda_\chi} + (\sqrt{2}\kappa_3 + 4\lambda_{\phi\xi})\sqrt{\lambda_\xi} + 2\Sigma_3\sqrt{\lambda_\phi} + \sqrt{2\Sigma_1\Sigma_3\Sigma_4} > 0, \\
& \lambda_{\phi\xi} + \lambda_{\phi\chi}x^2 - |\kappa_3|x + 2\sqrt{\lambda_\phi(\lambda_\xi + (2\lambda_\chi - 4\lambda_\xi)x^2 + (\lambda_\chi + \tilde{\lambda}_\chi)x^4)} > 0, \\
& 2\lambda_{\phi\xi} + (\sqrt{2}\kappa_3 + 4\lambda_{\phi\xi})x^2 - 2\sqrt{2}|\kappa_3|x + 4\sqrt{\lambda_\phi(\lambda_\xi + (2\lambda_\chi - 4\lambda_\xi)x^2 + \lambda_\chi x^4)} > 0, \\
& 4\lambda_\chi - 8\lambda_\xi + \kappa_1 + (4\lambda_\chi - 8\lambda_\xi + \kappa_1)x^2 - 2|\kappa_1|x + 4\sqrt{\lambda_\xi(\lambda_\chi + (2\lambda_\chi + 4\tilde{\lambda}_\chi)x^2 + \lambda_\chi x^4)} > 0, \tag{B11}
\end{aligned}$$

In case of the GM model, we get the following 3-field BFB conditions:

$$\begin{aligned}
& \lambda_1 > 0, \quad \Omega_1 = 2\sqrt{\lambda_1(\lambda_2 + \lambda_3)} + \lambda_4 > 0, \quad \Omega_4 = 4\sqrt{\lambda_1(4\lambda_2 + 2\lambda_3)} + 4\lambda_4 + \lambda_5 > 0, \\
& \lambda_2 + \lambda_3 > 0, \quad 2\lambda_2 + \lambda_3 > 0, \quad \Omega_6 = 4\sqrt{\lambda_1(4\lambda_2 + 2\lambda_3)} + 4\lambda_4 - \lambda_5 > 0, \\
& \Omega_2 = \sqrt{(\lambda_2 + \lambda_3)(4\lambda_2 + 2\lambda_3)} + 2\lambda_2 + \lambda_3 > 0, \\
& \Omega_3 = \sqrt{(\lambda_2 + \lambda_3)(4\lambda_2 + 2\lambda_3)} + 2\lambda_2 > 0, \\
& 16\sqrt{4\lambda_2 + 2\lambda_3}\lambda_1 + 16\sqrt{\lambda_1}\lambda_4 + 4\sqrt{\lambda_1\Omega_4\Omega_6} > 0,
\end{aligned}$$

$$\begin{aligned}
& 8\sqrt{4\lambda_2 + 2\lambda_3}(\lambda_2 + \lambda_3) + 4\sqrt{\lambda_2 + \lambda_3}(4\lambda_2 + \lambda_3) + 8\sqrt{(\lambda_2 + \lambda_3)\Omega_2\Omega_3} > 0, \\
& 4(\lambda_2 + \lambda_3)^{3/2} + \sqrt{2}(2\lambda_2 + \lambda_3)^{3/2} + 2\sqrt{\lambda_2 + \lambda_3}\Omega_2 > 0, \\
& 8(\lambda_2 + \lambda_3)^{3/2} + 4\sqrt{4\lambda_2 + 2\lambda_3}\lambda_2 + 4\sqrt{\lambda_2 + \lambda_3}\Omega_3 > 0, \\
& 16\sqrt{\lambda_2 + \lambda_3}\lambda_2 + 12\sqrt{\lambda_2 + \lambda_3}\lambda_3 + 8\sqrt{2}\sqrt{2\lambda_2 + \lambda_3}(\lambda_2 + \lambda_3) > 0, \\
& 8\lambda_4\sqrt{\lambda_2 + \lambda_3} + 2\sqrt{\lambda_1}(\lambda_2 + \lambda_3) + \sqrt{\lambda_2 + \lambda_3}\Omega_1 > 0, \\
& 8\sqrt{\lambda_1}(2\lambda_2 + \lambda_3) + 8\sqrt{\lambda_2 + \lambda_3}\lambda_4 + 4\sqrt{4\lambda_2 + 2\lambda_3}\Omega_1 > 0, \\
& 4\sqrt{\lambda_2 + \lambda_3}(4\lambda_2 + \lambda_3) + 8\sqrt{4\lambda_2 + 2\lambda_3}(\lambda_2 + \lambda_3) + 8\sqrt{(\lambda_2 + \lambda_3)\Omega_2\Omega_3} > 0, \\
& 8\sqrt{\lambda_1}(\lambda_2 + \lambda_3) + 2\sqrt{4\lambda_2 + 2\lambda_3}\lambda_4 + \sqrt{(\lambda_2 + \lambda_3)\Omega_4\Omega_6} > 0, \\
& (2\lambda_2 + \lambda_3)\sqrt{\lambda_2 + \lambda_3} + \sqrt{4\lambda_2 + 2\lambda_3}\lambda_2 + \sqrt{\lambda_2 + \lambda_3}\Omega_2 + \sqrt{4\lambda_2 + 2\lambda_3}\Omega_2 > 0, \\
& 16\sqrt{\lambda_1}(2\lambda_2 + \lambda_3) + 8\sqrt{4\lambda_2 + 2\lambda_3}\lambda_4 + 8\sqrt{\Omega_1\Omega_2\Omega_4} + 4\sqrt{\lambda_2 + \lambda_3}\Omega_4 > 0, \\
& 16\sqrt{\lambda_1}(2\lambda_2 + \lambda_3) + 8\sqrt{4\lambda_2 + 2\lambda_3}\lambda_4 + 8\sqrt{\Omega_1\Omega_2\Omega_6} + 4\sqrt{\lambda_2 + \lambda_3}\Omega_6 > 0, \\
& 4\sqrt{4\lambda_2 + 2\lambda_3}\lambda_4 + \sqrt{\lambda_2 + \lambda_3}(8\lambda_4 - 2\lambda_5) + 4\sqrt{\Omega_1\Omega_2\Omega_6} + 8\sqrt{\lambda_1}\Omega_2 > 0, \\
& 4\sqrt{4\lambda_2 + 2\lambda_3}\lambda_4 + 2\sqrt{\lambda_2 + \lambda_3}(4\lambda_4 + \lambda_5) + 4\sqrt{\Omega_1\Omega_2\Omega_4} + 8\sqrt{\lambda_1}\Omega_2 > 0, \\
& 4\sqrt{4\lambda_2 + 2\lambda_3}\lambda_4 + \sqrt{\lambda_2 + \lambda_3}(8\lambda_4 - 2\lambda_5) + 4\sqrt{\Omega_1\Omega_3\Omega_6} + 8\sqrt{\lambda_1}\Omega_3 > 0, \\
& 4\sqrt{4\lambda_2 + 2\lambda_3}\lambda_4 + 2\sqrt{\lambda_2 + \lambda_3}(4\lambda_4 + \lambda_5) + 4\sqrt{\Omega_1\Omega_3\Omega_4} + 8\sqrt{\lambda_1}\Omega_3 > 0, \\
& \lambda_4(4x^2 + 2) + 4\sqrt{\lambda_1\left(\lambda_3(4x^4 + 1) + \lambda_2(2x^2 + 1)^2\right)} - \sqrt{2}|\lambda_5|x > 0, \\
& 4\lambda_4 + 2(4\lambda_4 + \lambda_5)x^2 + 8\sqrt{\lambda_1\left(\lambda_3(2x^4 + 1) + \lambda_2(2x^2 + 1)^2\right)} - 4|\lambda_5|x > 0, \\
& (2\lambda_2 + \lambda_3)(x^2 + 1) + \sqrt{2(\lambda_2 + \lambda_3)\left(2\lambda_2(x^2 + 1)^2 + \lambda_3(x^4 + 6x^2 + 1)\right)} - 2|\lambda_3|x > 0,
\end{aligned} \tag{B12}$$

Appendix C: Necessary and sufficient bounded-from-below conditions

In general, the above BFB conditions for specific field directions are necessary but not sufficient to ensure boundedness of the scalar potential of the GM and the eGM models. To obtain the necessary and sufficient BFB conditions, one need to consider all the field directions simultaneously in the field space. The necessary and sufficient BFB conditions considering all 13-field directions for the GM model is given in Refs. [28, 77], while Ref. [77] also provides the necessary and sufficient BFB conditions considering all 13-field directions for the most general two-triplet model as given in Eq. (13). To obtain all 13-field BFB conditions for the eGM model, we follow the approach of Ref. [77]. We parameterize the scalar quartic

potential in Eq. (13) by considering a number of dimensionless ratio of invariants,

$$\begin{aligned}\zeta_1 &= \frac{|\tilde{\chi}^\dagger \chi|^2}{(\chi^\dagger \chi)^2}, & \zeta_2 &= \frac{(\phi^\dagger \tau_a \phi)(\chi^\dagger t_a \chi)}{(\phi^\dagger \phi)(\chi^\dagger \chi)}, \\ \zeta_3 &= \frac{|\xi^\dagger \chi|^2}{(\chi^\dagger \chi)(\xi^\dagger \xi)}, & \zeta_4 &= \frac{[(\phi^T \epsilon \tau_a \phi)(\chi^\dagger t_a \xi) + \text{h.c.}]}{(\phi^\dagger \phi) \sqrt{(\chi^\dagger \chi)(\xi^\dagger \xi)}} ,\end{aligned}\quad (\text{C1})$$

where

$$\zeta_1 \in [0, 1], \quad \zeta_2 \in [-1/2, 1/2], \quad \zeta_3 \in [0, 1], \quad \zeta_4 \in [-\sqrt{2}, \sqrt{2}].$$

Following Ref. [77], we obtain the necessary and sufficient 13-field BFB conditions for the eGM model,

$$\begin{aligned}\lambda_\phi > 0, \quad \lambda_\xi > 0, \quad \lambda_\chi > 0, \quad \lambda_\chi + \tilde{\lambda}_\chi > 0, \quad \zeta_3 \kappa_1 + 2\lambda_\chi - 4\lambda_\xi + 2\sqrt{\lambda_\xi (\zeta_1 \tilde{\lambda}_\chi + \lambda_\chi)} > 0, \\ \lambda_{\phi\xi} + x\kappa_3 (\sqrt{2}\zeta_2 x + \zeta_4) + 4x^2 \zeta_2 \lambda_{\phi\xi} + (1 - 2\zeta_2)x^2 \lambda_{\phi\chi} \\ + 2\sqrt{\lambda_\phi (\lambda_\xi + x^4 \zeta_1 \tilde{\lambda}_\chi + x^2 (\zeta_3 \kappa_1 - 4\lambda_\xi) + (x^4 + 2x^2) \lambda_\chi)} > 0,\end{aligned}\quad (\text{C2})$$

where $x (\equiv \sqrt{\chi^\dagger \chi / \xi^\dagger \xi}) \in \mathbb{R}_+$. Note that, the parameters ζ_i ($i = 1, \dots, 4$) are correlated. Despite considering the entire four-dimensional domain of the ζ -parameter space, we show the six possible projected planes. The boundary curves in the ζ_i vs. ζ_j planes are listed in Table VI, and their allowed domains are displayed in Figure 10. In numerical analysis, while considering the 13-field BFB conditions, we scan over the allowed parameter spaces of ζ_i 's and x for given model parameters.

Appendix D: Results for one-loop scattering amplitudes

For a given process, $i \rightarrow f$, the amplitudes given in this Appendix correspond to $256\pi^3 (a_0)_{i,f}$. In these amplitudes, the contributions from wave function renormalization are not considered. Therefore, all of the scattering amplitudes form a block diagonal structure in the S -matrix of $2 \rightarrow 2$ scattering. We have cross-checked our results by generating amplitudes using **FeynRules-2.3** [109] and **FeynArts-3.11** [110].

- $\mathbf{Q} = \mathbf{0}, \mathbf{Y} = \mathbf{0}$:

$$\begin{aligned}\phi^{0*} \phi^0 \rightarrow \phi^{0*} \phi^0 &= -64\pi^2 \lambda_\phi + 12\beta_{\lambda_\phi} + (i\pi - 1) \left[20\lambda_\phi^2 + 6\lambda_{\phi\xi}^2 + 3\lambda_{\phi\chi}^2 + \frac{1}{2}\kappa_2^2 \right], \\ \phi^{0*} \phi^0 \rightarrow \chi^{0*} \chi^0 &= -16\pi^2 \left(\lambda_{\phi\chi} + \frac{1}{2}\kappa_2 \right) + 3 \left(\beta_{\lambda_{\phi\chi}} + \frac{1}{2}\beta_{\kappa_2} \right) + (i\pi - 1) \left[2\lambda_{\phi\xi} (\kappa_1 + 3\lambda_{\chi\xi}) \right. \\ &\quad \left. + \kappa_2 (\lambda_\phi + \lambda_\chi - 2\tilde{\lambda}_\chi) + 2\lambda_{\phi\chi} (3\lambda_\phi + 4\lambda_\chi + 2\tilde{\lambda}_\chi) \right],\end{aligned}$$

| Projected planes | Boundary curves |
|-------------------------|--|
| ζ_1 vs. ζ_2 | (i) $0 \leq \zeta_1 \leq 1 - 4\zeta_2^2$, $\forall \zeta_2 \in [-\frac{1}{2}, \frac{1}{2}]$. |
| ζ_1 vs. ζ_3 | (i) $\zeta_3 = 0$, $\forall \zeta_1 \in [0, 1]$. (ii) $\zeta_1 = 1$, $\forall \zeta_3 \in [0, 1]$. (iii) $\zeta_1 = 0$, $\forall \zeta_3 \in [0, \frac{1}{2}]$. (iv) $\zeta_1 = 1 - 4\zeta_3(1 - \zeta_3)$, $\forall \zeta_3 \in [\frac{1}{2}, 1]$. |
| ζ_1 vs. ζ_4 | (i) $\zeta_1 = 0$, $\forall \zeta_4 \in [-\sqrt{2}, \sqrt{2}]$. (ii) $\zeta_1 = 1$, $\forall \zeta_4 \in [-1, 1]$. (iii) $\zeta_1 = 2\zeta_4^2 - \zeta_4^4$, $\forall \zeta_4 \in [-\sqrt{2}, -1) \cup (1, \sqrt{2}]$. |
| ζ_2 vs. ζ_3 | (i) $\zeta_2 = -\frac{1}{2}$, $\forall \zeta_3 \in [0, \frac{1}{2}]$. (ii) $\zeta_2 = \frac{1}{2}$, $\forall \zeta_3 \in [0, \frac{1}{2}]$. (iii) $\zeta_3 = 0$, $\forall \zeta_2 \in [-\frac{1}{2}, \frac{1}{2}]$. (iv) $\zeta_3 = \frac{1}{2} + \sqrt{\frac{1}{4} - \zeta_2^2}$, $\forall \zeta_2 \in [-\frac{1}{2}, \frac{1}{2}]$. |
| ζ_2 vs. ζ_4 | (i) $\zeta_2 = \frac{1}{2}$. (ii) $\zeta_2 = \frac{1}{2}(\zeta_4^2 - 1)$, $\forall \zeta_4 \in [-\sqrt{2}, \sqrt{2}]$ |
| ζ_3 vs. ζ_4 | (i) $0 \leq \zeta_3 \leq 1 - \frac{1}{2}\zeta_4^2$, $\forall \zeta_4 \in [-\sqrt{2}, \sqrt{2}]$. |

TABLE VI. Boundary curves in the six projected planes of the ζ -parameter space [77].

$$\phi^{0*}\phi^0 \rightarrow \phi^+\phi^- = -32\pi^2\lambda_\phi + 6\beta_{\lambda_\phi} + (i\pi - 1) \left[16\lambda_\phi^2 + 6\lambda_{\phi\xi}^2 + 3\lambda_{\phi\chi}^2 - \frac{1}{2}\kappa_2^2 \right],$$

$$\begin{aligned} \phi^{0*}\phi^0 \rightarrow \xi^+\xi^- = & -32\pi^2\lambda_{\phi\xi} + 6\beta_{\lambda_{\phi\xi}} \\ & + 2(i\pi - 1) \left[20\lambda_\xi\lambda_{\phi\xi} + 6\lambda_\phi\lambda_{\phi\xi} + \lambda_{\phi\chi}(\kappa_1 + 3\lambda_{\chi\xi}) \right], \end{aligned}$$

$$\begin{aligned} \phi^{0*}\phi^0 \rightarrow \chi^+\chi^- = & -16\pi^2\lambda_{\phi\chi} + 3\beta_{\lambda_{\phi\chi}} \\ & + (i\pi - 1) \left[2\lambda_{\phi\chi} \left(2\tilde{\lambda}_\chi + 4\lambda_\chi + 3\lambda_\phi \right) + 2\lambda_{\phi\xi}(\kappa_1 + 3\lambda_{\chi\xi}) \right], \end{aligned}$$

$$\begin{aligned} \chi^{0*}\chi^0 \rightarrow \phi^{0*}\phi^0 &= \phi^{0*}\phi^0 \rightarrow \chi^{0*}\chi^0, \\ \phi^+\phi^- \rightarrow \phi^{0*}\phi^0 &= \phi^{0*}\phi^0 \rightarrow \phi^+\phi^-, \\ \xi^+\xi^- \rightarrow \phi^{0*}\phi^0 &= \phi^{0*}\phi^0 \rightarrow \xi^+\xi^-, \\ \chi^+\chi^- \rightarrow \phi^{0*}\phi^0 &= \phi^{0*}\phi^0 \rightarrow \chi^+\chi^-, \end{aligned}$$

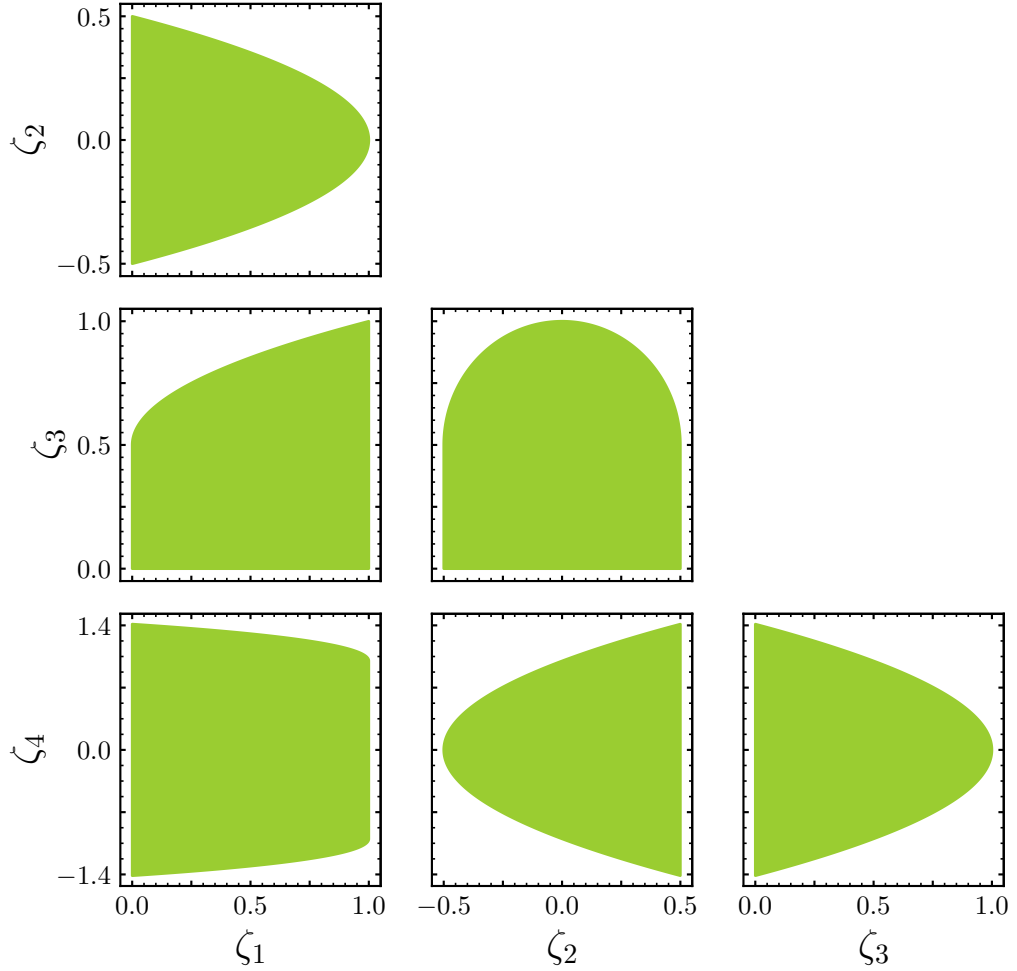


FIG. 10. The green region manifests allowed ζ -parameter space onto the projected planes.

$$\begin{aligned}
\phi^{0*}\phi^0 \rightarrow \frac{1}{\sqrt{2}}(\xi^0\xi^0) = & -16\sqrt{2}\pi^2\lambda_{\phi\xi} + 3\sqrt{2}\beta_{\lambda_{\phi\xi}} \\
& + \sqrt{2}(i\pi - 1)\left[6\lambda_\phi\lambda_{\phi\xi} + \lambda_{\phi\chi}(\kappa_1 + 3\lambda_{\chi\xi}) + 20\lambda_{\phi\xi}\lambda_\xi\right], \\
\phi^{0*}\phi^0 \rightarrow \chi^{++}\chi^{--} = & -16\pi^2\left(\lambda_{\phi\chi} - \frac{1}{2}\kappa_2\right) + 3\left(\beta_{\lambda_{\phi\chi}} - \frac{1}{2}\beta_{\kappa_2}\right) + (i\pi - 1)\left[2\lambda_{\phi\xi}(\kappa_1\right. \\
& \left.+ 3\lambda_{\chi\xi}) + \kappa_2(2\tilde{\lambda}_\chi - \lambda_\chi - \lambda_\phi) + 2\lambda_{\phi\chi}(2\tilde{\lambda}_\chi + 4\lambda_\chi + 3\lambda_\phi)\right],
\end{aligned}$$

$$\begin{aligned}
\frac{1}{\sqrt{2}}(\xi^0\xi^0) \rightarrow \phi^{0*}\phi^0 = \phi^{0*}\phi^0 \rightarrow \frac{1}{\sqrt{2}}(\xi^0\xi^0), \\
\chi^{++}\chi^{--} \rightarrow \phi^{0*}\phi^0 = \phi^{0*}\phi^0 \rightarrow \chi^{++}\chi^{--},
\end{aligned}$$

$$\begin{aligned}
\frac{1}{\sqrt{2}}(\xi^0\xi^0) \rightarrow \frac{1}{\sqrt{2}}(\xi^0\xi^0) = & -192\pi^2\lambda_\xi + 36\beta_{\lambda_\xi} + 2(i\pi - 1) \left[2\kappa_1\lambda_{\chi\xi} \right. \\
& \left. + \kappa_1^2 + 88\lambda_\xi^2 + 3\lambda_{\chi\xi}^2 + 2\lambda_{\phi\xi}^2 \right], \\
\frac{1}{\sqrt{2}}(\xi^0\xi^0) \rightarrow \chi^{0*}\chi^0 = & -16\sqrt{2}\pi^2\lambda_{\chi\xi} + 3\sqrt{2}\beta_{\lambda_{\chi\xi}} + 2\sqrt{2}(i\pi - 1) \left[2\lambda_{\chi\xi} \left(\tilde{\lambda}_\chi \right. \right. \\
& \left. \left. + 5\lambda_\xi + 2\lambda_\chi \right) + \kappa_1(2\lambda_\xi + \lambda_\chi) + \lambda_{\phi\xi}\lambda_{\phi\chi} \right], \\
\frac{1}{\sqrt{2}}(\xi^0\xi^0) \rightarrow \chi^{++}\chi^{--} = & -16\sqrt{2}\pi^2\lambda_{\chi\xi} + 3\sqrt{2}\beta_{\lambda_{\chi\xi}} + 2\sqrt{2}(i\pi - 1) \left[\lambda_{\phi\xi}\lambda_{\phi\chi} \right. \\
& \left. + 2\lambda_{\chi\xi} \left(\tilde{\lambda}_\chi + 5\lambda_\xi + 2\lambda_\chi \right) + \kappa_1(2\lambda_\xi + \lambda_\chi) \right],
\end{aligned}$$

$$\begin{aligned}
\chi^{0*}\chi^0 \rightarrow \frac{1}{\sqrt{2}}(\xi^0\xi^0) = & \frac{1}{\sqrt{2}}(\xi^0\xi^0) \rightarrow \chi^{0*}\chi^0, \\
\chi^{++}\chi^{--} \rightarrow \frac{1}{\sqrt{2}}(\xi^0\xi^0) = & \frac{1}{\sqrt{2}}(\xi^0\xi^0) \rightarrow \chi^{++}\chi^{--},
\end{aligned}$$

$$\begin{aligned}
\frac{1}{\sqrt{2}}(\xi^0\xi^0) \rightarrow \phi^+\phi^- = & -16\sqrt{2}\pi^2\lambda_{\phi\xi} + 3\sqrt{2}\beta_{\lambda_{\phi\xi}} \\
& + \sqrt{2}(i\pi - 1) \left[\lambda_{\phi\chi}(\kappa_1 + 3\lambda_{\chi\xi}) + 20\lambda_\xi\lambda_{\phi\xi} + 6\lambda_\phi\lambda_{\phi\xi} \right], \\
\frac{1}{\sqrt{2}}(\xi^0\xi^0) \rightarrow \xi^+\xi^- = & -64\sqrt{2}\pi^2\lambda_\xi + 12\sqrt{2}\beta_{\lambda_\xi} \\
& + 2\sqrt{2}(i\pi - 1) \left[\lambda_{\chi\xi}(2\kappa_1 + 3\lambda_{\chi\xi}) + 56\lambda_\xi^2 + 2\lambda_{\phi\xi}^2 \right], \\
\frac{1}{\sqrt{2}}(\xi^0\xi^0) \rightarrow \chi^+\chi^- = & -16\sqrt{2}\pi^2(\kappa_1 + \lambda_{\chi\xi}) + 3\sqrt{2}(\beta_{\kappa_1} + \beta_{\lambda_{\chi\xi}}) + \sqrt{2}(i\pi - 1) \left[2\lambda_{\phi\xi}\lambda_{\phi\chi} \right. \\
& \left. + 4\kappa_1(\tilde{\lambda}_\chi + 3\lambda_\xi + \lambda_\chi) + 4\lambda_{\chi\xi}(\tilde{\lambda}_\chi + 5\lambda_\xi + 2\lambda_\chi) \right],
\end{aligned}$$

$$\begin{aligned}
\phi^+\phi^- \rightarrow \frac{1}{\sqrt{2}}(\xi^0\xi^0) = & \frac{1}{\sqrt{2}}(\xi^0\xi^0) \rightarrow \phi^+\phi^-, \\
\xi^+\xi^- \rightarrow \frac{1}{\sqrt{2}}(\xi^0\xi^0) = & \frac{1}{\sqrt{2}}(\xi^0\xi^0) \rightarrow \xi^+\xi^-, \\
\chi^+\chi^- \rightarrow \frac{1}{\sqrt{2}}(\xi^0\xi^0) = & \frac{1}{\sqrt{2}}(\xi^0\xi^0) \rightarrow \chi^+\chi^-,
\end{aligned}$$

$$\begin{aligned}
\chi^{0*}\chi^0 \rightarrow \chi^{0*}\chi^0 &= -64\pi^2\lambda_\chi + 12\beta_{\lambda_\chi} + (i\pi - 1) \left[4\kappa_1\lambda_{\chi\xi} \right. \\
&\quad \left. + 2 \left(8\tilde{\lambda}_\chi^2 + 8\lambda_\chi\tilde{\lambda}_\chi + 12\lambda_\chi^2 + 3\lambda_{\chi\xi}^2 + \lambda_{\phi\chi}^2 \right) + \kappa_1^2 + \frac{1}{2}\kappa_2^2 \right], \\
\chi^{0*}\chi^0 \rightarrow \phi^+\phi^- &= -16\pi^2 \left(\lambda_{\phi\chi} - \frac{1}{2}\kappa_2 \right) + 3 \left(\beta_{\lambda_{\phi\chi}} - \frac{1}{2}\beta_{\kappa_2} \right) + (i\pi - 1) \left[2\lambda_{\phi\xi}(\kappa_1 \right. \\
&\quad \left. + 3\lambda_{\chi\xi}) + \kappa_2 \left(2\tilde{\lambda}_\chi - \lambda_\chi - \lambda_\phi \right) + 2\lambda_{\phi\chi} \left(2\tilde{\lambda}_\chi + 4\lambda_\chi + 3\lambda_\phi \right) \right], \\
\chi^{0*}\chi^0 \rightarrow \xi^+\xi^- &= -16\pi^2 (\kappa_1 + 2\lambda_{\chi\xi}) + 3 \left(\beta_{\kappa_1} + 2\beta_{\lambda_{\chi\xi}} \right) + (i\pi - 1) \left[4\lambda_{\phi\xi}\lambda_{\phi\chi} \right. \\
&\quad \left. + 2\kappa_1 \left(2\tilde{\lambda}_\chi + 8\lambda_\xi + 3\lambda_\chi \right) + 8\lambda_{\chi\xi} \left(\tilde{\lambda}_\chi + 5\lambda_\xi + 2\lambda_\chi \right) \right], \\
\chi^{0*}\chi^0 \rightarrow \chi^+\chi^- &= -32\pi^2\lambda_\chi + 6\beta_{\lambda_\chi} + 2(i\pi - 1) \left[8\lambda_\chi\tilde{\lambda}_\chi \right. \\
&\quad \left. + \lambda_{\chi\xi} (2\kappa_1 + 3\lambda_{\chi\xi}) + 10\lambda_\chi^2 + \lambda_{\phi\chi}^2 \right], \\
\chi^{0*}\chi^0 \rightarrow \chi^{++}\chi^{--} &= -32\pi^2 \left(2\tilde{\lambda}_\chi + \lambda_\chi \right) + 6 \left(2\beta_{\tilde{\lambda}_\chi} + \beta_{\lambda_\chi} \right) + (i\pi - 1) \left[4\kappa_1\lambda_{\chi\xi} \right. \\
&\quad \left. + 4\lambda_\chi \left(8\tilde{\lambda}_\chi + 5\lambda_\chi \right) + \kappa_1^2 - \frac{\kappa_2^2}{2} + 6\lambda_{\chi\xi}^2 + 2\lambda_{\phi\chi}^2 \right],
\end{aligned}$$

$$\begin{aligned}
\phi^+\phi^- \rightarrow \chi^{0*}\chi^0 &= \chi^{0*}\chi^0 \rightarrow \phi^+\phi^-, \\
\xi^+\xi^- \rightarrow \chi^{0*}\chi^0 &= \chi^{0*}\chi^0 \rightarrow \xi^+\xi^-, \\
\chi^+\chi^- \rightarrow \chi^{0*}\chi^0 &= \chi^{0*}\chi^0 \rightarrow \chi^+\chi^-, \\
\chi^{++}\chi^{--} \rightarrow \chi^{0*}\chi^0 &= \chi^{0*}\chi^0 \rightarrow \chi^{++}\chi^{--},
\end{aligned}$$

$$\begin{aligned}
\phi^+\phi^- \rightarrow \phi^+\phi^- &= -64\pi^2\lambda_\phi + 12\beta_{\lambda_\phi} + (i\pi - 1) \left[20\lambda_\phi^2 + 6\lambda_{\phi\xi}^2 + 3\lambda_{\phi\chi}^2 + \frac{1}{2}\kappa_2^2 \right], \\
\phi^+\phi^- \rightarrow \xi^+\xi^- &= -32\pi^2\lambda_{\phi\xi} + 6\beta_{\lambda_{\phi\xi}} \\
&\quad + 2(i\pi - 1) \left[\lambda_{\phi\chi} (\kappa_1 + 3\lambda_{\chi\xi}) + 20\lambda_\xi\lambda_{\phi\xi} + 6\lambda_\phi\lambda_{\phi\xi} \right], \\
\phi^+\phi^- \rightarrow \chi^+\chi^- &= -16\pi^2\lambda_{\phi\chi} + 3\beta_{\lambda_{\phi\chi}} \\
&\quad + (i\pi - 1) \left[2\lambda_{\phi\chi} \left(2\tilde{\lambda}_\chi + 4\lambda_\chi + 3\lambda_\phi \right) + 2\lambda_{\phi\xi} (\kappa_1 + 3\lambda_{\chi\xi}) \right], \\
\phi^+\phi^- \rightarrow \chi^{++}\chi^{--} &= -16\pi^2 \left(\frac{1}{2}\kappa_2 + \lambda_{\phi\chi} \right) + 3 \left(\frac{1}{2}\beta_{\kappa_2} + \beta_{\lambda_{\phi\chi}} \right) + (i\pi - 1) \left[2\lambda_{\phi\xi}(\kappa_1 \right. \\
&\quad \left. + 3\lambda_{\chi\xi}) + \kappa_2 \left(-2\tilde{\lambda}_\chi + \lambda_\chi + \lambda_\phi \right) + 2\lambda_{\phi\chi} \left(2\tilde{\lambda}_\chi + 4\lambda_\chi + 3\lambda_\phi \right) \right],
\end{aligned}$$

$$\begin{aligned}
\xi^+\xi^- \rightarrow \phi^+\phi^- &= \phi^+\phi^- \rightarrow \xi^+\xi^-, \\
\chi^+\chi^- \rightarrow \phi^+\phi^- &= \phi^+\phi^- \rightarrow \chi^+\chi^-, \\
\chi^{++}\chi^{--} \rightarrow \phi^+\phi^- &= \phi^+\phi^- \rightarrow \chi^{++}\chi^{--},
\end{aligned}$$

$$\begin{aligned}
\xi^+ \xi^- \rightarrow \xi^+ \xi^- &= -256\pi^2 \lambda_\xi + 48\beta_{\lambda_\xi} + (i\pi - 1) \left[2(\kappa_1 + 2\lambda_{\chi\xi})^2 \right. \\
&\quad \left. + 288\lambda_\xi^2 + 4\lambda_{\chi\xi}^2 + 8\lambda_{\phi\xi}^2 \right], \\
\xi^+ \xi^- \rightarrow \chi^+ \chi^- &= -32\pi^2 \lambda_{\chi\xi} + 6\beta_{\lambda_{\chi\xi}} \\
&\quad + 4(i\pi - 1) \left[2\lambda_{\chi\xi} (\tilde{\lambda}_\chi + 5\lambda_\xi + 2\lambda_\chi) + \kappa_1 (2\lambda_\xi + \lambda_\chi) + \lambda_{\phi\xi} \lambda_{\phi\chi} \right], \\
\xi^+ \xi^- \rightarrow \chi^{++} \chi^{--} &= -16\pi^2 (\kappa_1 + 2\lambda_{\chi\xi}) + 3(\beta_{\kappa_1} + 2\beta_{\lambda_{\chi\xi}}) + (i\pi - 1) \left[4\lambda_{\phi\xi} \lambda_{\phi\chi} \right. \\
&\quad \left. + 2\kappa_1 (2\tilde{\lambda}_\chi + 8\lambda_\xi + 3\lambda_\chi) + 8\lambda_{\chi\xi} (\tilde{\lambda}_\chi + 5\lambda_\xi + 2\lambda_\chi) \right],
\end{aligned}$$

$$\begin{aligned}
\chi^+ \chi^- \rightarrow \xi^+ \xi^- &= \xi^+ \xi^- \rightarrow \chi^+ \chi^-, \\
\chi^{++} \chi^{--} \rightarrow \xi^+ \xi^- &= \xi^+ \xi^- \rightarrow \chi^{++} \chi^{--},
\end{aligned}$$

$$\begin{aligned}
\chi^+ \chi^- \rightarrow \chi^+ \chi^- &= -64\pi^2 (\tilde{\lambda}_\chi + \lambda_\chi) + 12(\beta_{\tilde{\lambda}_\chi} + \beta_{\lambda_\chi}) + 2(i\pi - 1) \left[8(\tilde{\lambda}_\chi + \lambda_\chi)^2 \right. \\
&\quad \left. + (\kappa_1 + \lambda_{\chi\xi})^2 + 4\lambda_\chi^2 + 2\lambda_{\chi\xi}^2 + \lambda_{\phi\chi}^2 \right], \\
\chi^+ \chi^- \rightarrow \chi^{++} \chi^{--} &= -32\pi^2 \lambda_\chi + 6\beta_{\lambda_\chi} + 2(i\pi - 1) \left[8\lambda_\chi \tilde{\lambda}_\chi + 10\lambda_\chi^2 \right. \\
&\quad \left. + \lambda_{\chi\xi} (2\kappa_1 + 3\lambda_{\chi\xi}) + \lambda_{\phi\chi}^2 \right],
\end{aligned}$$

$$\chi^{++} \chi^{--} \rightarrow \chi^+ \chi^- = \chi^+ \chi^- \rightarrow \chi^{++} \chi^{--},$$

$$\begin{aligned}
\chi^{++} \chi^{--} \rightarrow \chi^{++} \chi^{--} &= -64\pi^2 \lambda_\chi + 12\beta_{\lambda_\chi} + (i\pi - 1) \left[4\kappa_1 \lambda_{\chi\xi} \right. \\
&\quad \left. + 2(8\tilde{\lambda}_\chi^2 + 8\lambda_\chi \tilde{\lambda}_\chi + 12\lambda_\chi^2 + 3\lambda_{\chi\xi}^2 + \lambda_{\phi\chi}^2) + \kappa_1^2 + \frac{1}{2}\kappa_2^2 \right]. \quad (\text{D1})
\end{aligned}$$

• $\mathbf{Q} = \mathbf{0}, \mathbf{Y} = \mathbf{1}/2$:

$$\begin{aligned}
\phi^+ \xi^- \rightarrow \phi^+ \xi^- &= -32\pi^2 \lambda_{\phi\xi} + 6\beta_{\lambda_{\phi\xi}} + (i\pi - 1) \left[3\kappa_3^2 + 4\lambda_{\phi\xi}^2 \right], \\
\phi^+ \xi^- \rightarrow \phi^0 \xi^0 &= \sqrt{2}(i\pi - 1)\kappa_3^2, \\
\phi^+ \xi^- \rightarrow \chi^+ \phi^- &= -16\sqrt{2}\pi^2 \kappa_3 + 3\sqrt{2}\beta_{\kappa_3} + \frac{1}{\sqrt{2}}(i\pi - 1) \left[\kappa_3 (\kappa_2 + 4\lambda_{\phi\xi} + 2\lambda_{\phi\chi}) \right], \\
\phi^+ \xi^- \rightarrow \phi^{0*} \chi^0 &= -16\pi^2 \kappa_3 + 3\beta_{\kappa_3} + (i\pi - 1) \left[\frac{1}{2}\kappa_3 (3\kappa_2 + 4\lambda_{\phi\xi} + 2\lambda_{\phi\chi}) \right],
\end{aligned}$$

$$\begin{aligned}
\phi^0 \xi^0 \rightarrow \phi^+ \xi^- &= \phi^+ \xi^- \rightarrow \phi^0 \xi^0, \\
\chi^+ \phi^- \rightarrow \phi^+ \xi^- &= \phi^+ \xi^- \rightarrow \chi^+ \phi^-, \\
\phi^{0*} \chi^0 \rightarrow \phi^+ \xi^- &= \phi^+ \xi^- \rightarrow \phi^{0*} \chi^0,
\end{aligned}$$

$$\begin{aligned}
\phi^0 \xi^0 \rightarrow \phi^0 \xi^0 &= -32\pi^2 \lambda_{\phi\xi} + 6\beta_{\lambda_{\phi\xi}} + 2(i\pi - 1) \left[\kappa_3^2 + 2\lambda_{\phi\xi}^2 \right], \\
\phi^0 \xi^0 \rightarrow \chi^+ \phi^- &= (i\pi - 1) \kappa_2 \kappa_3, \\
\phi^0 \xi^0 \rightarrow \phi^{0*} \chi^0 &= -16\sqrt{2}\pi^2 \kappa_3 + 3\sqrt{2}\beta_{\kappa_3} + \frac{1}{\sqrt{2}}(i\pi - 1) \left[\kappa_3 (\kappa_2 + 4\lambda_{\phi\xi} + 2\lambda_{\phi\chi}) \right],
\end{aligned}$$

$$\begin{aligned}
\chi^+ \phi^- \rightarrow \phi^0 \xi^0 &= \phi^0 \xi^0 \rightarrow \chi^+ \phi^-, \\
\phi^{0*} \chi^0 \rightarrow \phi^0 \xi^0 &= \phi^0 \xi^0 \rightarrow \phi^{0*} \chi^0, \\
\chi^+ \phi^- \rightarrow \chi^+ \phi^- &= -16\pi^2 \lambda_{\phi\chi} + 3\beta_{\lambda_{\phi\chi}} + (i\pi - 1) \left[\frac{\kappa_2^2}{2} + 2\kappa_3^2 + \lambda_{\phi\chi}^2 \right], \\
\chi^+ \phi^- \rightarrow \phi^{0*} \chi^0 &= -8\sqrt{2}\pi^2 \kappa_2 + \frac{3}{\sqrt{2}}\beta_{\kappa_2} + \frac{1}{2\sqrt{2}}(i\pi - 1) \left[4\kappa_2 \lambda_{\phi\chi} + \kappa_2^2 + 4\kappa_3^2 \right],
\end{aligned}$$

$$\phi^{0*} \chi^0 \rightarrow \chi^+ \phi^- = \chi^+ \phi^- \rightarrow \phi^{0*} \chi^0,$$

$$\begin{aligned}
\phi^{0*} \chi^0 \rightarrow \phi^{0*} \chi^0 &= -16\pi^2 \left(\lambda_{\phi\chi} + \frac{1}{2}\kappa_2 \right) + 3 \left(\beta_{\lambda_{\phi\chi}} + \frac{1}{2}\beta_{\kappa_2} \right) \\
&\quad + (i\pi - 1) \left[\kappa_2 \lambda_{\phi\chi} + \frac{3\kappa_2^2}{4} + 3\kappa_3^2 + \lambda_{\phi\chi}^2 \right]. \tag{D2}
\end{aligned}$$

• $Q = 0, Y = 1$:

$$\begin{aligned}
\chi^+ \xi^- \rightarrow \chi^+ \xi^- &= -32\pi^2 \lambda_{\chi\xi} + 6\beta_{\lambda_{\chi\xi}} + (i\pi - 1) \left[\kappa_1^2 + \kappa_3^2 + 4\lambda_{\chi\xi}^2 \right], \\
\chi^+ \xi^- \rightarrow \chi^0 \xi^0 &= 16\pi^2 \kappa_1 - 3\beta_{\kappa_1} + (i\pi - 1) \left[\kappa_3^2 - 4\kappa_1 \lambda_{\chi\xi} \right], \\
\chi^+ \xi^- \rightarrow \frac{1}{\sqrt{2}}(\phi^0 \phi^0) &= -16\pi^2 \kappa_3 + 3\beta_{\kappa_3} + (i\pi - 1) \left[\kappa_3 (2(\lambda_{\chi\xi} + \lambda_\phi) - \kappa_1) \right],
\end{aligned}$$

$$\begin{aligned}
\chi^0 \xi^0 \rightarrow \chi^+ \xi^- &= \chi^+ \xi^- \rightarrow \chi^0 \xi^0, \\
\frac{1}{\sqrt{2}}(\phi^0 \phi^0) \rightarrow \chi^+ \xi^- &= \chi^+ \xi^- \rightarrow \frac{1}{\sqrt{2}}(\phi^0 \phi^0),
\end{aligned}$$

$$\begin{aligned}
\chi^0 \xi^0 \rightarrow \chi^0 \xi^0 &= -32\pi^2 \lambda_{\chi\xi} + 6\beta_{\lambda_{\chi\xi}} + (i\pi - 1) \left[\kappa_1^2 + \kappa_3^2 + 4\lambda_{\chi\xi}^2 \right], \\
\chi^0 \xi^0 \rightarrow \frac{1}{\sqrt{2}}(\phi^0 \phi^0) &= -16\pi^2 \kappa_3 + 3\beta_{\kappa_3} + (i\pi - 1) \left[\kappa_3 (2(\lambda_{\chi\xi} + \lambda_\phi) - \kappa_1) \right],
\end{aligned}$$

$$\frac{1}{\sqrt{2}}(\phi^0 \phi^0) \rightarrow \chi^0 \xi^0 = \chi^0 \xi^0 \rightarrow \frac{1}{\sqrt{2}}(\phi^0 \phi^0),$$

$$\frac{1}{\sqrt{2}}(\phi^0\phi^0) \rightarrow \frac{1}{\sqrt{2}}(\phi^0\phi^0) = -32\pi^2\lambda_\phi + 6\beta_{\lambda_\phi} + 2(i\pi - 1)\left[\kappa_3^2 + 2\lambda_\phi^2\right]. \quad (\text{D3})$$

• $Q = 0, Y = 3/2$:

$$\begin{aligned} \phi^0\chi^0 \rightarrow \phi^0\chi^0 = & -16\pi^2\left(\frac{1}{2}\kappa_2 + \lambda_{\phi\chi}\right) + 3\left(\beta_{\lambda_{\phi\chi}} + \frac{1}{2}\beta_{\kappa_2}\right) \\ & + (i\pi - 1)\left[\kappa_2\lambda_{\phi\chi} + \frac{\kappa_2^2}{4} + \lambda_{\phi\chi}^2\right]. \end{aligned} \quad (\text{D4})$$

• $Q = 0, Y = 2$:

$$\frac{1}{\sqrt{2}}(\chi^0\chi^0) \rightarrow \frac{1}{\sqrt{2}}(\chi^0\chi^0) = -32\pi^2\lambda_\chi + 6\beta_{\lambda_\chi} + 4(i\pi - 1)\lambda_\chi^2. \quad (\text{D5})$$

• $Q = 1, Y = 0$:

$$\begin{aligned} \chi^{++}\chi^- \rightarrow \chi^{++}\chi^- = & -32\pi^2\lambda_\chi + 6\beta_{\lambda_\chi} + (i\pi - 1)\left[16\tilde{\lambda}_\chi^2 + \kappa_1^2 + \frac{\kappa_2^2}{2} + 4\lambda_\chi^2\right], \\ \chi^{++}\chi^- \rightarrow \chi^+\chi^{0*} = & 64\pi^2\tilde{\lambda}_\chi - 12\beta_{\tilde{\lambda}_\chi} + \frac{1}{2}(i\pi - 1)\left[-2\kappa_1^2 + \kappa_2^2 - 32\lambda_\chi\tilde{\lambda}_\chi\right], \\ \chi^{++}\chi^- \rightarrow \xi^+\xi^0 = & -16\pi^2\kappa_1 + 3\beta_{\kappa_1} + 2(i\pi - 1)\left[\kappa_1\left(4\lambda_\xi + \lambda_\chi + 2\tilde{\lambda}_\chi\right)\right], \\ \chi^{++}\chi^- \rightarrow \phi^+\phi^{0*} = & -8\sqrt{2}\kappa_2 + \frac{3}{\sqrt{2}}\beta_{\kappa_2} + \sqrt{2}(i\pi - 1)\left[\kappa_2\left(\lambda_\phi + \lambda_\chi - 2\tilde{\lambda}_\chi\right)\right], \end{aligned}$$

$$\begin{aligned} \chi^+\chi^{0*} \rightarrow \chi^{++}\chi^- = & \chi^{++}\chi^- \rightarrow \chi^+\chi^{0*}, \\ \xi^+\xi^0 \rightarrow \chi^{++}\chi^- = & \chi^{++}\chi^- \rightarrow \xi^+\xi^0, \\ \phi^+\phi^{0*} \rightarrow \chi^{++}\chi^- = & \chi^{++}\chi^- \rightarrow \phi^+\phi^{0*}, \end{aligned}$$

$$\begin{aligned} \chi^+\chi^{0*} \rightarrow \chi^+\chi^{0*} = & -32\pi^2\lambda_\chi + 6\beta_{\lambda_\chi} + (i\pi - 1)\left[\kappa_1^2 + \frac{\kappa_2^2}{2} + 4\lambda_\chi^2 + 16\tilde{\lambda}_\chi^2\right], \\ \chi^+\chi^{0*} \rightarrow \xi^+\xi^0 = & 16\pi^2\kappa_1 - 3\beta_{\kappa_1} - 2(i\pi - 1)\left[\kappa_1\left(4\lambda_\xi + \lambda_\chi + 2\tilde{\lambda}_\chi\right)\right], \\ \chi^+\chi^{0*} \rightarrow \phi^+\phi^{0*} = & -8\sqrt{2}\pi^2\kappa_2 + \frac{3}{\sqrt{2}}\beta_{\kappa_2} + \sqrt{2}(i\pi - 1)\left[\kappa_2\left(\lambda_\phi + \lambda_\chi - 2\tilde{\lambda}_\chi\right)\right], \end{aligned}$$

$$\begin{aligned} \xi^+\xi^0 \rightarrow \chi^+\chi^{0*} = & \chi^+\chi^{0*} \rightarrow \xi^+\xi^0, \\ \phi^+\phi^{0*} \rightarrow \chi^+\chi^{0*} = & \chi^+\chi^{0*} \rightarrow \phi^+\phi^{0*}, \end{aligned}$$

$$\begin{aligned}
\xi^+ \xi^0 &\rightarrow \xi^+ \xi^0 = -128\pi^2 \lambda_\xi + 24\beta_{\lambda_\xi} + 2(i\pi - 1) \left[\kappa_1^2 + 32\lambda_\xi^2 \right], \\
\xi^+ \xi^0 &\rightarrow \phi^+ \phi^{0*} = 0 = \phi^+ \phi^{0*} \rightarrow \xi^+ \xi^0, \\
\phi^+ \phi^{0*} &\rightarrow \phi^+ \phi^{0*} = -32\pi^2 \lambda_\phi + 6\beta_{\lambda_\phi} + (i\pi - 1) \left[\kappa_2^2 + 4\lambda_\phi^2 \right]. \tag{D6}
\end{aligned}$$

• $Q = 1, Y = 1/2$:

$$\begin{aligned}
\phi^0 \xi^+ &\rightarrow \phi^0 \xi^+ = -32\pi^2 \lambda_{\phi\xi} + 6\beta_{\lambda_{\phi\xi}} + (i\pi - 1) \left[3\kappa_3^2 + 4\lambda_{\phi\xi}^2 \right], \\
\phi^0 \xi^+ &\rightarrow \phi^+ \xi^0 = -\sqrt{2}(i\pi - 1)\kappa_3^2, \\
\phi^0 \xi^+ &\rightarrow \chi^+ \phi^{0*} = -16\sqrt{2}\pi^2 \kappa_3 + 3\sqrt{2}\beta_{\kappa_3} + \frac{(i\pi - 1)}{\sqrt{2}} \left[\kappa_3 (\kappa_2 + 4\lambda_{\phi\xi} + 2\lambda_{\phi\chi}) \right], \\
\phi^0 \xi^+ &\rightarrow \phi^- \chi^{++} = -16\pi^2 \kappa_3 + 3\beta_{\kappa_3} + (i\pi - 1) \left[\frac{1}{2}\kappa_3 (3\kappa_2 + 4\lambda_{\phi\xi} + 2\lambda_{\phi\chi}) \right],
\end{aligned}$$

$$\begin{aligned}
\phi^+ \xi^0 &\rightarrow \phi^0 \xi^+ = \phi^0 \xi^+ \rightarrow \phi^+ \xi^0, \\
\chi^+ \phi^{0*} &\rightarrow \phi^0 \xi^+ = \phi^0 \xi^+ \rightarrow \chi^+ \phi^{0*}, \\
\phi^- \chi^{++} &\rightarrow \phi^0 \xi^+ = \phi^0 \xi^+ \rightarrow \phi^- \chi^{++},
\end{aligned}$$

$$\begin{aligned}
\phi^+ \xi^0 &\rightarrow \phi^+ \xi^0 = -32\pi^2 \lambda_{\phi\xi} + 6\beta_{\lambda_{\phi\xi}} + 2(i\pi - 1) \left[\kappa_3^2 + 2\lambda_{\phi\xi}^2 \right], \\
\phi^+ \xi^0 &\rightarrow \chi^+ \phi^{0*} = -(i\pi - 1)\kappa_2 \kappa_3, \\
\phi^+ \xi^0 &\rightarrow \phi^- \chi^{++} = 16\sqrt{2}\pi^2 \kappa_3 - 3\sqrt{2}\beta_{\kappa_3} - \frac{1}{\sqrt{2}}(i\pi - 1) \left[\kappa_3 (\kappa_2 + 4\lambda_{\phi\xi} + 2\lambda_{\phi\chi}) \right],
\end{aligned}$$

$$\begin{aligned}
\chi^+ \phi^{0*} &\rightarrow \phi^+ \xi^0 = \phi^+ \xi^0 \rightarrow \chi^+ \phi^{0*}, \\
\phi^- \chi^{++} &\rightarrow \phi^+ \xi^0 = \phi^+ \xi^0 \rightarrow \phi^- \chi^{++},
\end{aligned}$$

$$\begin{aligned}
\phi^- \chi^{++} &\rightarrow \phi^- \chi^{++} = -16\pi^2 \left(\lambda_{\phi\chi} + \frac{\kappa_2}{2} \right) + 3 \left(\beta_{\lambda_{\phi\chi}} + \frac{1}{2}\beta_{\kappa_2} \right) \\
&\quad + (i\pi - 1) \left[\frac{3}{4}\kappa_2^2 + 3\kappa_3^2 + \kappa_2 \lambda_{\phi\chi} + \lambda_{\phi\chi}^2 \right], \\
\phi^- \chi^{++} &\rightarrow \chi^+ \phi^{0*} = -8\sqrt{2}\kappa_2 + \frac{3}{\sqrt{2}}\beta_{\kappa_2} + \frac{1}{2\sqrt{2}}(i\pi - 1) \left[\kappa_2^2 + 4\kappa_3^2 + 4\kappa_2 \lambda_{\phi\chi} \right],
\end{aligned}$$

$$\chi^+ \phi^{0*} \rightarrow \phi^- \chi^{++} = \phi^- \chi^{++} \rightarrow \chi^+ \phi^{0*},$$

$$\chi^+ \phi^{0*} \rightarrow \chi^+ \phi^{0*} = -16\pi^2 \lambda_{\phi\chi} + 3\beta_{\lambda_{\phi\chi}} + (i\pi - 1) \left[\frac{\kappa_2^2}{2} + 2\kappa_3^2 + \lambda_{\phi\chi}^2 \right]. \tag{D7}$$

- $Q = 1, Y = 1$:

$$\begin{aligned}
\phi^+ \phi^0 \rightarrow \phi^+ \phi^0 &= -32\pi^2 \lambda_\phi + 6\beta_{\lambda_\phi} + 2(i\pi - 1) \left[\kappa_3^2 + 2\lambda_\phi^2 \right], \\
\phi^+ \phi^0 \rightarrow \chi^+ \xi^0 &= 0 = \chi^+ \xi^0 \rightarrow \phi^+ \phi^0, \\
\phi^+ \phi^0 \rightarrow \chi^0 \xi^+ &= -16\pi^2 \kappa_3 + 3\beta_{\kappa_3} + (i\pi - 1) \left[\kappa_3 (-\kappa_1 + 2(\lambda_\phi + \lambda_{\chi\xi})) \right], \\
\phi^+ \phi^0 \rightarrow \chi^{++} \xi^- &= -16\pi^2 \kappa_3 + 3\beta_{\kappa_3} + (i\pi - 1) \left[\kappa_3 (-\kappa_1 + 2(\lambda_\phi + \lambda_{\chi\xi})) \right],
\end{aligned}$$

$$\begin{aligned}
\chi^0 \xi^+ \rightarrow \phi^+ \phi^0 &= \phi^+ \phi^0 \rightarrow \chi^0 \xi^+, \\
\chi^{++} \xi^- \rightarrow \phi^+ \phi^0 &= \phi^+ \phi^0 \rightarrow \chi^{++} \xi^-,
\end{aligned}$$

$$\begin{aligned}
\chi^+ \xi^0 \rightarrow \chi^+ \xi^0 &= -32\pi^2 (\lambda_{\chi\xi} + \kappa_1) + 6(\beta_{\lambda_{\chi\xi}} + \beta_{\kappa_1}) + (i\pi - 1) \left[2\kappa_1^2 + 4(\kappa_1 + \lambda_{\chi\xi})^2 \right], \\
\chi^+ \xi^0 \rightarrow \chi^{++} \xi^- &= -16\pi^2 \kappa_1 + 3\beta_{\kappa_1} + (i\pi - 1) \left[\kappa_1 (5\kappa_1 + 4\lambda_{\chi\xi}) \right], \\
\chi^+ \xi^0 \rightarrow \chi^0 \xi^+ &= 16\pi^2 \kappa_1 - 3\beta_{\kappa_1} - (i\pi - 1) \left[\kappa_1 (5\kappa_1 + 4\lambda_{\chi\xi}) \right],
\end{aligned}$$

$$\begin{aligned}
\chi^{++} \xi^- \rightarrow \chi^+ \xi^0 &= \chi^+ \xi^0 \rightarrow \chi^{++} \xi^-, \\
\chi^0 \xi^+ \rightarrow \chi^+ \xi^0 &= \chi^+ \xi^0 \rightarrow \chi^0 \xi^+,
\end{aligned}$$

$$\begin{aligned}
\chi^{++} \xi^- \rightarrow \chi^{++} \xi^- &= -16\pi^2 (\kappa_1 + 2\lambda_{\chi\xi}) + 3(\beta_{\kappa_1} + 2\beta_{\lambda_{\chi\xi}}) \\
&\quad + (i\pi - 1) \left[5\kappa_1^2 + \kappa_3^2 + (\kappa_1 + 2\lambda_{\chi\xi})^2 \right], \\
\chi^{++} \xi^- \rightarrow \chi^0 \xi^+ &= 32\pi^2 \kappa_1 - 6\beta_{\kappa_1} + (i\pi - 1) \left[-5\kappa_1^2 + \kappa_3^2 - 8\kappa_1 \lambda_{\chi\xi} \right],
\end{aligned}$$

$$\chi^0 \xi^+ \rightarrow \chi^{++} \xi^- = \chi^{++} \xi^- \rightarrow \chi^0 \xi^+,$$

$$\begin{aligned}
\chi^0 \xi^+ \rightarrow \chi^0 \xi^+ &= -16\pi^2 (2\lambda_{\chi\xi} + \kappa_1) + 3(2\beta_{\chi\xi} + \beta_{\kappa_1}) \\
&\quad + (i\pi - 1) \left[5\kappa_1^2 + \kappa_3^2 + (\kappa_1 + 2\lambda_{\chi\xi})^2 \right].
\end{aligned} \tag{D8}$$

- $Q = 1, Y = 3/2$:

$$\begin{aligned}
\phi^+ \chi^0 \rightarrow \phi^0 \chi^+ &= -8\sqrt{2}\pi^2 \kappa_2 + \frac{3}{\sqrt{2}}\beta_{\kappa_2} - \frac{1}{2\sqrt{2}}(i\pi - 1) \left[\kappa_2 (\kappa_2 - 4\lambda_{\phi\chi}) \right], \\
\phi^0 \chi^+ \rightarrow \phi^0 \chi^+ &= -16\pi^2 \lambda_{\phi\chi} + 3\beta_{\lambda_{\phi\chi}} + (i\pi - 1) \left[\frac{\kappa_2^2}{2} + \lambda_{\phi\chi}^2 \right],
\end{aligned}$$

$$\phi^0 \chi^+ \rightarrow \phi^+ \chi^0 = \phi^+ \chi^0 \rightarrow \phi^0 \chi^+,$$

$$\begin{aligned} \phi^+ \chi^0 \rightarrow \phi^+ \chi^0 = & -16\pi^2 \left(\lambda_{\phi\chi} - \frac{1}{2}\kappa_2 \right) + 3 \left(\beta_{\lambda_{\phi\chi}} - \frac{1}{2}\beta_{\kappa_2} \right) \\ & + (i\pi - 1) \left[-\kappa_2 \lambda_{\phi\chi} + \frac{3}{4}\kappa_2^2 + \lambda_{\phi\chi}^2 \right]. \end{aligned} \quad (\text{D9})$$

• $Q = 1, Y = 2$:

$$\chi^+ \chi^0 \rightarrow \chi^+ \chi^0 = -32\pi^2 \lambda_\chi + 6\beta_{\lambda_\chi} + 4(i\pi - 1)\lambda_\chi^2. \quad (\text{D10})$$

• $Q = 2, Y = 0$:

$$\begin{aligned} \chi^{++} \chi^{0*} \rightarrow \chi^{++} \chi^{0*} = & -32\pi^2 (\lambda_\chi + 2\tilde{\lambda}_\chi) + 6 \left(\beta_{\lambda_\chi} + 2\beta_{\tilde{\lambda}_\chi} \right) \\ & + (i\pi - 1) \left[2\kappa_1^2 + 4 \left(\lambda_\chi + 2\tilde{\lambda}_\chi \right)^2 \right], \\ \chi^{++} \chi^{0*} \rightarrow \frac{1}{\sqrt{2}} (\xi^+ \xi^+) = & 16\sqrt{2}\pi^2 \kappa_1 - 3\sqrt{2}\beta_{\kappa_1} \\ & + \frac{1}{\sqrt{2}} (i\pi - 1) \left[-4\kappa_1 \left(4\lambda_\xi + \lambda_\chi + 2\tilde{\lambda}_\chi \right) \right], \\ \frac{1}{\sqrt{2}} (\xi^+ \xi^+) \rightarrow \chi^{++} \chi^{0*} = & \chi^{++} \chi^{0*} \rightarrow \frac{1}{\sqrt{2}} (\xi^+ \xi^+), \end{aligned}$$

$$\frac{1}{\sqrt{2}} (\xi^+ \xi^+) \rightarrow \frac{1}{\sqrt{2}} (\xi^+ \xi^+) = -128\pi^2 \lambda_\xi + 24\beta_{\lambda_\xi} + 2(i\pi - 1) \left[\left(\kappa_1^2 + 32\lambda_\xi^2 \right) \right]. \quad (\text{D11})$$

• $Q = 2, Y = 1/2$:

$$\begin{aligned} \phi^+ \xi^+ \rightarrow \phi^+ \xi^+ = & -32\pi^2 \lambda_{\phi\xi} + 6\beta_{\lambda_{\phi\xi}} + (i\pi - 1) \left[\left(\kappa_3^2 + 4\lambda_{\phi\xi}^2 \right) \right], \\ \phi^+ \xi^+ \rightarrow \chi^{++} \phi^{0*} = & -16\pi^2 \kappa_3 + 3\beta_{\kappa_3} + (i\pi - 1) \left[\kappa_3 \left(-\frac{\kappa_2}{2} + 2\lambda_{\phi\xi} + \lambda_{\phi\chi} \right) \right], \end{aligned}$$

$$\chi^{++} \phi^{0*} \rightarrow \phi^+ \xi^+ = \phi^+ \xi^+ \rightarrow \chi^{++} \phi^{0*},$$

$$\begin{aligned} \chi^{++} \phi^{0*} \rightarrow \chi^{++} \phi^{0*} = & -16\pi^2 \left(\lambda_{\phi\chi} - \frac{1}{2}\kappa_2 \right) + 3 \left(\beta_{\lambda_{\phi\chi}} - \frac{1}{2}\beta_{\kappa_2} \right) \\ & + (i\pi - 1) \left[\kappa_3^2 + \left(-\frac{\kappa_2}{2} + \lambda_{\phi\chi} \right)^2 \right]. \end{aligned} \quad (\text{D12})$$

- $Q = 2, Y = 3/2$:

$$\begin{aligned}\phi^+ \chi^+ \rightarrow \phi^+ \chi^+ &= -16\pi^2 \lambda_{\phi\chi} + 3\beta_{\lambda_{\phi\chi}} + (i\pi - 1) \left[\frac{1}{2} \kappa_2^2 + \lambda_{\phi\chi}^2 \right], \\ \phi^+ \chi^+ \rightarrow \chi^{++} \phi^0 &= -8\sqrt{2}\pi^2 \kappa_2 + \frac{3}{\sqrt{2}} \beta_{\kappa_2} - \frac{1}{2\sqrt{2}} (i\pi - 1) \left[\kappa_2 (\kappa_2 - 4\lambda_{\phi\chi}) \right],\end{aligned}$$

$$\chi^{++} \phi^0 \rightarrow \phi^+ \chi^+ = \phi^+ \chi^+ \rightarrow \chi^{++} \phi^0,$$

$$\begin{aligned}\chi^{++} \phi^0 \rightarrow \chi^{++} \phi^0 &= -16\pi^2 \left(\lambda_{\phi\chi} - \frac{\kappa_2}{2} \right) + 3 \left(\beta_{\lambda_{\phi\chi}} - \frac{1}{2} \beta_{\kappa_2} \right) \\ &\quad + (i\pi - 1) \left[\frac{3\kappa_2^2}{4} - \kappa_2 \lambda_{\phi\chi} + \lambda_{\phi\chi}^2 \right].\end{aligned}\tag{D13}$$

- $Q = 2, Y = 2$:

$$\begin{aligned}\chi^{++} \chi^0 \rightarrow \chi^{++} \chi^0 &= -32\pi^2 \left(\lambda_\chi + 2\tilde{\lambda}_\chi \right) + 6 \left(\beta_{\lambda_\chi} + 2\beta_{\tilde{\lambda}_\chi} \right) \\ &\quad + (i\pi - 1) \left[8\tilde{\lambda}_\chi^2 + 4 \left(\lambda_\chi + 2\tilde{\lambda}_\chi \right)^2 \right], \\ \chi^{++} \chi^0 \rightarrow \frac{1}{\sqrt{2}} (\chi^+ \chi^+) &= 32\sqrt{2}\pi^2 \tilde{\lambda}_\chi - 6\sqrt{2} \beta_{\tilde{\lambda}_\chi} + (i\pi - 1) \left[-4\sqrt{2} \tilde{\lambda}_\chi \left(2\lambda_\chi + 3\tilde{\lambda}_\chi \right) \right],\end{aligned}$$

$$\frac{1}{\sqrt{2}} (\chi^+ \chi^+) \rightarrow \chi^{++} \chi^0 = \chi^{++} \chi^0 \rightarrow \frac{1}{\sqrt{2}} (\chi^+ \chi^+),$$

$$\begin{aligned}\frac{1}{\sqrt{2}} (\chi^+ \chi^+) \rightarrow \frac{1}{\sqrt{2}} (\chi^+ \chi^+) &= -32\pi^2 \left(\lambda_\chi + \tilde{\lambda}_\chi \right) + 6 \left(\beta_{\lambda_\chi} + \beta_{\tilde{\lambda}_\chi} \right) \\ &\quad + 4(i\pi - 1) \left[2\tilde{\lambda}_\chi^2 + \left(\tilde{\lambda}_\chi + \lambda_\chi \right)^2 \right].\end{aligned}\tag{D14}$$

- $Q = 2, Y = 1$:

$$\begin{aligned}\frac{1}{\sqrt{2}} (\phi^+ \phi^+) \rightarrow \chi^{++} \xi^0 &= 16\pi^2 \kappa_3 - 3\beta_{\kappa_3} + (i\pi - 1) \left[\kappa_3 \left(\kappa_1 - 2(\lambda_\phi + \lambda_{\chi\xi}) \right) \right], \\ \frac{1}{\sqrt{2}} (\phi^+ \phi^+) \rightarrow \chi^+ \xi^+ &= -16\pi^2 \kappa_3 + 3\beta_{\kappa_3} + (i\pi - 1) \left[\kappa_3 \left(-\kappa_1 + 2(\lambda_\phi + \lambda_{\chi\xi}) \right) \right], \\ \frac{1}{\sqrt{2}} (\phi^+ \phi^+) \rightarrow \frac{1}{\sqrt{2}} (\phi^+ \phi^+) &= -32\pi^2 \lambda_\phi + 6\beta_{\lambda_\phi} + 2(i\pi - 1) \left[\kappa_3^2 + 2\lambda_\phi^2 \right],\end{aligned}$$

$$\begin{aligned}\chi^{++}\xi^0 &\rightarrow \frac{1}{\sqrt{2}}(\phi^+\phi^+) = \frac{1}{\sqrt{2}}(\phi^+\phi^+) \rightarrow \chi^{++}\xi^0, \\ \chi^+\xi^+ &\rightarrow \frac{1}{\sqrt{2}}(\phi^+\phi^+) = \frac{1}{\sqrt{2}}(\phi^+\phi^+) \rightarrow \chi^+\xi^+, \end{aligned}$$

$$\begin{aligned}\chi^{++}\xi^0 &\rightarrow \chi^{++}\xi^0 = -32\pi^2\lambda_{\chi\xi} + 6\beta_{\lambda_{\chi\xi}} + (i\pi - 1)\left[\kappa_1^2 + \kappa_3^2 + 4\lambda_{\chi\xi}^2\right], \\ \chi^{++}\xi^0 &\rightarrow \chi^+\xi^+ = -16\pi^2\kappa_1 + 3\beta_{\kappa_1} + (i\pi - 1)\left[-\kappa_3^2 + 4\kappa_1\lambda_{\chi\xi}\right], \end{aligned}$$

$$\chi^+\xi^+ \rightarrow \chi^{++}\xi^0 = \chi^{++}\xi^0 \rightarrow \chi^+\xi^+,$$

$$\chi^+\xi^+ \rightarrow \chi^+\xi^+ = -32\pi^2\lambda_{\chi\xi} + 6\beta_{\lambda_{\chi\xi}} + (i\pi - 1)\left[\kappa_1^2 + \kappa_3^2 + 4\lambda_{\chi\xi}^2\right]. \quad (\text{D15})$$

• $Q = 3, Y = 1$:

$$\begin{aligned}\chi^{++}\xi^+ &\rightarrow \chi^{++}\xi^+ = -16\pi^2(2\lambda_{\chi\xi} + \kappa_1) + 3(2\beta_{\lambda_{\chi\xi}} + \beta_{\kappa_1}) \\ &\quad + (i\pi - 1)\left[4\kappa_1\lambda_{\chi\xi} + \kappa_1^2 + 4\lambda_{\chi\xi}^2\right]. \end{aligned} \quad (\text{D16})$$

• $Q = 3, Y = 3/2$:

$$\begin{aligned}\chi^{++}\phi^+ &\rightarrow \chi^{++}\phi^+ = -16\pi^2\left(\lambda_{\phi\chi} + \frac{\kappa_2}{2}\right) + 3\left(\beta_{\lambda_{\phi\chi}} + \frac{1}{2}\beta_{\kappa_2}\right) \\ &\quad + (i\pi - 1)\left[\kappa_2\lambda_{\phi\chi} + \frac{\kappa_2^2}{4} + \lambda_{\phi\chi}^2\right]. \end{aligned} \quad (\text{D17})$$

• $Q = 3, Y = 2$:

$$\chi^{++}\chi^+ \rightarrow \chi^{++}\chi^+ = -32\pi^2\lambda_\chi + 6\beta_{\lambda_\chi} + 4(i\pi - 1)\lambda_\chi^2. \quad (\text{D18})$$

• $Q = 4, Y = 2$:

$$\frac{1}{\sqrt{2}}(\chi^{++}\chi^{++}) \rightarrow \frac{1}{\sqrt{2}}(\chi^{++}\chi^{++}) = -32\pi^2\lambda_\chi + 6\beta_{\lambda_\chi} + 4(i\pi - 1)\lambda_\chi^2. \quad (\text{D19})$$

Appendix E: Two-loop renormalization group equations

In this appendix, we list the renormalization group equations (RGEs) for the quartic couplings of the most general potential given in Eq. (1), obtained using the public code PyR@TE [104]. For any coupling A , the complete β function up to two-loop order can be

sub-divided into leading and next-to-leading order contributions separately as,

$$\beta_A \equiv \frac{dA}{d \ln \mu} = \frac{1}{16\pi^2} \beta_A^{(0)} + \frac{1}{(16\pi^2)^2} \beta_A^{(1)}. \quad (\text{E1})$$

The two-loop RGEs for the Yukawa couplings are the same as in the SM [111] and the type-I 2HDM [112], since the contributions of Higgs triplets to the Yukawa Lagrangian are not considered in this analysis [26]. The RGEs of the gauge couplings up to two-loop order are given by,

$$\begin{aligned} \beta_{g_1}^{(0)} &= \frac{47}{6} g_1^3, & \beta_{g_1}^{(1)} &= \frac{1}{18} g_1^3 \left(415g_1^2 + 513g_2^2 + 264g_3^2 - 15y_b^2 - 51y_t^2 - 45y_\tau^2 \right), \\ \beta_{g_2}^{(0)} &= -\frac{13}{6} g_2^3, & \beta_{g_2}^{(1)} &= \frac{1}{6} g_2^3 \left(57g_1^2 + 203g_2^2 + 72g_3^2 - 9y_b^2 - 9y_t^2 - 3y_\tau^2 \right), \\ \beta_{g_3}^{(0)} &= -7g_3^3, & \beta_{g_3}^{(1)} &= \frac{1}{6} g_3^3 \left(11g_1^2 + 27g_2^2 - 156g_3^2 - 12y_b^2 - 12y_t^2 \right), \end{aligned}$$

The running of the quartic couplings are given by the following:

$$\begin{aligned} \beta_{\lambda_\phi}^{(0)} &= +24\lambda_\phi^2 + \frac{3}{8} \left(g_1^4 + 2g_1^2g_2^2 + 3g_2^4 \right) - 6y_b^4 - 6y_t^4 - 2y_\tau^4 \\ &\quad + \lambda_\phi \left(12y_b^2 + 12y_t^2 + 4y_\tau^2 - 3g_1^2 - 9g_2^2 \right) + 6\lambda_{\phi\xi}^2 + 3\lambda_{\phi\chi}^2 + \frac{1}{2}\kappa_2^2 + 2\kappa_3^2, \\ \beta_{\lambda_\phi}^{(1)} &= -312\lambda_\phi^3 + \frac{1}{48}g_1^4 \left(60y_b^2 - 643g_2^2 - 228y_t^2 - 300y_\tau^2 \right) + \frac{1}{48}g_1^2 \left(24g_2^2 \left(9y_b^2 + 21y_t^2 + 11y_\tau^2 \right) \right. \\ &\quad \left. + 64 \left(y_b^4 - 2y_t^4 - 3y_\tau^4 \right) - 373g_2^4 \right) - \frac{3}{4}g_2^4 \left(3y_b^2 + 3y_t^2 + y_\tau^2 \right) + \frac{25}{6}g_1^2y_b^2\lambda_\phi + \frac{45}{2}g_2^2y_b^2\lambda_\phi \\ &\quad + 80g_3^2y_b^2\lambda_\phi - 32g_3^2y_b^4 - 42y_b^2\lambda_\phi y_t^2 - 6y_b^2y_t^4 - 6y_b^4y_t^2 - 144y_b^2\lambda_\phi^2 - 3y_b^4\lambda_\phi + 30y_b^6 \\ &\quad + 2\kappa_3^2 \left(g_1^2 + 10g_2^2 - 14\lambda_\phi - 20\lambda_{\phi\xi} - 10\lambda_{\phi\chi} \right) + \kappa_2^2 \left(4g_1^2 + 5g_2^2 - 7\lambda_\phi - 10\lambda_{\phi\chi} \right) \\ &\quad + 2\kappa_2 \left(5g_1^2g_2^2 - 3\kappa_3^2 \right) + 6\lambda_{\phi\chi}^2 \left(4g_1^2 + 8g_2^2 - 5\lambda_\phi \right) + \frac{761}{24}g_1^4\lambda_\phi + 36g_1^2\lambda_\phi^2 + \frac{39}{4}g_2^2g_1^2\lambda_\phi \\ &\quad + 108g_2^2\lambda_\phi^2 + \frac{59}{8}g_2^4\lambda_\phi + 96g_2^2\lambda_{\phi\xi}^2 + 30g_2^4\lambda_{\phi\xi} + 15 \left(g_1^4 + 2g_2^4 \right) \lambda_{\phi\chi} + \frac{85}{6}g_1^2\lambda_\phi y_t^2 \\ &\quad + \frac{45}{2}g_2^2\lambda_\phi y_t^2 + \frac{25}{2}g_1^2\lambda_\phi y_\tau^2 + \frac{15}{2}g_2^2\lambda_\phi y_\tau^2 - \frac{463g_1^6}{48} + \frac{221g_2^6}{16} + 80g_3^2\lambda_\phi y_t^2 - 32g_3^2y_t^4 \\ &\quad - 60\lambda_\phi\lambda_{\phi\xi}^2 - 48\lambda_{\phi\xi}^3 - 12\lambda_{\phi\chi}^3 - 144\lambda_\phi^2y_t^2 - 3\lambda_\phi y_t^4 + 30y_t^6 - 48\lambda_\phi^2y_\tau^2 - \lambda_\phi y_\tau^4 + 10y_\tau^6, \end{aligned}$$

$$\beta_{\lambda_\xi}^{(0)} = +88\lambda_\xi^2 + 3g_2^4 - 24g_2^2\lambda_\xi + 2\kappa_1\lambda_{\chi\xi} + \kappa_1^2 + 3\lambda_{\chi\xi}^2 + 2\lambda_{\phi\xi}^2,$$

$$\begin{aligned}\beta_{\lambda_\xi}^{(1)} = & -4416\lambda_\xi^3 + 2\lambda_{\phi\xi}\left(2\lambda_{\phi\xi}\left(-3y_b^2 - 3y_t^2 + g_1^2 + 3g_2^2 - 4\lambda_{\phi\xi} - y_\tau^2\right) + 5g_2^4 - 4\kappa_3^2\right) \\ & + 4\kappa_1^2\left(2g_1^2 + g_2^2 - 12\lambda_\xi - 8\lambda_{\chi\xi}\right) + 4\kappa_1\left(4\lambda_{\chi\xi}\left(g_1^2 + 2g_2^2 - 5\lambda_\xi\right) + 5g_2^4 - 6\lambda_{\chi\xi}^2\right) \\ & + \lambda_\xi\left(\frac{470}{3}g_2^4 + 8\kappa_3^2 - 80\lambda_{\phi\xi}^2\right) + 4\left(10g_2^4 - \kappa_3^2\right)\lambda_{\chi\xi} + 24\lambda_{\chi\xi}^2\left(g_1^2 + 2g_2^2 - 5\lambda_\xi\right) \\ & + 1024g_2^2\lambda_\xi^2 - \frac{83}{3}g_2^6 - 12\kappa_1^3 - 24\lambda_{\chi\xi}^3,\end{aligned}$$

$$\begin{aligned}\beta_{\lambda_\chi}^{(0)} = & +28\lambda_\chi^2 + 12g_1^2\left(g_2^2 - \lambda_\chi\right) - 24g_2^2\lambda_\chi + 6g_1^4 + 9g_2^4 + 4\kappa_1\lambda_{\chi\xi} + \kappa_1^2 + \frac{1}{2}\kappa_2^2 \\ & + 6\lambda_{\chi\xi}^2 + 16\tilde{\lambda}_\chi^2 + 16\lambda_\chi\tilde{\lambda}_\chi + 2\lambda_{\phi\chi}^2,\end{aligned}$$

$$\begin{aligned}\beta_{\lambda_\chi}^{(1)} = & -384\lambda_\chi^3 + 2g_2^2\left(16\left(8\lambda_\chi\tilde{\lambda}_\chi + 5\tilde{\lambda}_\chi^2 + 11\lambda_\chi^2 + 3\lambda_{\chi\xi}^2\right) + 32\kappa_1\lambda_{\chi\xi} + 5\kappa_1^2 + 6\lambda_{\phi\chi}^2\right) \\ & + g_2^4\left(128\tilde{\lambda}_\chi + 30\kappa_1 + \frac{638}{3}\lambda_\chi + 80\lambda_{\chi\xi} + 20\lambda_{\phi\chi}\right) + \frac{1}{3}g_1^2\left(6g_2^2\left(-80\tilde{\lambda}_\chi + 5\kappa_2 + 68\lambda_\chi\right)\right. \\ & \left.+ 3\left(4\left(32\tilde{\lambda}_\chi^2 + 32\lambda_\chi\tilde{\lambda}_\chi + 44\lambda_\chi^2 + \lambda_{\phi\chi}^2\right) + \kappa_2^2\right) - 958g_2^4\right) + g_1^4\left(80\tilde{\lambda}_\chi - \frac{1138}{3}g_2^2\right. \\ & \left.+ \frac{811}{3}\lambda_\chi + 10\lambda_{\phi\chi}\right) - \kappa_2^2\left(3y_b^2 + 3y_t^2 + y_\tau^2\right) - \frac{598}{3}g_1^6 - 29g_2^6 - 2\left[2\left(80\tilde{\lambda}_\chi^3 + 156\lambda_\chi\tilde{\lambda}_\chi^2\right.\right. \\ & \left.\left.+ 88\lambda_\chi^2\tilde{\lambda}_\chi + 3y_b^2\lambda_{\phi\chi}^2 + \kappa_3^2\left(-\lambda_\chi + 2\lambda_{\chi\xi} + 2\lambda_{\phi\chi}\right) + 15\lambda_\chi\lambda_{\chi\xi}^2 + 12\lambda_{\chi\xi}^3 + 5\lambda_\chi\lambda_{\phi\chi}^2\right.\right. \\ & \left.\left.+ 2\lambda_{\phi\chi}^3 + 3\lambda_{\phi\chi}^2y_t^2 + \lambda_{\phi\chi}^2y_\tau^2\right) + 8\kappa_1^2\left(\tilde{\lambda}_\chi + \lambda_\chi + 3\lambda_{\chi\xi}\right) + \kappa_1\left[\kappa_3^2 + 4\lambda_{\chi\xi}(5\lambda_\chi + 6\lambda_{\chi\xi})\right]\right. \\ & \left.+\kappa_2^2\left(3\lambda_\chi + 4\lambda_{\phi\chi}\right) + 7\kappa_1^3 + \kappa_2\kappa_3^2\right],\end{aligned}$$

$$\beta_{\tilde{\lambda}_\chi}^{(0)} = +12\tilde{\lambda}_\chi^2 + 24\tilde{\lambda}_\chi\left(\lambda_\chi - g_2^2\right) - 12g_1^2\left(\tilde{\lambda}_\chi + g_2^2\right) + 3g_2^4 + \kappa_1^2 - \frac{1}{2}\kappa_2^2,$$

$$\begin{aligned}\beta_{\tilde{\lambda}_\chi}^{(1)} = & -16\tilde{\lambda}_\chi^3 + \frac{1}{3}\left[g_2^4\left(86\tilde{\lambda}_\chi + 30\kappa_1 + 72\lambda_\chi\right) - 6g_2^2\left[\kappa_1^2 - 48\tilde{\lambda}_\chi\left(\tilde{\lambda}_\chi + 2\lambda_\chi\right)\right]\right. \\ & + g_1^2\left(-6g_2^2\left(-84\tilde{\lambda}_\chi + 5\kappa_2 + 48\lambda_\chi\right) - 3\left(48\tilde{\lambda}_\chi\left(\tilde{\lambda}_\chi - 2\lambda_\chi\right) + \kappa_2^2\right) + 598g_2^4\right) \\ & + g_1^4\left(331\tilde{\lambda}_\chi + 778g_2^2\right) + 6\left(-4\kappa_1^2\left(\tilde{\lambda}_\chi + \lambda_\chi + 2\lambda_{\chi\xi}\right) + \kappa_1\left(\kappa_3^2 - 20\lambda_{\chi\xi}\tilde{\lambda}_\chi\right)\right. \\ & \left.- 2\tilde{\lambda}_\chi\left(4\left(28\lambda_\chi\tilde{\lambda}_\chi + 28\lambda_\chi^2\right) - \kappa_3^2 + 15\lambda_{\chi\xi}^2 + 5\lambda_{\phi\chi}^2\right) + \kappa_2^2\left[3\tilde{\lambda}_\chi + 2\left(\lambda_\chi + \lambda_{\phi\chi}\right)\right]\right. \\ & \left.- 5\kappa_1^3 + \kappa_2\kappa_3^2\right) + 3\kappa_2^2\left(3y_b^2 + 3y_t^2 + y_\tau^2\right) - 245g_2^6\right],\end{aligned}$$

$$\beta_{\kappa_1}^{(0)} = +10\kappa_1^2 - 24g_2^2\kappa_1 + 6g_2^4 + 2\kappa_1\left(4\tilde{\lambda}_\chi - 3g_1^2 + 8\lambda_\xi + 2\lambda_\chi + 8\lambda_{\chi\xi}\right) - 2\kappa_3^2,$$

$$\begin{aligned}\beta_{\kappa_1}^{(1)} = & -22\kappa_1^3 + 2\kappa_1^2\left(-60\tilde{\lambda}_\chi + 5g_1^2 + 80g_2^2 - 152\lambda_\xi - 46\lambda_\chi - 66\lambda_{\chi\xi}\right) \\ & + 2\kappa_3^2\left(4\tilde{\lambda}_\chi + 6y_b^2 + 6y_t^2 + g_1^2 + 2\kappa_2 + 8\lambda_\xi + 2\lambda_\chi + 4\lambda_{\chi\xi} + 8\lambda_{\phi\xi} + 4\lambda_{\phi\chi} + 2y_\tau^2\right) \\ & + \frac{1}{6}\kappa_1\left[12\left(-8\tilde{\lambda}_\chi\left(g_2^2 + 5\lambda_\chi + 12\lambda_{\chi\xi}\right) - 12\tilde{\lambda}_\chi^2 + 8\lambda_{\chi\xi}\left(13g_2^2 - 36\lambda_\xi - 12\lambda_\chi\right)\right) \right. \\ & - 4\left(4\lambda_\xi\left(g_2^2 + 13\lambda_\xi\right) + g_2^2\lambda_\chi + 4\lambda_\chi^2\right) - 57\lambda_{\chi\xi}^2\Big) + 96g_1^2\left(4\tilde{\lambda}_\chi + 2\lambda_\chi + \lambda_{\chi\xi}\right) \\ & + 307g_1^4 + 48g_2^2g_1^2 + 136g_2^4 + 12\kappa_2^2 + 84\kappa_3^2 - 12\left(16\lambda_{\phi\xi}\lambda_{\phi\chi} + 4\lambda_{\phi\xi}^2 + \lambda_{\phi\chi}^2\right)\Big] \\ & + \frac{2}{3}g_2^4\left(60\tilde{\lambda}_\chi - 45g_1^2 - 245g_2^2 + 120\lambda_\xi + 30\lambda_\chi + 12\lambda_{\chi\xi}\right),\end{aligned}$$

$$\begin{aligned}\beta_{\kappa_2}^{(0)} = & +\frac{3}{2}g_1^2\left(8g_2^2 - 5\kappa_2\right) - \frac{33}{2}g_2^2\kappa_2 + 4\kappa_3^2 \\ & + 2\kappa_2\left(-4\tilde{\lambda}_\chi + 2\lambda_\chi + 2\lambda_\phi + 4\lambda_{\phi\chi} + 3y_b^2 + 3y_t^2 + y_\tau^2\right),\end{aligned}$$

$$\begin{aligned}\beta_{\kappa_2}^{(1)} = & +\frac{1}{2}\kappa_2^3 + 6g_1^2\kappa_2^2 + \frac{1}{3}g_1^2g_2^2\left(120\lambda_\chi + 120\lambda_\phi - 240\tilde{\lambda}_\chi + 24\lambda_{\phi\chi} + 108y_b^2 + 252y_t^2\right. \\ & \left.+ 132y_\tau^2 - 643g_1^2 - 463g_2^2\right) + \kappa_3^2\left(16\tilde{\lambda}_\chi - 12y_b^2 + 8\kappa_1 - 8\lambda_\chi - 16\lambda_{\chi\xi} - 24\lambda_\phi\right. \\ & - 16\lambda_{\phi\xi} - 16\lambda_{\phi\chi} - 12y_t^2 - 4y_\tau^2 + g_1^2 + 47g_2^2\Big) + \frac{1}{48}\kappa_2\left[48\left(2\lambda_{\phi\chi}\left(16\tilde{\lambda}_\chi - 48\lambda_\chi\right)\right.\right. \\ & \left.\left.- 12y_b^2 - 12y_t^2 - 4y_\tau^2 + 5g_1^2 + 23g_2^2\right) + 8\left(4g_1^2\left(\lambda_\chi - 2\tilde{\lambda}_\chi\right) + 5g_2^2\left(\lambda_\chi - 2\tilde{\lambda}_\chi\right)\right.\right. \\ & \left.\left.+ 9\tilde{\lambda}_\chi^2 + 6\lambda_\chi\tilde{\lambda}_\chi - 4\lambda_\chi^2\right) + 8\lambda_\phi\left(-3y_b^2 - 3y_t^2 + g_1^2 - 10\lambda_{\phi\chi} - y_\tau^2\right) - 28\lambda_\phi^2\right. \\ & \left.- 29\lambda_{\phi\chi}^2\right) + 10g_1^2\left(10y_b^2 + 489g_2^2 + 34y_t^2 + 30y_\tau^2\right) + 180g_2^2\left(3y_b^2 + 3y_t^2 + y_\tau^2\right) \\ & + 24\left(80g_3^2\left(y_b^2 + y_t^2\right) - 27\left(y_b^2 - y_t^2\right)^2 - 9y_\tau^4\right) + 96\left[-2\kappa_1\left(\lambda_{\chi\xi} + 4\lambda_{\phi\xi}\right)\right. \\ & \left.+ 3\kappa_1^2 - 3\left(\lambda_{\chi\xi}^2 + 8\lambda_{\chi\xi}\lambda_{\phi\xi} + \lambda_{\phi\xi}^2\right)\right] + 3121g_1^4 - 911g_2^4 + 192\kappa_3^2\Big],\end{aligned}$$

$$\beta_{\kappa_3}^{(0)} = -\frac{1}{2}\kappa_3\left(9g_1^2 + 33g_2^2\right) + 2\kappa_3\left(3y_b^2 - \kappa_1 + \kappa_2 + 2\lambda_{\chi\xi} + 2\lambda_\phi + 4\lambda_{\phi\xi} + 2\lambda_{\phi\chi} + 3y_t^2 + y_\tau^2\right),$$

$$\begin{aligned}
\beta_{\kappa_3}^{(1)} = & +3\kappa_3^3 + \frac{1}{48}\kappa_3 \left[1797g_1^4 - 911g_2^4 - 24 \left(\kappa_2 \left(-16\tilde{\lambda}_\chi + 4 \left(3y_b^2 + 3y_t^2 + y_\tau^2 \right) - 17g_1^2 - 47g_2^2 \right. \right. \right. \\
& + 8\lambda_\chi + 16\lambda_{\chi\xi} + 24\lambda_\phi + 16\lambda_{\phi\xi} + 16\lambda_{\phi\chi} \left. \right) + 2 \left(-12\tilde{\lambda}_\chi^2 + 8\tilde{\lambda}_\chi \left(-\lambda_\chi + 2\lambda_{\chi\xi} + 2\lambda_{\phi\chi} \right) \right. \\
& + \lambda_{\phi\xi} \left(8 \left(3y_b^2 + 3y_t^2 + y_\tau^2 \right) - 2g_1^2 - 46g_2^2 + 160\lambda_\xi + 56\lambda_{\chi\xi} + 24\lambda_{\phi\chi} \right) + 4\lambda_\phi \left(6y_b^2 + 6y_t^2 \right. \\
& + g_1^2 + 20\lambda_{\phi\xi} + 10\lambda_{\phi\chi} + 2y_\tau^2 \left. \right) + 12y_b^2\lambda_{\phi\chi} - 4g_1^2\lambda_{\chi\xi} - 40g_2^2\lambda_{\chi\xi} - 17g_1^2\lambda_{\phi\chi} - 23g_2^2\lambda_{\phi\chi} \\
& + 80\lambda_\xi\lambda_{\chi\xi} + 32\lambda_\chi\lambda_{\chi\xi} - 8\lambda_\chi^2 - \lambda_{\chi\xi}^2 + 28\lambda_\phi^2 + 34\lambda_{\phi\xi}^2 + 32\lambda_\chi\lambda_{\phi\chi} + 40\lambda_{\chi\xi}\lambda_{\phi\chi} + 10\lambda_{\phi\chi}^2 \\
& + 12\lambda_{\phi\chi}y_t^2 + 4\lambda_{\phi\chi}y_\tau^2 \left. \right) + 4\kappa_1 \left(-4\tilde{\lambda}_\chi + g_1^2 + 10g_2^2 - 2\kappa_2 + 2\lambda_\chi - 7\lambda_{\chi\xi} - 4\lambda_{\phi\xi} \right) - 28\kappa_1^2 \\
& - 2\kappa_2^2 \left. \right) + 10g_1^2 \left(10y_b^2 + 45g_2^2 + 34y_t^2 + 30y_\tau^2 \right) + 180g_2^2 \left(3y_b^2 + 3y_t^2 + y_\tau^2 \right) \\
& + 24 \left(80g_3^2 \left(y_b^2 + y_t^2 \right) - 3 \left(y_b^2 - y_t^2 \right)^2 - y_\tau^4 \right) + 3840\lambda_\xi^2 \left. \right],
\end{aligned}$$

$$\begin{aligned}
\beta_{\lambda_{\phi\xi}}^{(0)} = & +8\lambda_{\phi\xi}^2 - \frac{33}{2}g_2^2\lambda_{\phi\xi} + \frac{1}{2}\lambda_{\phi\xi} \left(12y_b^2 + 80\lambda_\xi + 24\lambda_\phi + 12y_t^2 + 4y_\tau^2 - 3g_1^2 \right) \\
& + 3g_2^4 + 2\lambda_{\phi\chi} \left(\kappa_1 + 3\lambda_{\chi\xi} \right) + 4\kappa_3^2,
\end{aligned}$$

$$\begin{aligned}
\beta_{\lambda_{\phi\xi}}^{(1)} = & -46\lambda_{\phi\xi}^3 + \frac{1609}{48}g_2^4\lambda_{\phi\xi} + 640g_2^2\lambda_\xi\lambda_{\phi\xi} + 100g_2^4\lambda_\xi + 72g_2^2\lambda_\phi\lambda_{\phi\xi} + 24g_1^2\lambda_\phi\lambda_{\phi\xi} + 30g_2^4\lambda_\phi \\
& + 22g_2^2\lambda_{\phi\xi}^2 + \frac{15}{8}g_1^2g_2^2\lambda_{\phi\xi} + 2g_1^2\lambda_{\phi\xi}^2 + 40g_2^4\lambda_{\phi\chi} + \frac{45}{4}g_2^2\lambda_{\phi\xi}y_t^2 + \frac{85}{12}g_1^2\lambda_{\phi\xi}y_t^2 + \frac{15}{4}g_2^2\lambda_{\phi\xi}y_\tau^2 \\
& + \frac{25}{4}g_1^2\lambda_{\phi\xi}y_\tau^2 + 40g_3^2\lambda_{\phi\xi}y_t^2 - 8\kappa_1^2(\lambda_{\phi\xi} + 2\lambda_{\phi\chi}) - \frac{3}{2}\kappa_2^2\lambda_{\phi\xi} - 480\lambda_\xi\lambda_{\phi\xi}^2 - 800\lambda_\xi^2\lambda_{\phi\xi} \\
& - 144\lambda_\phi\lambda_{\phi\xi}^2 - 60\lambda_\phi^2\lambda_{\phi\xi} - 12\lambda_{\chi\xi}^2(\lambda_{\phi\xi} + 2\lambda_{\phi\chi}) - 3\lambda_{\phi\xi}\lambda_{\phi\chi}^2 - 72\lambda_\phi\lambda_{\phi\xi}y_t^2 - 24\lambda_{\phi\xi}^2y_t^2 \\
& - \frac{27}{2}\lambda_{\phi\xi}y_t^4 - 24\lambda_\phi\lambda_{\phi\xi}y_\tau^2 - 8\lambda_{\phi\xi}^2y_\tau^2 - \frac{9}{2}\lambda_{\phi\xi}y_\tau^4 + \kappa_3^2 \left(-4 \left(3y_b^2 + 3y_t^2 + y_\tau^2 \right) + 17g_1^2 \right. \\
& + 23g_2^2 - 4\kappa_2 - 80\lambda_\xi - 28\lambda_{\chi\xi} - 40\lambda_\phi - 34\lambda_{\phi\xi} - 12\lambda_{\phi\chi} \left. \right) + \frac{1}{48} \left[689g_1^4\lambda_{\phi\xi} \right. \\
& - 4g_2^4 \left(12 \left(3y_b^2 + 3y_t^2 + y_\tau^2 \right) + 45g_1^2 - 217g_2^2 \right) \left. \right] + \frac{45}{4}g_2^2y_b^2\lambda_{\phi\xi} + \frac{25}{12}g_1^2y_b^2\lambda_{\phi\xi} - \frac{27}{2}y_b^4\lambda_{\phi\xi} \\
& + 40g_3^2y_b^2\lambda_{\phi\xi} - 21y_b^2\lambda_{\phi\xi}y_t^2 - 72y_b^2\lambda_\phi\lambda_{\phi\xi} - 24y_b^2\lambda_{\phi\xi}^2 + 3\lambda_{\chi\xi} \left(4\lambda_{\phi\chi} \left(4g_1^2 + 8g_2^2 - 4\lambda_{\phi\xi} \right) \right. \\
& - \lambda_{\phi\chi} \left. \right) + 5 \left(g_1^4 + 2g_2^4 \right) - 2\kappa_2^2 \left. \right) + \kappa_1 \left[4\lambda_{\phi\chi} \left(4g_1^2 + 8g_2^2 - 4\lambda_{\phi\xi} - \lambda_{\phi\chi} \right) + 5 \left(g_1^4 + 2g_2^4 \right) \right. \\
& \left. \left. - 2\kappa_2^2 + 4\kappa_3^2 - 8\lambda_{\chi\xi} \left(\lambda_{\phi\xi} + 2\lambda_{\phi\chi} \right) \right] \right],
\end{aligned}$$

$$\begin{aligned}
\beta_{\lambda_{\phi\chi}}^{(0)} = & +4\lambda_{\phi\chi}^2 + 2\lambda_{\phi\chi} \left(4\tilde{\lambda}_\chi + 3y_b^2 + 8\lambda_\chi + 6\lambda_\phi + 3y_t^2 + y_\tau^2 \right) + 4\lambda_{\phi\xi} \left(\kappa_1 + 3\lambda_{\chi\xi} \right) \\
& + 2\kappa_2^2 + 4\kappa_3^2 - \frac{15}{2}g_1^2\lambda_{\phi\chi} - \frac{33}{2}g_2^2\lambda_{\phi\chi} + 3g_1^4 + 6g_2^4,
\end{aligned}$$

$$\begin{aligned}
\beta_{\lambda_{\phi\chi}}^{(1)} = & -13\lambda_{\phi\chi}^3 - \frac{1061}{12}g_1^6 + \frac{217}{6}g_2^6 + g_1^4 \left(-\frac{165}{4}g_2^2 + 5y_b^2 - 19y_t^2 - 25y_\tau^2 + 30\lambda_\phi + 40\lambda_\chi \right. \\
& + 20\tilde{\lambda}_\chi + \frac{6121}{48}\lambda_{\phi\chi} \left. \right) + g_2^4 \left(-6y_b^2 - 6y_t^2 - 2y_\tau^2 + 10\kappa_1 + 60\lambda_\phi + 80\lambda_{\phi\xi} + \frac{3529}{48}\lambda_{\phi\chi} \right. \\
& + 80\lambda_\chi + 30\lambda_{\chi\xi} + 40\tilde{\lambda}_\chi \left. \right) + \frac{1}{24}g_1^2 \left[-900g_2^4 + (96\kappa_2 + 525\lambda_{\phi\chi})g_2^2 + 60\kappa_2^2 + 24\kappa_3^2 \right. \\
& + 2\lambda_{\phi\chi} \left(25y_b^2 + 85y_t^2 + 75y_\tau^2 + 288\lambda_\phi + 60\lambda_{\phi\chi} + 1536\lambda_\chi + 768\tilde{\lambda}_\chi \right) \left. \right] + \frac{1}{4}g_2^2 \left[46\kappa_2^2 \right. \\
& + 92\kappa_3^2 + 256\lambda_{\phi\xi} \left(\kappa_1 + 3\lambda_{\chi\xi} \right) + \lambda_{\phi\chi} \left(45y_b^2 + 45y_t^2 + 15y_\tau^2 + 288\lambda_\phi + 44\lambda_{\phi\chi} \right. \\
& \left. \left. \left. + 1024\lambda_\chi + 512\tilde{\lambda}_\chi \right) \right] - 6y_b^2\kappa_2^2 - 6y_t^2\kappa_2^2 - 2y_\tau^2\kappa_2^2 - 12y_b^2\kappa_3^2 - 12y_t^2\kappa_3^2 - 4y_\tau^2\kappa_3^2 \\
& - 8\kappa_2\kappa_3^2 - 16\kappa_1\lambda_{\phi\xi}^2 - 12y_b^2\lambda_{\phi\chi}^2 - 12y_t^2\lambda_{\phi\chi}^2 - 4y_\tau^2\lambda_{\phi\chi}^2 - 72\lambda_\phi\lambda_{\phi\chi}^2 - 80\lambda_{\phi\chi}\lambda_\chi^2 \\
& - 48\lambda_{\phi\xi}\lambda_{\chi\xi}^2 - 6\lambda_{\phi\chi}\lambda_{\chi\xi}^2 - 120\lambda_{\phi\chi}\tilde{\lambda}_\chi^2 - 20\kappa_2^2\lambda_\phi - 40\kappa_3^2\lambda_\phi - 32\kappa_1^2\lambda_{\phi\xi} - 24\kappa_3^2\lambda_{\phi\xi} \\
& - \frac{27}{2}y_b^4\lambda_{\phi\chi} - \frac{27}{2}y_t^4\lambda_{\phi\chi} - \frac{9}{2}y_\tau^4\lambda_{\phi\chi} + 40g_3^2y_b^2\lambda_{\phi\chi} + 40g_3^2y_t^2\lambda_{\phi\chi} - 21y_b^2y_t^2\lambda_{\phi\chi} - 4\kappa_1^2\lambda_{\phi\chi} \\
& - \frac{29}{2}\kappa_2^2\lambda_{\phi\chi} - 20\kappa_3^2\lambda_{\phi\chi} - 60\lambda_\phi^2\lambda_{\phi\chi} - 6\lambda_{\phi\xi}^2\lambda_{\phi\chi} - 96\lambda_{\phi\chi}^2\lambda_\chi - 72y_b^2\lambda_\phi\lambda_{\phi\chi} - 72y_t^2\lambda_\phi\lambda_{\phi\chi} \\
& - 24y_\tau^2\lambda_\phi\lambda_{\phi\chi} - 16\kappa_1\lambda_{\phi\xi}\lambda_{\phi\chi} - 24\kappa_2^2\lambda_\chi - 32\kappa_3^2\lambda_\chi - 40\kappa_3^2\lambda_{\chi\xi} - 48\lambda_{\phi\xi}^2\lambda_{\chi\xi} - 4\kappa_1\lambda_{\phi\chi}\lambda_{\chi\xi} \\
& - 32\kappa_1\lambda_{\phi\xi}\lambda_{\chi\xi} - 48\lambda_{\phi\xi}\lambda_{\phi\chi}\lambda_{\chi\xi} + 8\tilde{\lambda}_\chi \left[\kappa_2^2 - 2 \left(\kappa_3^2 + 3\lambda_{\phi\chi}^2 + 5\lambda_{\phi\chi}\lambda_\chi \right) \right],
\end{aligned}$$

$$\begin{aligned}
\beta_{\lambda_{\chi\xi}}^{(0)} = & +8\lambda_{\chi\xi}^2 + 2\lambda_{\chi\xi} \left(4\tilde{\lambda}_\chi + 20\lambda_\xi + 8\lambda_\chi - 3g_1^2 \right) - 24g_2^2\lambda_{\chi\xi} + 6g_2^4 + 4\kappa_1 \left(2\lambda_\xi + \lambda_\chi \right) \\
& + 2\kappa_1^2 + 2\kappa_3^2 + 4\lambda_{\phi\xi}\lambda_{\phi\chi},
\end{aligned}$$

$$\begin{aligned}
\beta_{\lambda_{\chi\xi}}^{(1)} = & -50\lambda_{\chi\xi}^3 - 120\lambda_{\chi\xi}\tilde{\lambda}_\chi^2 + \frac{667}{6}g_1^4\lambda_{\chi\xi} + 10g_1^4\lambda_{\phi\xi} + 20g_1^2g_2^2\lambda_{\chi\xi} + 100g_2^4\lambda_\chi + 20g_2^4\lambda_{\phi\xi} \\
& + \frac{2}{3}g_2^4 \left(-45g_1^2 + 79g_2^2 + 360\lambda_\xi \right) + 128g_1^2\lambda_\chi\lambda_{\chi\xi} + 8g_1^2\lambda_{\chi\xi}^2 + 8g_1^2\lambda_{\phi\xi}\lambda_{\phi\chi} + 10g_2^4\lambda_{\phi\chi} \\
& + 640g_2^2\lambda_\xi\lambda_{\chi\xi} + \frac{326}{3}g_2^4\lambda_{\chi\xi} + 256g_2^2\lambda_\chi\lambda_{\chi\xi} + 32g_2^2\lambda_{\chi\xi}^2 + 24g_2^2\lambda_{\phi\xi}\lambda_{\phi\chi} - \kappa_2^2\lambda_{\chi\xi} - 26\kappa_1^3 \\
& - 4\kappa_2^2\lambda_{\phi\xi} - 480\lambda_\xi\lambda_{\chi\xi}^2 - 800\lambda_\xi^2\lambda_{\chi\xi} - 192\lambda_\chi\lambda_{\chi\xi}^2 - 80\lambda_\chi^2\lambda_{\chi\xi} - 8\lambda_{\chi\xi}\lambda_{\phi\xi}^2 - 32\lambda_{\chi\xi}\lambda_{\phi\xi}\lambda_{\phi\chi} \\
& - 8\lambda_{\phi\xi}\lambda_{\phi\chi}^2 - 16\lambda_{\phi\xi}^2\lambda_{\phi\chi} - 2\lambda_{\chi\xi}\lambda_{\phi\chi}^2 - 24y_b^2\lambda_{\phi\xi}\lambda_{\phi\chi} - 24y_t^2\lambda_{\phi\xi}\lambda_{\phi\chi} - 8y_\tau^2\lambda_{\phi\xi}\lambda_{\phi\chi} \\
& + 2\kappa_1^2 \left(-12\tilde{\lambda}_\chi + g_1^2 + 4g_2^2 - 56\lambda_\xi - 22\lambda_\chi - 18\lambda_{\chi\xi} \right) + 8\tilde{\lambda}_\chi \left[2\lambda_{\chi\xi} \left(4g_1^2 + 8g_2^2 - 5\lambda_\chi \right. \right. \\
& \left. \left. - 6\lambda_{\chi\xi} \right) + 5g_2^4 \right] - 2\kappa_3^2 \left(4\tilde{\lambda}_\chi + g_1^2 + 2\kappa_2 + 16\lambda_\xi + 6\lambda_\chi + \lambda_{\chi\xi} + 12\lambda_{\phi\xi} + 8\lambda_{\phi\chi} + 2y_\tau^2 \right. \\
& \left. + 6y_b^2 + 6y_t^2 \right) + \kappa_1 \left[-4 \left(-12g_2^2\tilde{\lambda}_\chi + 8\tilde{\lambda}_\chi^2 + 8\lambda_\xi \left(4\lambda_{\chi\xi} - 7g_2^2 \right) \right) + \lambda_\chi \left(16\lambda_{\chi\xi} - 22g_2^2 \right) \right. \\
& \left. + 3\lambda_{\chi\xi} \left(4g_2^2 + \lambda_{\chi\xi} \right) + 32\lambda_\xi^2 + 4\lambda_\chi^2 \right] + 20g_1^4 + 4g_1^2g_2^2 + 32g_1^2\lambda_\chi + 34g_2^4 - \kappa_2^2.
\end{aligned}$$

For the sake of completeness, the beta functions of the dimensionful parameters at one-loop are given in Ref. [97].

Appendix F: Supplementary figures

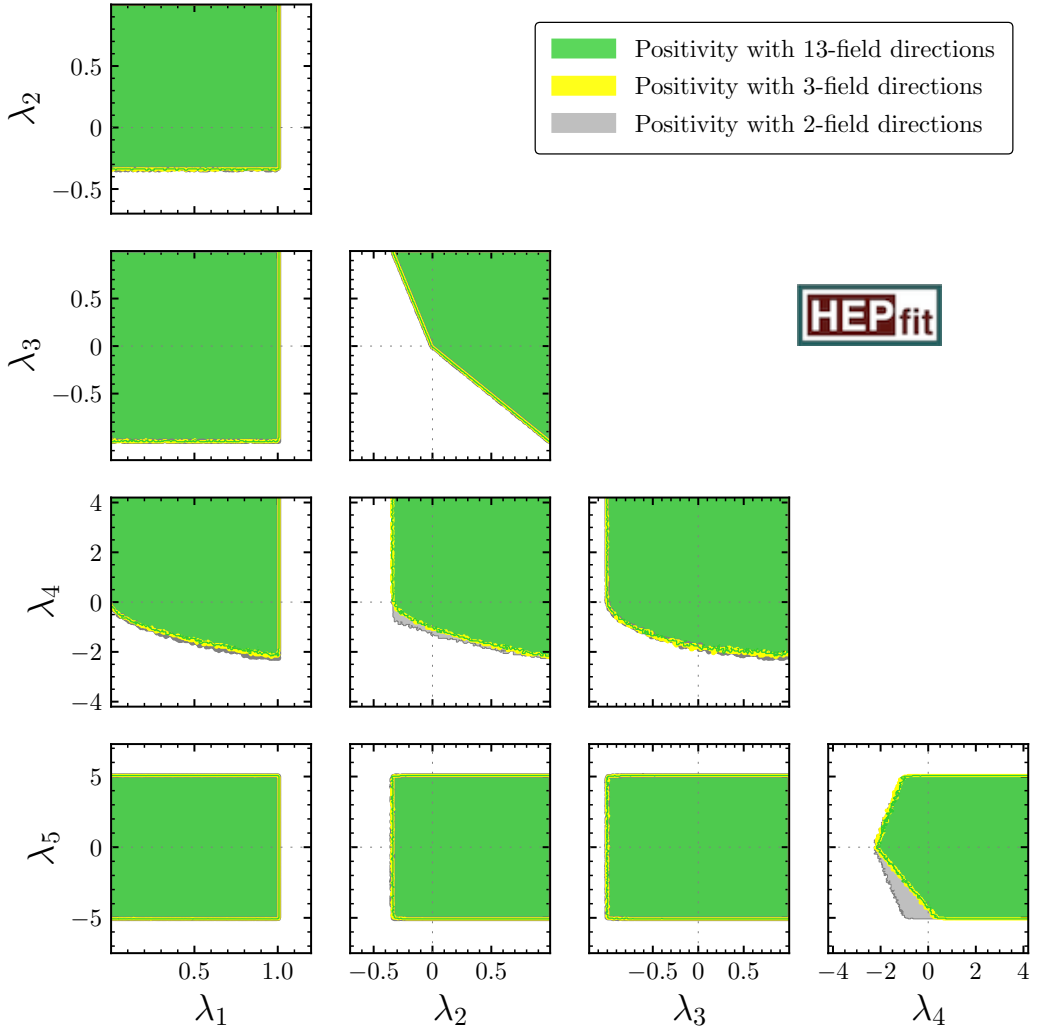


FIG. 11. Allowed regions on the quartic coupling planes of the GM model with three different BFB constraints. The colors of the shaded regions have the same meaning here as in Figure 2.

In this appendix, we present supplementary figures of the GM (eGM) model parameter space. The comparison of the three different BFB constraints in the quartic coupling planes of the GM model is shown in Figure 11. The colors in Figure 11 have the same meaning as in Figure 2, and from this figure, we observe that the regions allowed from the 3-field BFB constraints largely overlap with the allowed regions considering all 13-field BFB constraints [28, 77].

The allowed regions with different unitarity conditions in the $\lambda_{\phi\chi}$ vs. κ_2 ($\lambda_{\chi\xi}$ vs. κ_1) plane are shown in Figure 12. From Eq. (23), the tree-level amplitudes vanish along the lines, $\kappa_2 = \lambda_{\phi\chi}$, $\kappa_2 = -2\lambda_{\phi\chi}$, $\kappa_1 = -2\lambda_{\chi\xi}$, and $\kappa_1 = -\lambda_{\chi\xi}/2$, which are denoted by the cyan

dotted lines in Figure 12. The perturbativity test ($R'_1 < 1$) fails for coupling values lying in the neighborhood region of these lines. In Figure 12, the effects of such cancellations are visible in the NLO unitarity with R'_1 contour. The colors in Figure 12 have the same meaning as in Figure 3.

In the top left (right) panel of Figure 13, we show the allowed ranges in $r_{Z\gamma}$ vs. r_{gg} plane for all different final states for the GM (eGM) model. The colors in Figure 13 have the same meaning as in Figure 6. From Figure 13, we see that the most significant constraints in the $r_{Z\gamma}$ vs. r_{gg} plane come from the WW , bb , and $\gamma\gamma$ decay channels. The SM predictions of $r_{Z\gamma}^{\text{SM}} = 1$ and $r_{gg}^{\text{SM}} = 1$ lie within the allowed regions (grey shaded area) of all signal strengths. The maximal deviation of $r_{Z\gamma}$ (r_{gg}) from its SM value is roughly 10% (15%) in both models. In the bottom left (right) panel of Figure 13, we show the allowed ranges in $r_{\gamma\gamma}$ vs. r_{gg} plane, for all different final states for the GM (eGM) model. The maximal deviation of $r_{\gamma\gamma}$ from its SM value ($r_{\gamma\gamma}^{\text{SM}} = 1$) is roughly 25% in both models.

The masses of the heavy Higgs bosons and their mass differences are shown in Figures 14 and 15, for the GM and the eGM models, respectively. The colors in Figures 14 and 15 have the same meaning as in Figure 7.

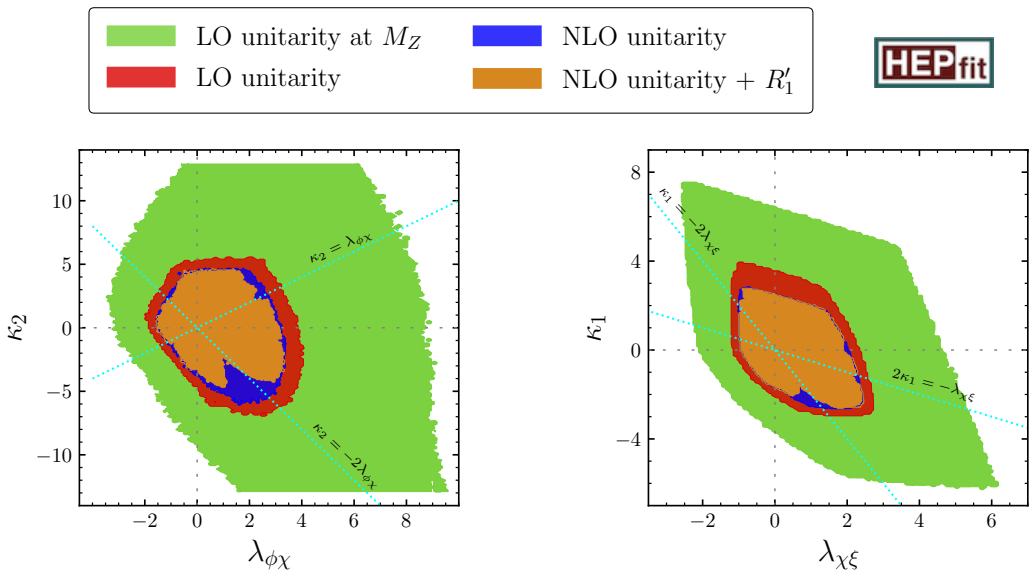


FIG. 12. Allowed regions in the λ_i vs. κ_j planes. The green, red, and blue regions have the same meaning as in Figure 3. The brown areas show the parameter space without violating the perturbativity conditions ($R'_1 < 1$) at the one-loop level. The cyan dashed lines represent directions along which the tree-level amplitudes vanish.

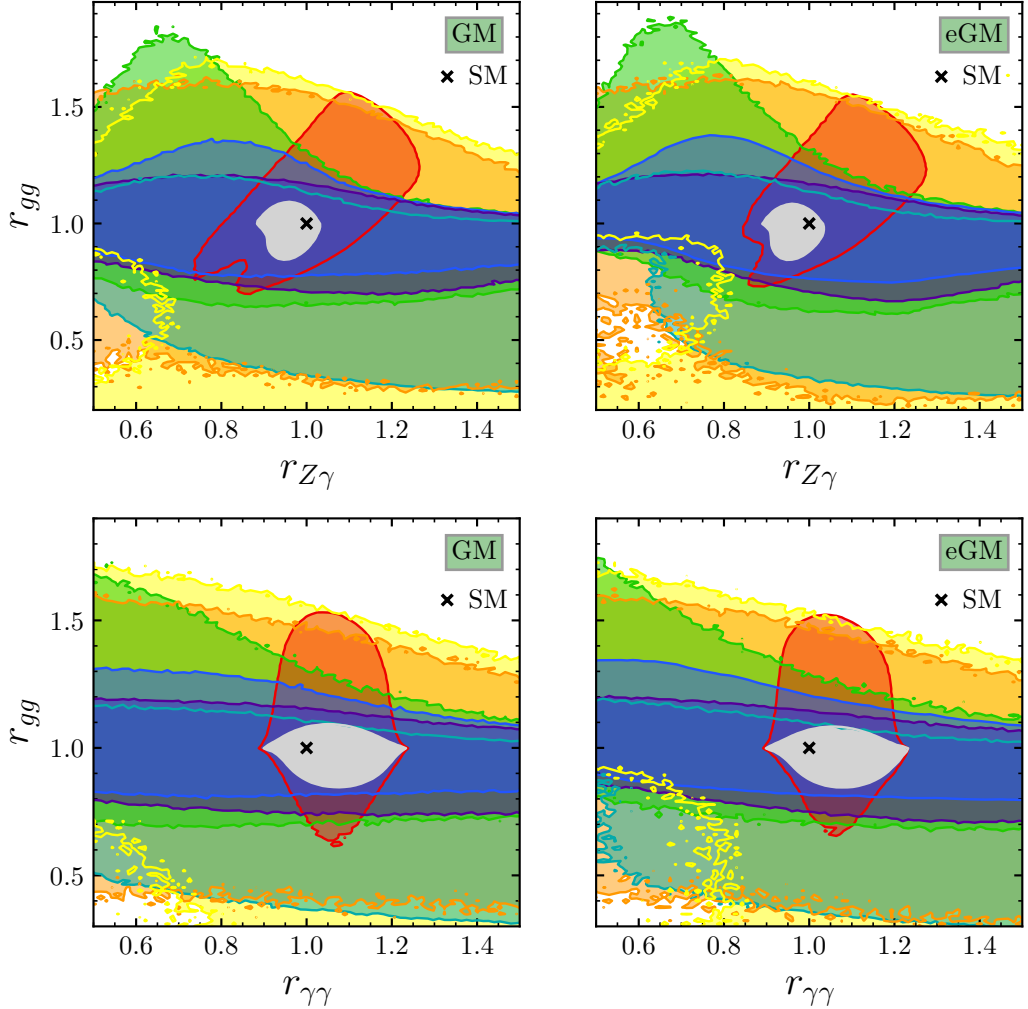
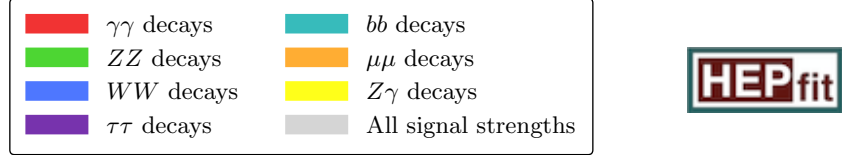


FIG. 13. 95.4% probability regions show the impact of the Higgs signal strengths for different final states in the r_{Vg} vs. r_{gg} ($V = \gamma, Z$) planes for the GM model (left panel) and the eGM model (right panel). The individual fits to full Run 1 and Run 2 data from h decays to $\gamma\gamma$, ZZ , WW , $\tau\tau$, bb , $\mu\mu$, and $Z\gamma$ are displayed in red, green, blue, purple, cyan, orange, and yellow, respectively. The results from the combined fits are shown in the grey color shaded regions, where the cross indicates the expected value for the SM Higgs boson.

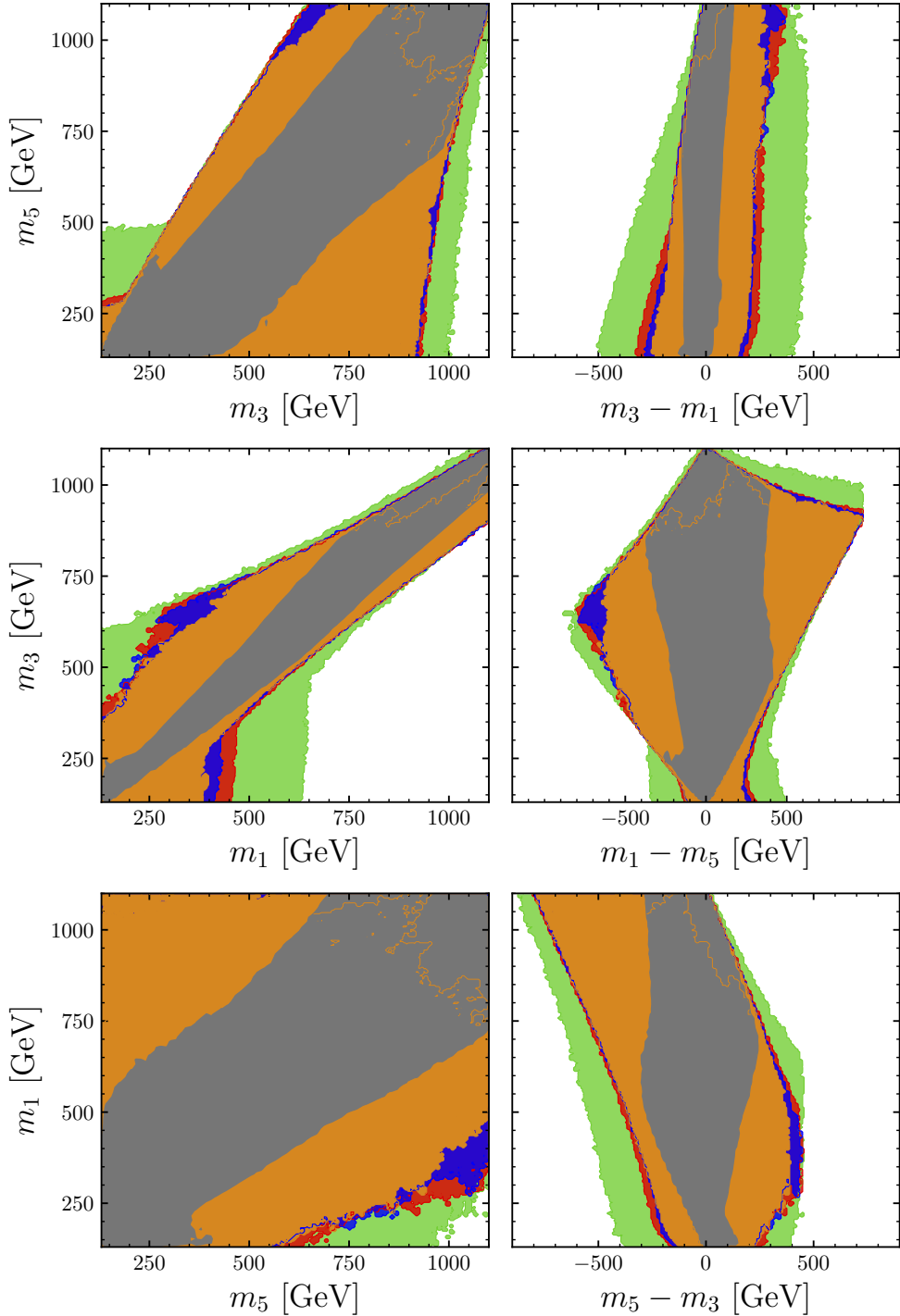
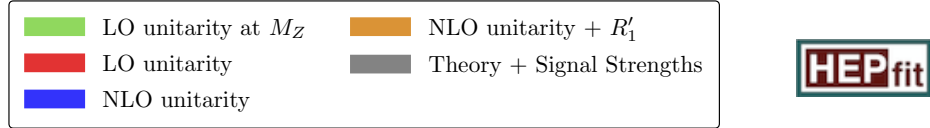


FIG. 14. Allowed regions in the m_i vs. m_j ($m_j - m_k$) planes in the GM model. The color shaded regions have the same meaning as in Figure 7.

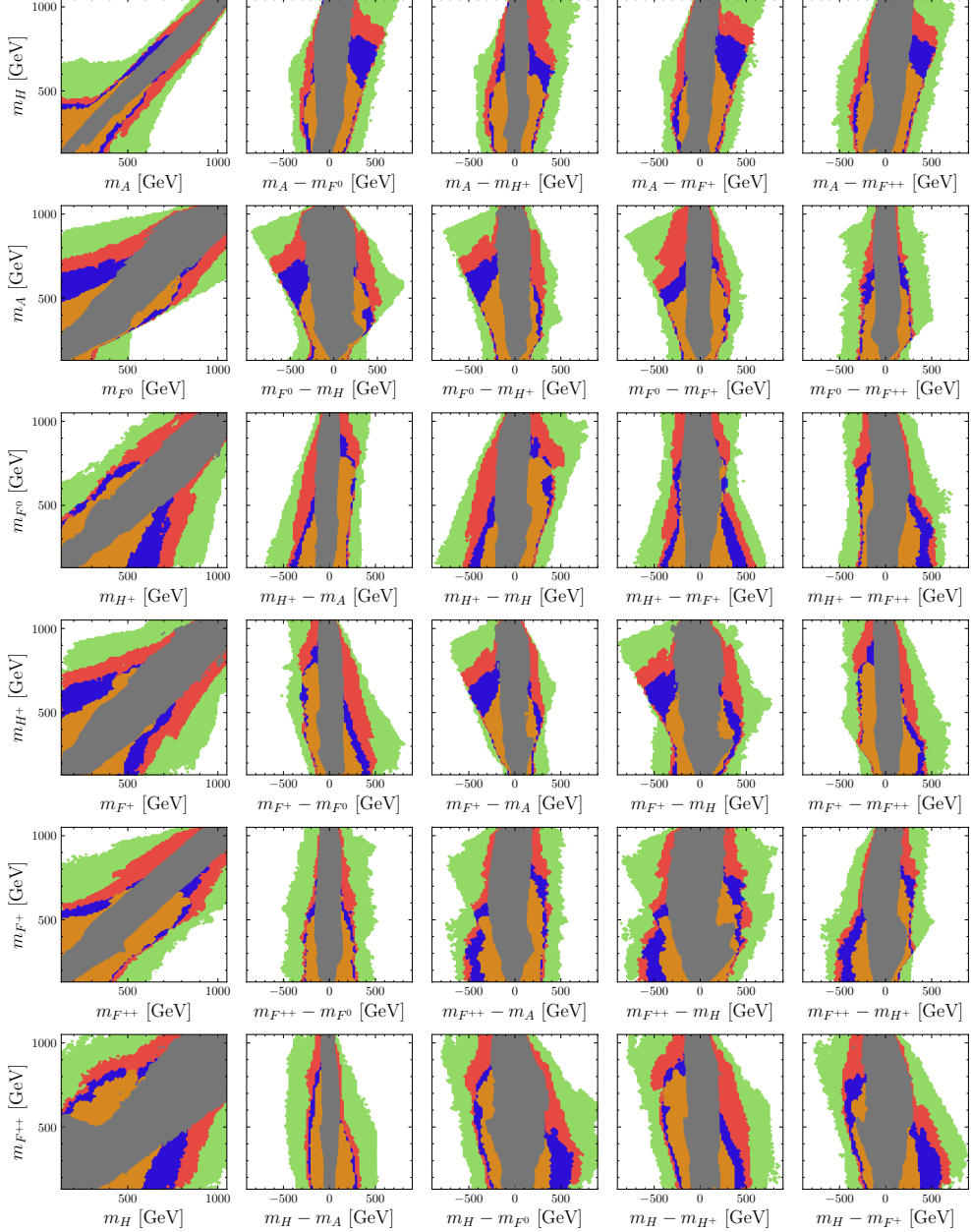
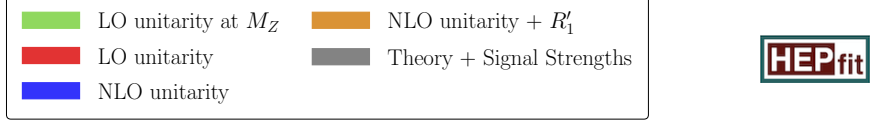


FIG. 15. Allowed regions in the m_i vs. m_j ($m_j - m_k$) planes in the eGM model. The color shaded regions have the same meaning as in Figure 7.

[1] ATLAS collaboration, *Observation of a new particle in the search for the Standard Model*

Higgs boson with the ATLAS detector at the LHC, *Phys. Lett. B* **716** (2012) 1 [[1207.7214](#)].

[2] CMS collaboration, *Observation of a New Boson at a Mass of 125 GeV with the CMS Experiment at the LHC*, *Phys. Lett. B* **716** (2012) 30 [[1207.7235](#)].

[3] ATLAS, CMS collaboration, *Measurements of the Higgs boson production and decay rates and constraints on its couplings from a combined ATLAS and CMS analysis of the LHC pp collision data at $\sqrt{s} = 7$ and 8 TeV*, *JHEP* **08** (2016) 045 [[1606.02266](#)].

[4] ATLAS collaboration, *Higgs boson production cross-section measurements and their EFT interpretation in the 4ℓ decay channel at $\sqrt{s} = 13$ TeV with the ATLAS detector*, *Eur. Phys. J. C* **80** (2020) 957 [[2004.03447](#)].

[5] ATLAS collaboration, *A search for the $Z\gamma$ decay mode of the Higgs boson in pp collisions at $\sqrt{s} = 13$ TeV with the ATLAS detector*, *Phys. Lett. B* **809** (2020) 135754 [[2005.05382](#)].

[6] ATLAS collaboration, *Measurements of WH and ZH production in the $H \rightarrow b\bar{b}$ decay channel in pp collisions at 13 TeV with the ATLAS detector*, *Eur. Phys. J. C* **81** (2021) 178 [[2007.02873](#)].

[7] ATLAS collaboration, *A search for the dimuon decay of the Standard Model Higgs boson with the ATLAS detector*, *Phys. Lett. B* **812** (2021) 135980 [[2007.07830](#)].

[8] CMS collaboration, *Evidence for Higgs boson decay to a pair of muons*, *JHEP* **01** (2021) 148 [[2009.04363](#)].

[9] ATLAS collaboration, *Measurements of Higgs bosons decaying to bottom quarks from vector boson fusion production with the ATLAS experiment at $\sqrt{s} = 13$ TeV*, *Eur. Phys. J. C* **81** (2021) 537 [[2011.08280](#)].

[10] CMS collaboration, *Measurements of production cross sections of the Higgs boson in the four-lepton final state in proton–proton collisions at $\sqrt{s} = 13$ TeV*, *Eur. Phys. J. C* **81** (2021) 488 [[2103.04956](#)].

[11] CMS collaboration, *Measurements of Higgs boson production cross sections and couplings in the diphoton decay channel at $\sqrt{s} = 13$ TeV*, *JHEP* **07** (2021) 027 [[2103.06956](#)].

[12] ATLAS collaboration, *Measurement of Higgs boson decay into b -quarks in associated production with a top-quark pair in pp collisions at $\sqrt{s} = 13$ TeV with the ATLAS detector*, *JHEP* **06** (2022) 097 [[2111.06712](#)].

[13] ATLAS collaboration, *Measurements of Higgs boson production cross-sections in the $H \rightarrow \tau^+\tau^-$ decay channel in pp collisions at $\sqrt{s} = 13$ TeV with the ATLAS detector*, *JHEP* **08** (2022) 175 [[2201.08269](#)].

[14] CMS collaboration, *Search for Higgs boson decays to a Z boson and a photon in proton-proton collisions at $\sqrt{s} = 13$ TeV*, *JHEP* **05** (2023) 233 [[2204.12945](#)].

[15] CMS collaboration, *Measurements of Higgs boson production in the decay channel with a pair of τ leptons in proton–proton collisions at $\sqrt{s} = 13$ TeV*, *Eur. Phys. J. C* **83** (2023) 562 [[2204.12957](#)].

[16] CMS collaboration, *Measurements of the Higgs boson production cross section and couplings in the W boson pair decay channel in proton-proton collisions at $\sqrt{s} = 13$ TeV*, *Eur. Phys. J. C* **83** (2023) 667 [[2206.09466](#)].

[17] CMS collaboration, *A portrait of the Higgs boson by the CMS experiment ten years after the discovery*, *Nature* **607** (2022) 60 [[2207.00043](#)].

[18] ATLAS collaboration, *A detailed map of Higgs boson interactions by the ATLAS experiment ten years after the discovery*, *Nature* **607** (2022) 52 [[2207.00092](#)].

[19] ATLAS collaboration, *Measurements of Higgs boson production by gluon-gluon fusion and vector-boson fusion using $H \rightarrow WW^* \rightarrow e\nu\mu\nu$ decays in pp collisions at $\sqrt{s} = 13$ TeV with*

the ATLAS detector, *Phys. Rev. D* **108** (2023) 032005 [[2207.00338](#)].

[20] ATLAS collaboration, *Measurement of the properties of Higgs boson production at $\sqrt{s} = 13$ TeV in the $H \rightarrow \gamma\gamma$ channel using 139 fb^{-1} of pp collision data with the ATLAS experiment*, *JHEP* **07** (2023) 088 [[2207.00348](#)].

[21] CMS collaboration, *Measurement of the Higgs boson production via vector boson fusion and its decay into bottom quarks in proton-proton collisions at $\sqrt{s} = 13$ TeV*, *JHEP* **01** (2024) 173 [[2308.01253](#)].

[22] H. Georgi and M. Machacek, *Doubly charged Higgs bosons*, *Nucl. Phys. B* **262** (1985) 463.

[23] M.S. Chanowitz and M. Golden, *Higgs Boson Triplets With $M(W) = M(Z) \cos \theta \omega$* , *Phys. Lett. B* **165** (1985) 105.

[24] J.F. Gunion, R. Vega and J. Wudka, *Higgs triplets in the standard model*, *Phys. Rev. D* **42** (1990) 1673.

[25] J.F. Gunion, R. Vega and J. Wudka, *Naturalness problems for $\rho = 1$ and other large one loop effects for a standard model Higgs sector containing triplet fields*, *Phys. Rev. D* **43** (1991) 2322.

[26] C.-W. Chiang and K. Yagyu, *Testing the custodial symmetry in the Higgs sector of the Georgi-Machacek model*, *JHEP* **01** (2013) 026 [[1211.2658](#)].

[27] C. Englert, E. Re and M. Spannowsky, *Triplet Higgs boson collider phenomenology after the LHC*, *Phys. Rev. D* **87** (2013) 095014 [[1302.6505](#)].

[28] K. Hartling, K. Kumar and H.E. Logan, *The decoupling limit in the Georgi-Machacek model*, *Phys. Rev. D* **90** (2014) 015007 [[1404.2640](#)].

[29] M. Garcia-Pepin, S. Gori, M. Quiros, R. Vega, R. Vega-Morales and T.-T. Yu, *Supersymmetric Custodial Higgs Triplets and the Breaking of Universality*, *Phys. Rev. D* **91** (2015) 015016 [[1409.5737](#)].

[30] K. Hartling, K. Kumar and H.E. Logan, *Indirect constraints on the Georgi-Machacek model and implications for Higgs boson couplings*, *Phys. Rev. D* **91** (2015) 015013 [[1410.5538](#)].

[31] C.-W. Chiang, A.-L. Kuo and T. Yamada, *Searches of exotic Higgs bosons in general mass spectra of the Georgi-Machacek model at the LHC*, *JHEP* **01** (2016) 120 [[1511.00865](#)].

[32] C.-W. Chiang, G. Cottin and O. Eberhardt, *Global fits in the Georgi-Machacek model*, *Phys. Rev. D* **99** (2019) 015001 [[1807.10660](#)].

[33] A. Banerjee, G. Bhattacharyya and N. Kumar, *Impact of Yukawa-like dimension-five operators on the Georgi-Machacek model*, *Phys. Rev. D* **99** (2019) 035028 [[1901.01725](#)].

[34] C.H. de Lima, D. Stolarski and Y. Wu, *Status of negative coupling modifiers for extended Higgs sectors*, *Phys. Rev. D* **105** (2022) 035019 [[2111.02533](#)].

[35] P. Mondal, *Enhancement of the W boson mass in the Georgi-Machacek model*, *Phys. Lett. B* **833** (2022) 137357 [[2204.07844](#)].

[36] T.-K. Chen, C.-W. Chiang, C.-T. Huang and B.-Q. Lu, *Updated constraints on the Georgi-Machacek model and its electroweak phase transition and associated gravitational waves*, *Phys. Rev. D* **106** (2022) 055019 [[2205.02064](#)].

[37] A. Kundu, A. Le Yaouanc, P. Mondal and F. Richard, *Searches for scalars at LHC and interpretation of the findings*, in *2022 ECFA Workshop on e+e- Higgs/EW/Top factories*, 11, 2022 [[2211.11723](#)].

[38] T.-K. Chen, C.-W. Chiang and K. Yagyu, *CP violation in a model with Higgs triplets*, *JHEP* **06** (2023) 069 [[2303.09294](#)].

[39] T.-K. Chen, C.-W. Chiang, S. Heinemeyer and G. Weiglein, *95 GeV Higgs boson in the Georgi-Machacek model*, *Phys. Rev. D* **109** (2024) 075043 [[2312.13239](#)].

[40] M. Chakraborti, D. Das, N. Ghosh, S. Mukherjee and I. Saha, *New physics implications of vector boson fusion searches exemplified through the Georgi-Machacek model*, *Phys. Rev. D* **109** (2024) 015016 [[2308.02384](#)].

[41] C.H. de Lima and D. Stolarski, *Influence of new states in searches for negative gauge-Higgs couplings*, [2404.10815](#).

[42] A. Crivellin, S. Ashanujaman, S. Banik, G. Coloretti, S.P. Maharathy and B. Mellado, *Growing Evidence for a Higgs Triplet*, [2404.14492](#).

[43] C. Henderson, *Future Physics Prospects with the CMS Detector at the High-Luminosity LHC*, *SciPost Phys. Proc.* (2022) 111.

[44] W. Bizoń, U. Haisch, L. Rottoli, Z. Gillis, B. Moser and P. Windischhofer, *Addendum to: Constraints on the quartic Higgs self-coupling from double-Higgs production at future hadron colliders* [*JHEP* 10 (2019) 267], *JHEP* **02** (2024) 170 [[2402.03463](#)].

[45] P. Stylianou and G. Weiglein, *Constraints on the trilinear and quartic Higgs couplings from triple Higgs production at the LHC and beyond*, *Eur. Phys. J. C* **84** (2024) 366 [[2312.04646](#)].

[46] J.M. Torndal, J. List, D. Ntounis and C. Vernieri, *Higgs self-coupling measurement at future e^+e^- colliders*, *PoS EPS-HEP2023* (2024) 406 [[2311.16774](#)].

[47] E. Celada, T. Giani, J. ter Hoeve, L. Mantani, J. Rojo, A.N. Rossia et al., *Mapping the SMEFT at High-Energy Colliders: from LEP and the (HL-)LHC to the FCC-ee*, [2404.12809](#).

[48] C. Aime et al., *Muon Collider Physics Summary*, [2203.07256](#).

[49] MUON COLLIDER collaboration, *The physics case of a 3 TeV muon collider stage*, [2203.07261](#).

[50] M. Forslund and P. Meade, *High precision higgs from high energy muon colliders*, *JHEP* **08** (2022) 185 [[2203.09425](#)].

[51] CMS collaboration, *Observation of electroweak production of same-sign W boson pairs in the two jet and two same-sign lepton final state in proton-proton collisions at $\sqrt{s} = 13$ TeV*, *Phys. Rev. Lett.* **120** (2018) 081801 [[1709.05822](#)].

[52] CMS collaboration, *Measurements of production cross sections of polarized same-sign W boson pairs in association with two jets in proton-proton collisions at $\sqrt{s} = 13$ TeV*, *Phys. Lett. B* **812** (2021) 136018 [[2009.09429](#)].

[53] ATLAS collaboration, *Search for doubly charged scalar bosons decaying into same-sign W boson pairs with the ATLAS detector*, *Eur. Phys. J. C* **79** (2019) 58 [[1808.01899](#)].

[54] ATLAS collaboration, *Measurement and interpretation of same-sign W boson pair production in association with two jets in pp collisions at $\sqrt{s} = 13$ TeV with the ATLAS detector*, [2312.00420](#).

[55] M. Ciuchini, E. Franco, S. Mishima and L. Silvestrini, *Electroweak Precision Observables, New Physics and the Nature of a 126 GeV Higgs Boson*, *JHEP* **08** (2013) 106 [[1306.4644](#)].

[56] J. de Blas, M. Ciuchini, E. Franco, S. Mishima, M. Pierini, L. Reina et al., *Electroweak precision observables and Higgs-boson signal strengths in the Standard Model and beyond: present and future*, *JHEP* **12** (2016) 135 [[1608.01509](#)].

[57] J. de Blas, M. Pierini, L. Reina and L. Silvestrini, *Impact of the Recent Measurements of the Top-Quark and W-Boson Masses on Electroweak Precision Fits*, *Phys. Rev. Lett.* **129** (2022) 271801 [[2204.04204](#)].

[58] PARTICLE DATA GROUP collaboration, *Review of Particle Physics*, *PTEP* **2022** (2022) 083C01.

[59] A. Kundu, P. Mondal and P.B. Pal, *Custodial symmetry, the Georgi-Machacek model, and other scalar extensions*, *Phys. Rev. D* **105** (2022) 115026 [[2111.14195](#)].

[60] D.A. Dicus and V.S. Mathur, *Upper bounds on the values of masses in unified gauge theories*, *Phys. Rev. D* **7** (1973) 3111.

[61] B.W. Lee, C. Quigg and H.B. Thacker, *The Strength of Weak Interactions at Very High-Energies and the Higgs Boson Mass*, *Phys. Rev. Lett.* **38** (1977) 883.

[62] B.W. Lee, C. Quigg and H.B. Thacker, *Weak Interactions at Very High-Energies: The Role of the Higgs Boson Mass*, *Phys. Rev. D* **16** (1977) 1519.

[63] G. Passarino, *Large masses, unitary and one-loop corrections*, *Physics Letters B* **156** (1985) 231.

[64] M. Luscher and P. Weisz, *Is There a Strong Interaction Sector in the Standard Lattice Higgs Model?*, *Phys. Lett. B* **212** (1988) 472.

[65] S. Dawson and S. Willenbrock, *Unitarity constraints on heavy higgs bosons*, *Phys. Rev. Lett.* **62** (1989) 1232.

[66] W.J. Marciano, G. Valencia and S. Willenbrock, *Renormalization Group Improved Unitarity Bounds on the Higgs Boson and Top Quark Masses*, *Phys. Rev. D* **40** (1989) 1725.

[67] S. Dawson and S. Willenbrock, *RADIATIVE CORRECTIONS TO LONGITUDINAL VECTOR BOSON SCATTERING*, *Phys. Rev. D* **40** (1989) 2880.

[68] G. Passarino, *Ww scattering and perturbative unitarity*, *Nuclear Physics B* **343** (1990) 31.

[69] L. Durand, J.M. Johnson and J.L. Lopez, *One-loop perturbative unitarity and the higgs-boson mass: A new approach*, *Phys. Rev. Lett.* **64** (1990) 1215.

[70] E. Lendvai, G. Pocsik and T. Torma, *Radiative corrections and unitarity bounds on the Higgs boson mass*, *Mod. Phys. Lett. A* **6** (1991) 1195.

[71] L. Durand, J.M. Johnson and J.L. Lopez, *Perturbative unitarity and high-energy W(L)+-, Z(L), H scattering. One loop corrections and the Higgs boson coupling*, *Phys. Rev. D* **45** (1992) 3112.

[72] P.N. Maher, L. Durand and K. Riesselmann, *Two loop renormalization constants and high-energy 2 → 2 scattering amplitudes in the Higgs sector of the Standard Model*, *Phys. Rev. D* **48** (1993) 1061 [[hep-ph/9303233](#)].

[73] L. Durand, P.N. Maher and K. Riesselmann, *Two loop unitarity constraints on the Higgs boson coupling*, *Phys. Rev. D* **48** (1993) 1084 [[hep-ph/9303234](#)].

[74] B. Grinstein, C.W. Murphy and P. Uttayarat, *One-loop corrections to the perturbative unitarity bounds in the CP-conserving two-Higgs doublet model with a softly broken \mathbb{Z}_2 symmetry*, *JHEP* **06** (2016) 070 [[1512.04567](#)].

[75] V. Cacchio, D. Chowdhury, O. Eberhardt and C.W. Murphy, *Next-to-leading order unitarity fits in Two-Higgs-Doublet models with soft \mathbb{Z}_2 breaking*, *JHEP* **11** (2016) 026 [[1609.01290](#)].

[76] M. Aoki and S. Kanemura, *Unitarity bounds in the Higgs model including triplet fields with custodial symmetry*, *Phys. Rev. D* **77** (2008) 095009 [[0712.4053](#)].

[77] G. Moultaka and M.C. Peyranère, *Vacuum stability conditions for Higgs potentials with $SU(2)_L$ triplets*, *Phys. Rev. D* **103** (2021) 115006 [[2012.13947](#)].

[78] K. Kannike, *Vacuum stability conditions from copositivity criteria*, *Eur. Phys. J. C* **72** (2012) 2093 [[1205.3781](#)].

[79] J. Chakrabortty, P. Konar and T. Mondal, *Copositive Criteria and Boundedness of the Scalar Potential*, *Phys. Rev. D* **89** (2014) 095008 [[1311.5666](#)].

[80] K. Kannike, *Vacuum Stability of a General Scalar Potential of a Few Fields*, *Eur. Phys. J. C* **76** (2016) 324 [[1603.02680](#)].

[81] M. Abud and G. Sartori, *The geometry of orbit-space and natural minima of higgs potentials*, *Physics Letters B* **104** (1981) 147.

[82] J. Kim, *General Method for Analyzing Higgs Potentials*, *Nucl. Phys. B* **196** (1982) 285.

[83] M. Abud and G. Sartori, *The Geometry of Spontaneous Symmetry Breaking*, *Annals Phys.* **150** (1983) 307.

[84] I.P. Ivanov, *Minkowski space structure of the Higgs potential in 2HDM*, *Phys. Rev. D* **75** (2007) 035001 [[hep-ph/0609018](#)].

[85] A.W. El Kaffas, W. Khater, O.M. Ogreid and P. Osland, *Consistency of the two Higgs doublet model and CP violation in top production at the LHC*, *Nucl. Phys. B* **775** (2007) 45 [[hep-ph/0605142](#)].

[86] A. Degee, I.P. Ivanov and V. Keus, *Geometric minimization of highly symmetric potentials*, *JHEP* **02** (2013) 125 [[1211.4989](#)].

[87] K.G. Klimenko, *On Necessary and Sufficient Conditions for Some Higgs Potentials to Be Bounded From Below*, *Theor. Math. Phys.* **62** (1985) 58.

[88] K.G. Murty and S.N. Kabadi, *Some np-complete problems in quadratic and nonlinear programming*, *Math. Program.* **39** (1987) 117–129.

[89] I.P. Ivanov, M. Köpke and M. Mühlleitner, *Algorithmic boundedness-from-below conditions for generic scalar potentials*, *Eur. Phys. J. C* **78** (2018) 413 [[1802.07976](#)].

[90] S. Blasi, S. De Curtis and K. Yagyu, *Effects of custodial symmetry breaking in the Georgi-Machacek model at high energies*, *Phys. Rev. D* **96** (2017) 015001 [[1704.08512](#)].

[91] M.E. Krauss and F. Staub, *Perturbativity Constraints in BSM Models*, *Eur. Phys. J. C* **78** (2018) 185 [[1709.03501](#)].

[92] A. Arhrib, R. Benbrik, M. Chabab, G. Moultaka, M.C. Peyranere, L. Rahili et al., *The Higgs Potential in the Type II Seesaw Model*, *Phys. Rev. D* **84** (2011) 095005 [[1105.1925](#)].

[93] L. Durand, J.M. Johnson and J.L. Lopez, *Perturbative unitarity and high-energy W_L^\pm , Z_L , h scattering. one-loop corrections and the higgs-boson coupling*, *Phys. Rev. D* **45** (1992) 3112.

[94] M.S. Chanowitz and M.K. Gaillard, *The TeV Physics of Strongly Interacting W 's and Z 's*, *Nucl. Phys. B* **261** (1985) 379.

[95] J. Bagger and C. Schmidt, *Equivalence theorem redux*, *Phys. Rev. D* **41** (1990) 264.

[96] S. Dawson and S. Willenbrock, *Radiative corrections to longitudinal-vector-boson scattering*, *Phys. Rev. D* **40** (1989) 2880.

[97] S. Blasi, S. De Curtis and K. Yagyu, *Effects of custodial symmetry breaking in the Georgi-Machacek model at high energies*, *Phys. Rev. D* **96** (2017) 015001 [[1704.08512](#)].

[98] B. Keeshan, H.E. Logan and T. Pilkington, *Custodial symmetry violation in the Georgi-Machacek model*, *Phys. Rev. D* **102** (2020) 015001 [[1807.11511](#)].

[99] C.W. Murphy, *NLO Perturbativity Bounds on Quartic Couplings in Renormalizable Theories with ϕ^4 -like Scalar Sectors*, *Phys. Rev. D* **96** (2017) 036006 [[1702.08511](#)].

[100] J. De Blas et al., *HEPfit: a code for the combination of indirect and direct constraints on high energy physics models*, *Eur. Phys. J. C* **80** (2020) 456 [[1910.14012](#)].

[101] A. Caldwell, D. Kollar and K. Kroninger, *BAT: The Bayesian Analysis Toolkit*, *Comput. Phys. Commun.* **180** (2009) 2197 [[0808.2552](#)].

[102] ATLAS, CMS collaboration, *Combined Measurement of the Higgs Boson Mass in pp Collisions at $\sqrt{s} = 7$ and 8 TeV with the ATLAS and CMS Experiments*, *Phys. Rev. Lett.* **114** (2015) 191803 [[1503.07589](#)].

[103] D. Chowdhury and O. Eberhardt, *Update of Global Two-Higgs-Doublet Model Fits*, *JHEP* **05** (2018) 161 [[1711.02095](#)].

- [104] L. Sartore and I. Schienbein, *PyR@TE 3*, *Comput. Phys. Commun.* **261** (2021) 107819 [[2007.12700](#)].
- [105] J.F. Gunion, H.E. Haber, G.L. Kane and S. Dawson, *The Higgs Hunter's Guide*, vol. 80 (2000).
- [106] D. Chowdhury, A. Kundu, P. Mondal, S. Samanta and A. Srivastava, *Oblique Parameters in the Extended Georgi-Machacek Model*, [2505.xxxxx](#).
- [107] K.P. Hadeler, *On copositive matrices*, *Linear Algebra and its Applications* **49** (1983) 79.
- [108] G. Chang and T.W. Sederberg, *Nonnegative quadratic b  zier triangular patches*, *Comput. Aided Geom. Des.* **11** (1994) 113.
- [109] N.D. Christensen and C. Duhr, *FeynRules - Feynman rules made easy*, *Comput. Phys. Commun.* **180** (2009) 1614 [[0806.4194](#)].
- [110] T. Hahn, *Generating Feynman diagrams and amplitudes with FeynArts 3*, *Comput. Phys. Commun.* **140** (2001) 418 [[hep-ph/0012260](#)].
- [111] M.-x. Luo and Y. Xiao, *Two loop renormalization group equations in the standard model*, *Phys. Rev. Lett.* **90** (2003) 011601 [[hep-ph/0207271](#)].
- [112] D. Chowdhury and O. Eberhardt, *Global fits of the two-loop renormalized Two-Higgs-Doublet model with soft Z_2 breaking*, *JHEP* **11** (2015) 052 [[1503.08216](#)].